Neutron stars & Pulsars

Outline

- What is a neutron star?
- When there is a pulsar
- Radio (but non only radio) properties
- The pulsar diagram
- Facts & models
- Look at https://www.youtube.com/watch?v=tWsWcWAcK2U for a schematic view

Further readings:

- Taylor, J. H. & Stinebring 1986, ARAA, 24, 285-327
  "Recent progress in the understanding of pulsars"
- Kramer 2003, "Pulsars" http://www.jb.man.ac.uk/~pulsar/Education/jenam.pdf
- Gensler & Slane 2006, ARAA, 44, 17-47
  "The Evolution and Structure of Pulsar Wind Nebulae"
- Lorimer 2008, Living Rev. Relativity, 2008, 11, 8 "Binary and Millisecond Pulsars"
- Kramer & Stairs 2008, ARAA, 46, 541-72 "The Double Pulsar"
- Caraveo 2014, ARAA, 52, 211-250 "Gamma – Ray Pulsar Revolution"
- Fanti + Fanti, Chap 17
- http://www.iap.fr/vie_scientifique/seminaires/Seminaire_IAP/2018/videos/Benoit_Cerutti_2018-01-12_1100/index.html

Neutron star is the final product of the most common type Ib, Ic and type II supernovae

Type Ia supernovae are not considered in the right side diagram (massive stars only!)

NS are believed to account for a fraction of the Dark Matter in our galaxy

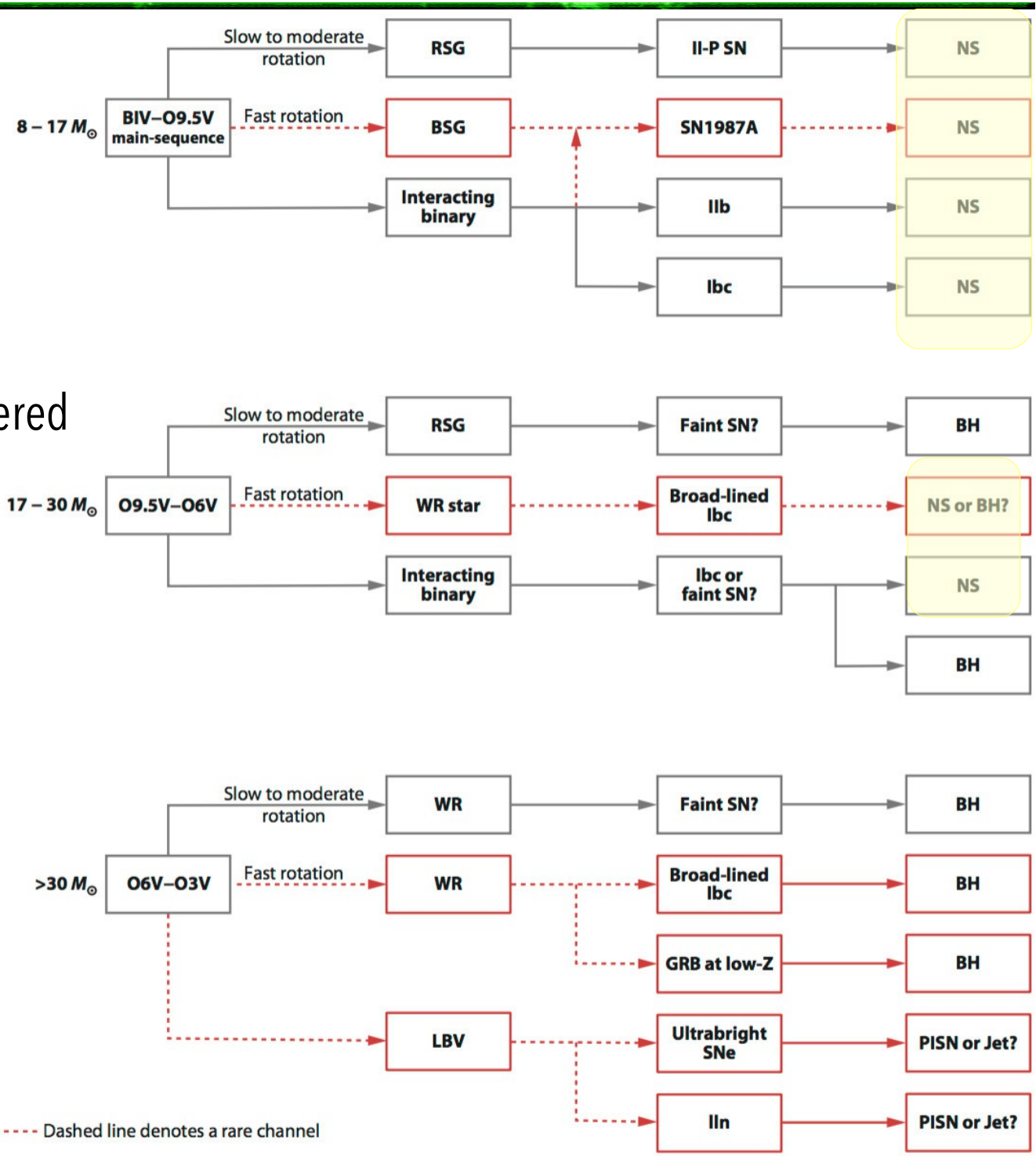

What is a neutron star?

- Small: radius ~ 10 km
- High mass 1 – 2 (3) $M_\odot$
- Dense: even denser than atomic nuclei:
  on average, $\rho \sim 4 \times 10^{17}$ kg m^{-3}
- Electrons & protons collide to generate neutrons
  whose (degenerate) pressure stops the collapse

$$e^- + p^+ \rightarrow n + \nu_e$$

- Hot: initial temperatures $T \sim 5 \times 10^{11}$ K
  but the neutrino release can drop it to a
  few in 10^6 K after a few years (leaving X-ray emission)

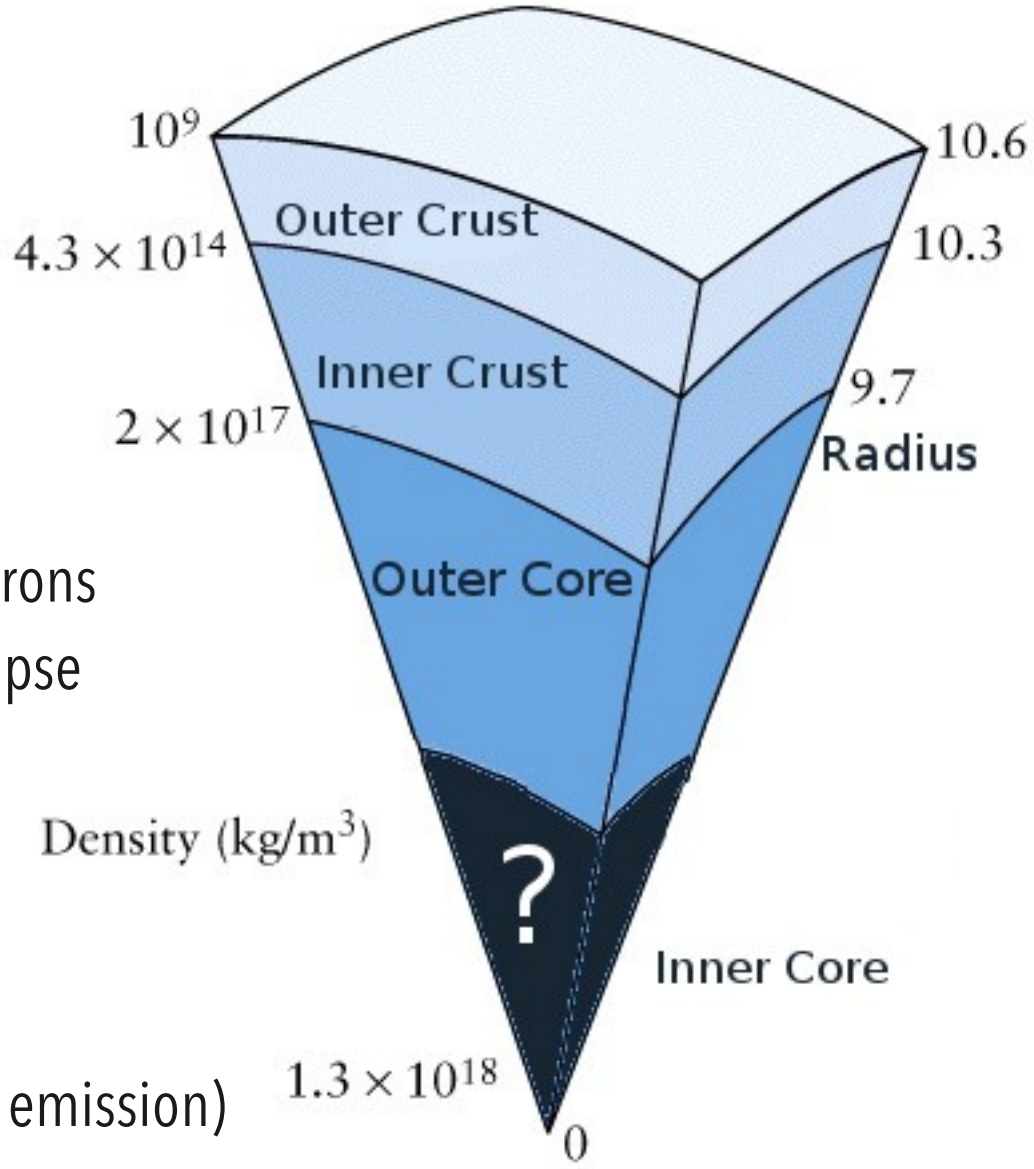

- Strong magnetic field (flux conservation), rapid rotation (angular momentum conservation)

What is a neutron star?

Equation of state defined by Openheimer & Volkov (1939)
... still an open question

1967
Pacini:
Rotating NS can produce Electromagnetic radiation.

Hewish & Bell:
Discovery of a pulsating radio signal

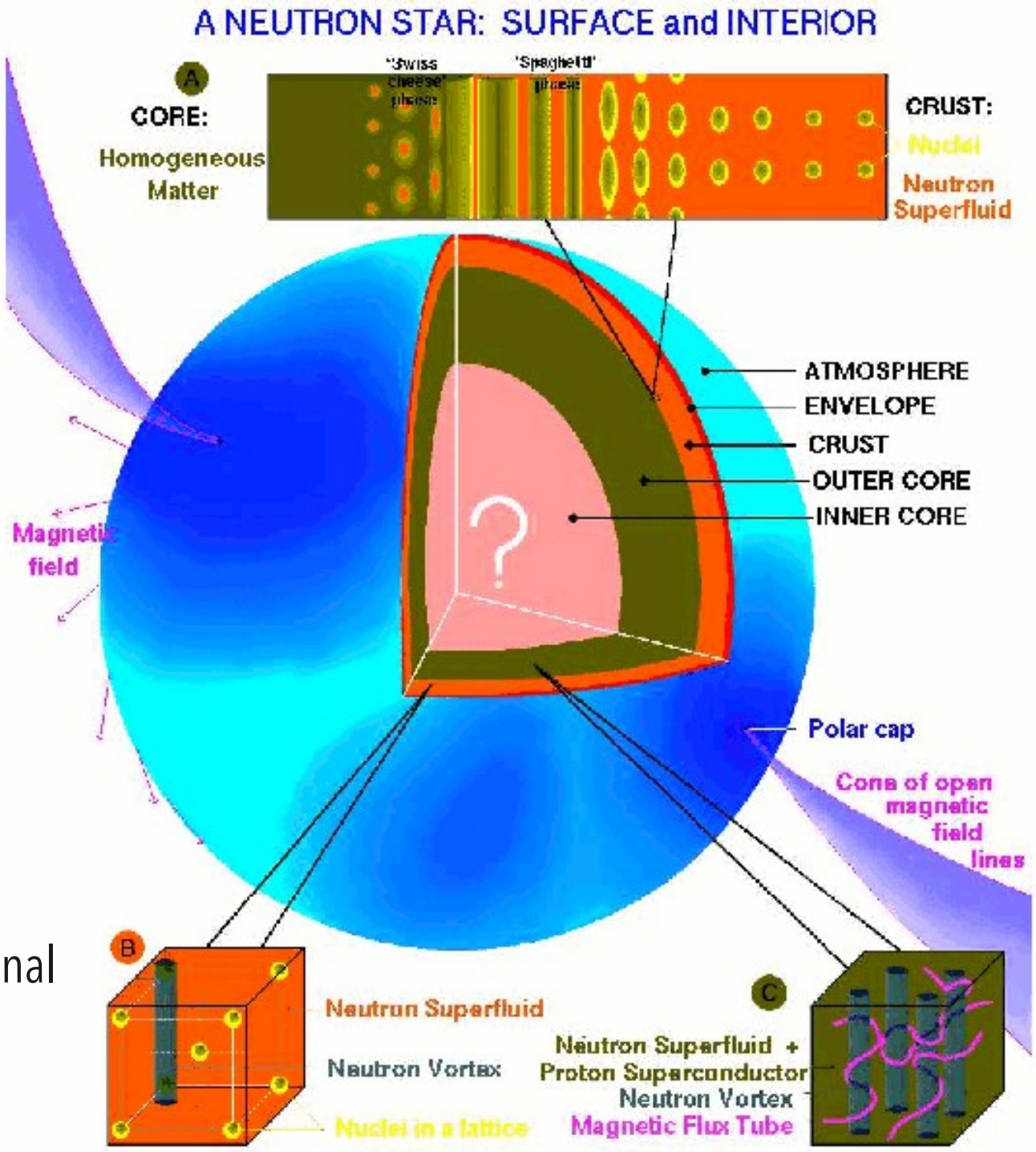

Direct view: NS at the center of Vela SNR (distance 250 pc, diameter 70 pc ~ 6°, ~12 kyr old)

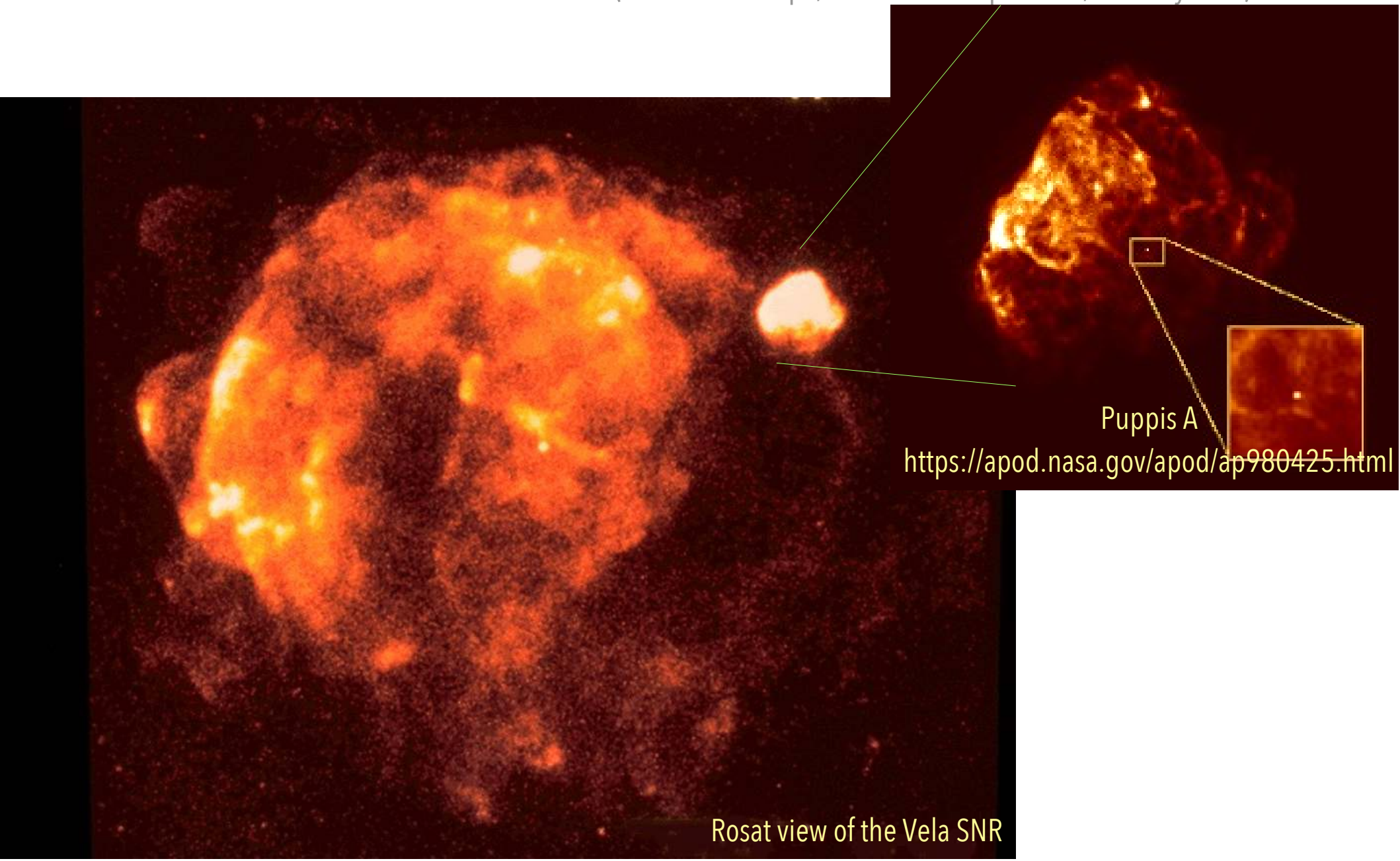

Pulsars

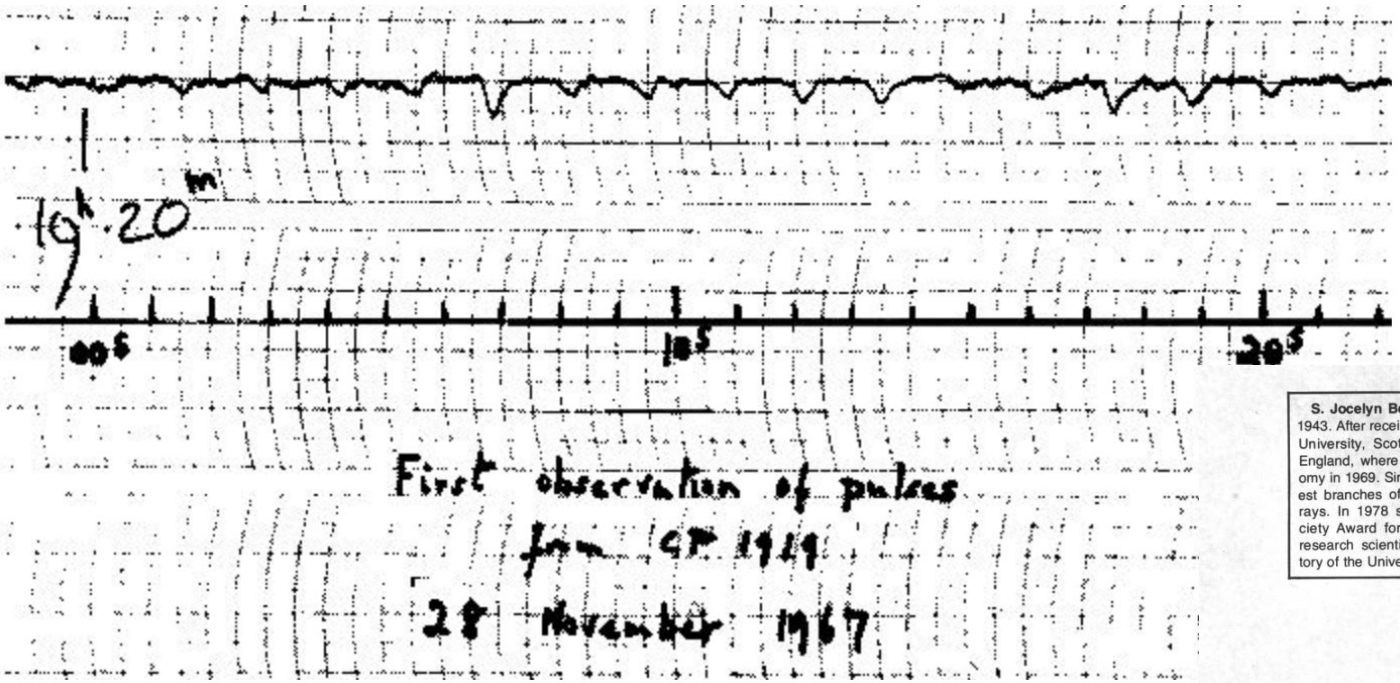

PSR B1919+21 has a period of 1.3373 seconds, a pulse width of 0.04 seconds. Discovered by Jocelyn Bell and Antony Hewish on November 28, 1967

S. Jocelyn Bell Burnell was born in northern Ireland in 1943. After receiving a B.S. degree in physics from Glasgow University, Scotland, she went to Cambridge University, England, where she earned her doctorate in radio astronomy in 1969. Since then she has done research in the newest branches of astronomy involving gamma-rays and x-rays. In 1978 she received the American Tentative Society Award for her pulsar research. Currently she is a research scientist at the Mullard Space Science Laboratory of the University College London.

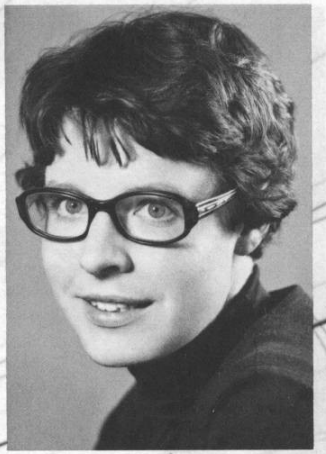

Burnell

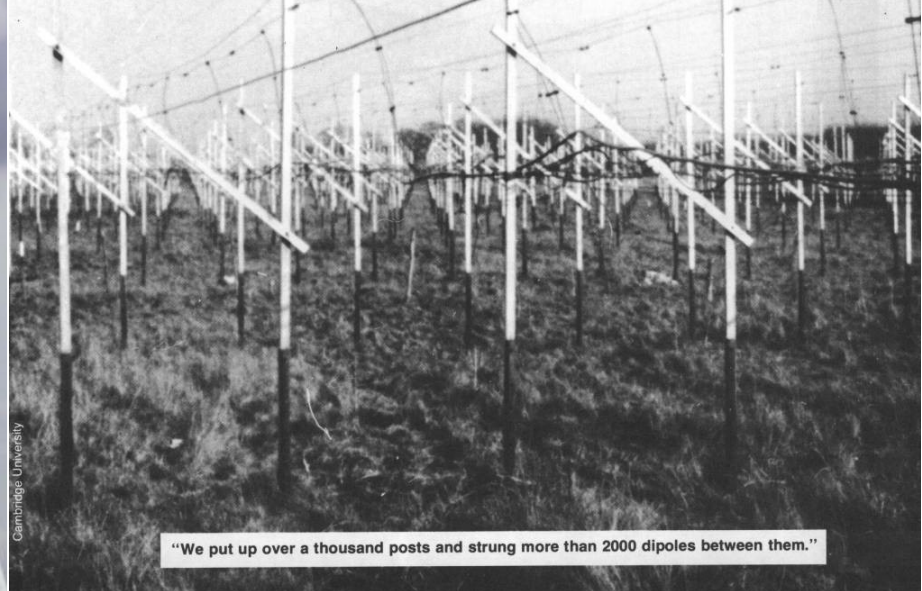

Progenitors:

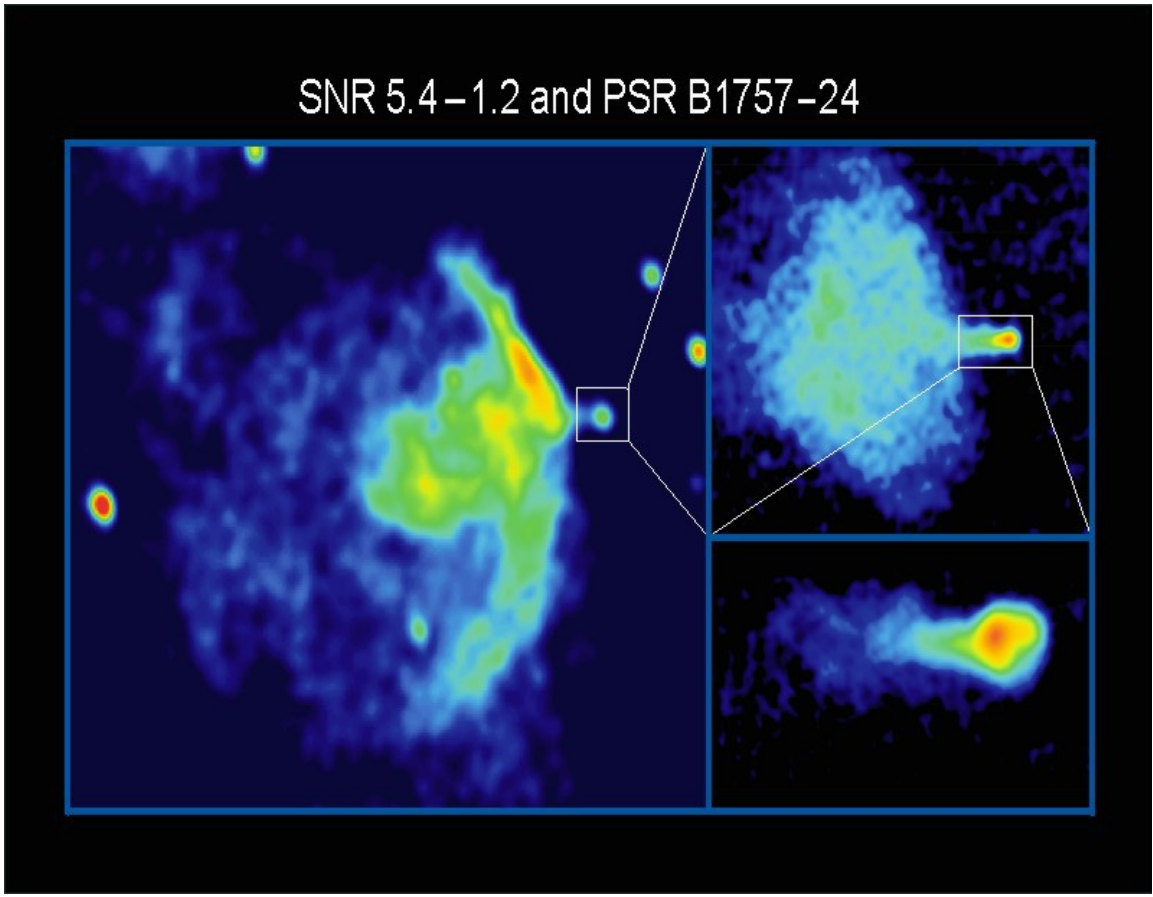

- SN explosions
  the number of associations between a pulsar and its SNR is difficult:
  SNR are visible for ~0.1 Myr max,
  pulsars are 10-100 times longer lived

  Pulsars have rather high peculiar velocities and this may prevent the association

- Best chances for associations with young SNR

Pulsars: Variable individual pulses in 1919+21 (the “discovery pulsar”)

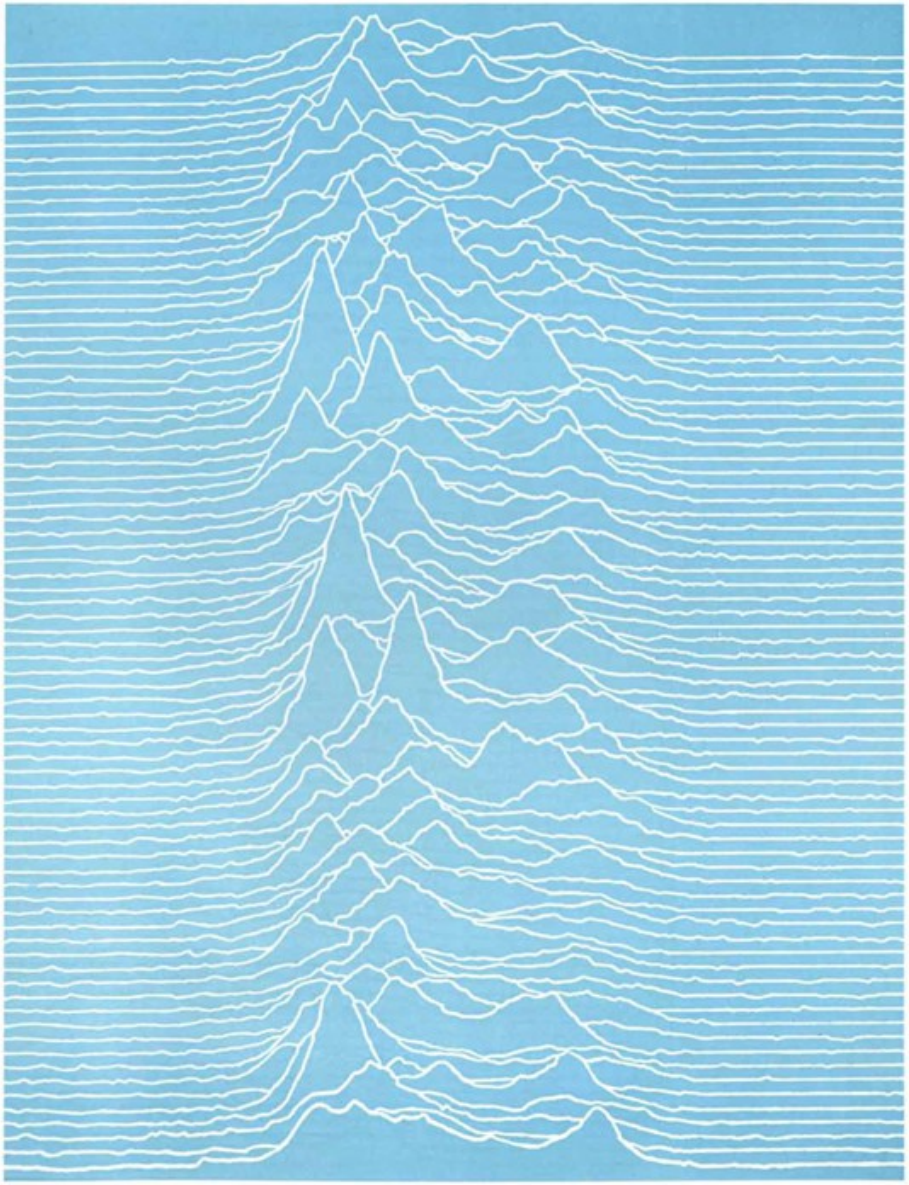

EIGHTY SUCCESSIVE PERIODS of the first pulsar observed, CP1919 (Cambridge pulsar at 19 hours 19 minutes right ascension), are stacked on top of one another using the average period of 1.33730 seconds in this computer-generated illustration produced at the Arecibo Radio Observatory in Puerto Rico. Although the leading edges of the radio pulses occur within a few thousandths of a second of the predicted times, the shape of the pulses is quite irregular. Some of this irregularity in radio reception is caused by the effects of transmission through the interstellar medium. The average pulse width is less than 50 thousandths of a second.

Pulsars: Radio profiles like the dna of each pulsar

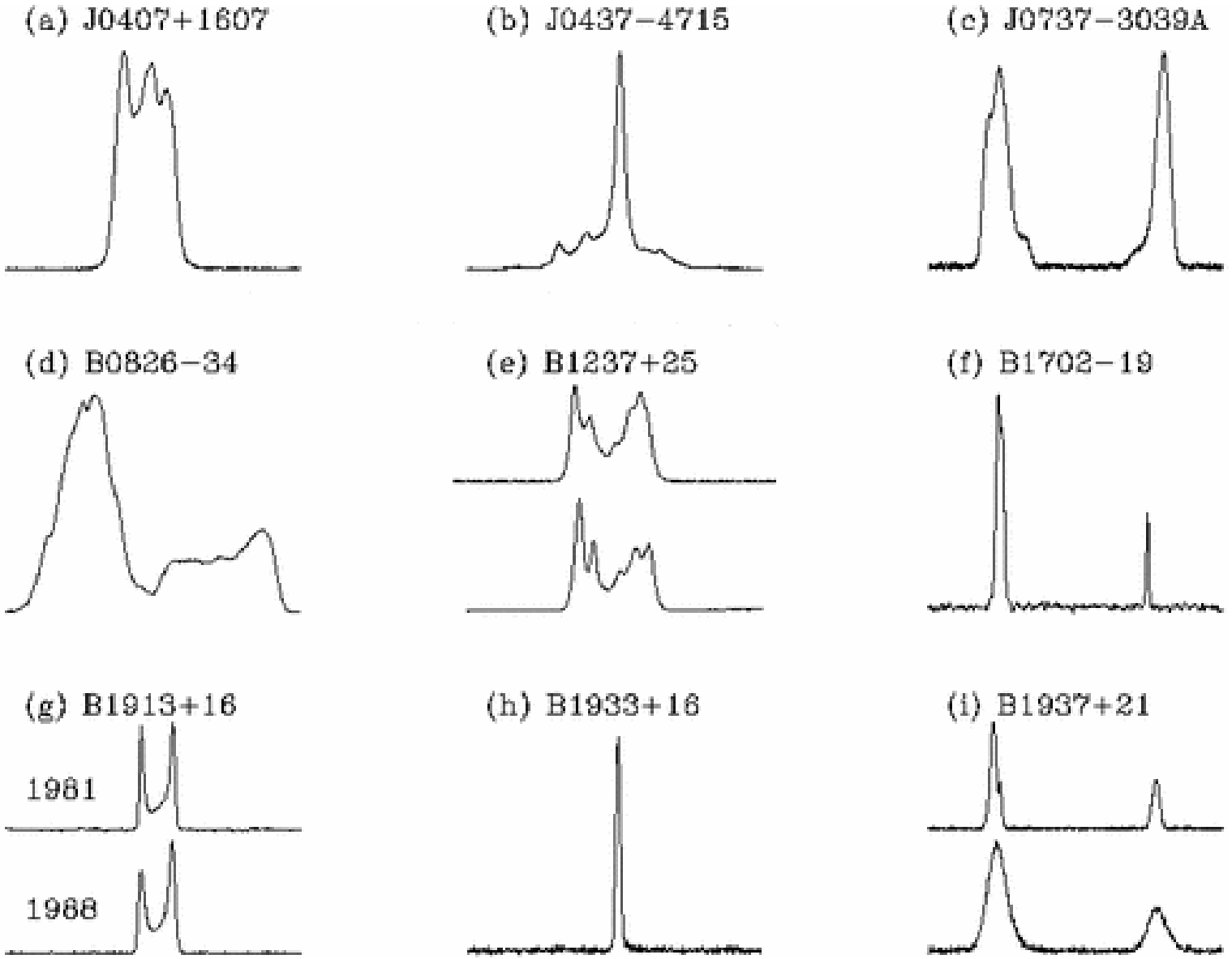

Pulsars: Glitches

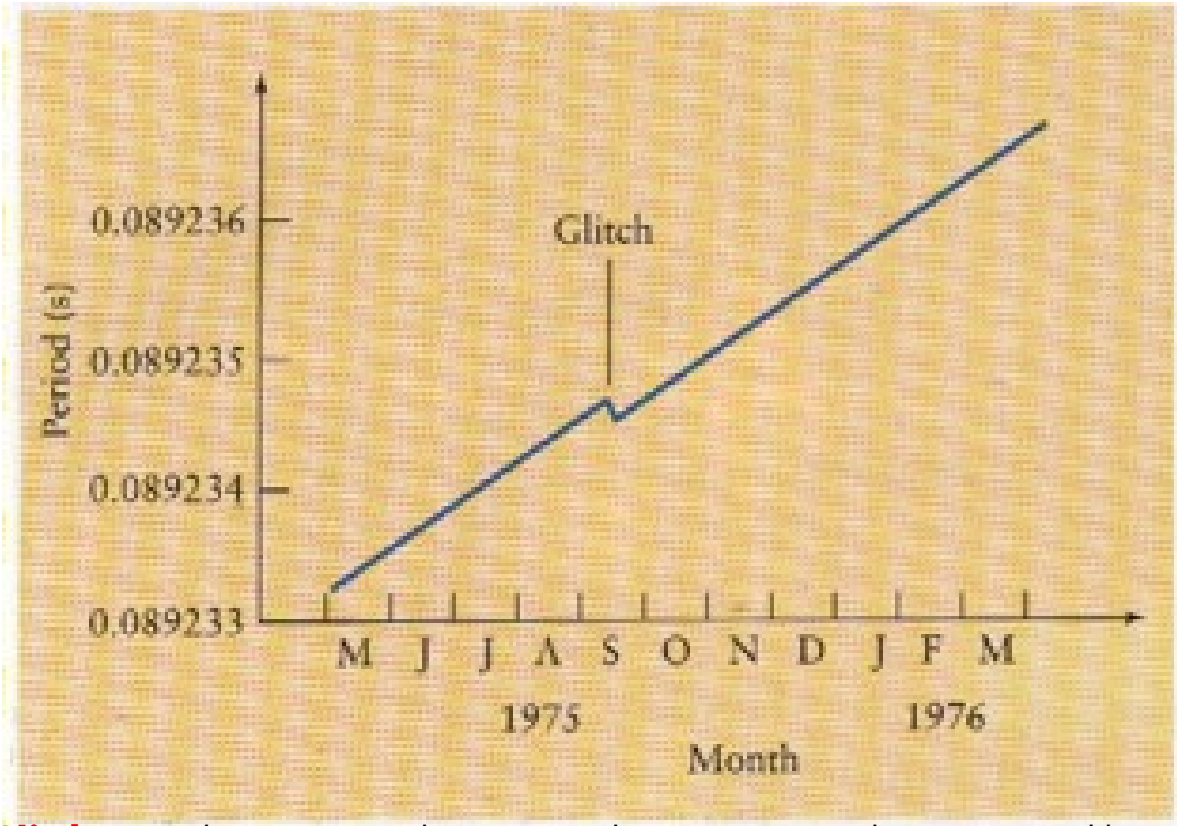

Glitches are discontinuous decreases in the rotation period, accompanied by quasi-exponential recoveries with timescales of hours up to years. Such variation can be interpreted as changes in the pulsar environment and/or neutron star interior. Here a glitch in the VELA PULSAR timing

They are likely common in young pulsars when the fast rotation causes stress between the crustand the NS interior. As the rotation slows down, such stress is reduced and glitches does not appear any more

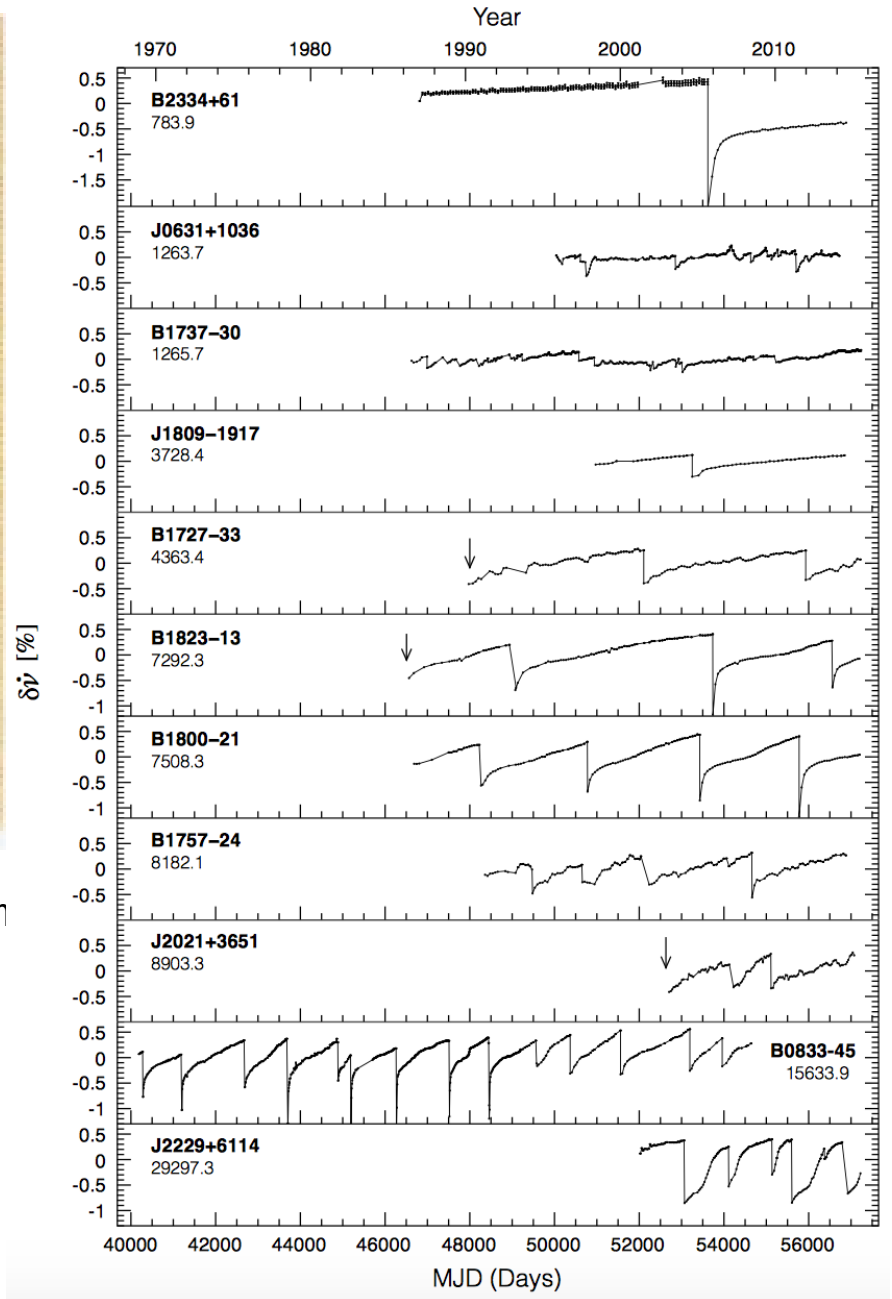

Espinoza +, 2017: glitches in young pulsars

Pulsars: the effect of the dispersion measure

$$n_r(\nu) \simeq \sqrt{1 - \frac{4\pi e^2}{m_e}\frac{n_e}{(2\pi\nu)^2}} = \sqrt{1 - \left(\frac{\nu_p}{\nu}\right)^2}$$

Dispersion measure $DM = \int_L n_e \, dl$

A frequency dependent time delay is introduced

$$\Delta t = 4.15 \cdot 10^3 \; DM \left(\frac{1}{\nu_1^2} - \frac{1}{\nu_2^2}\right) \quad [sec]$$

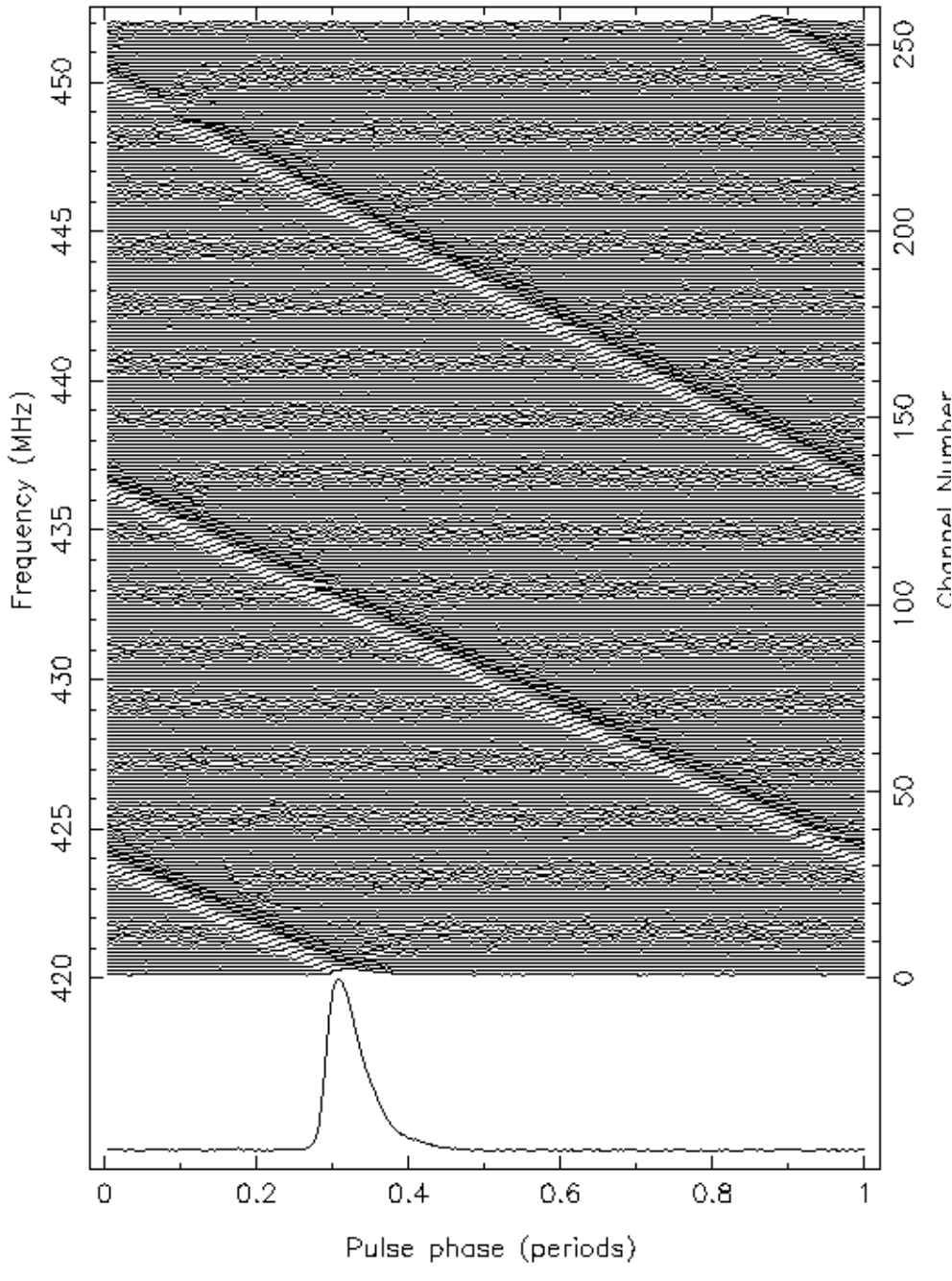

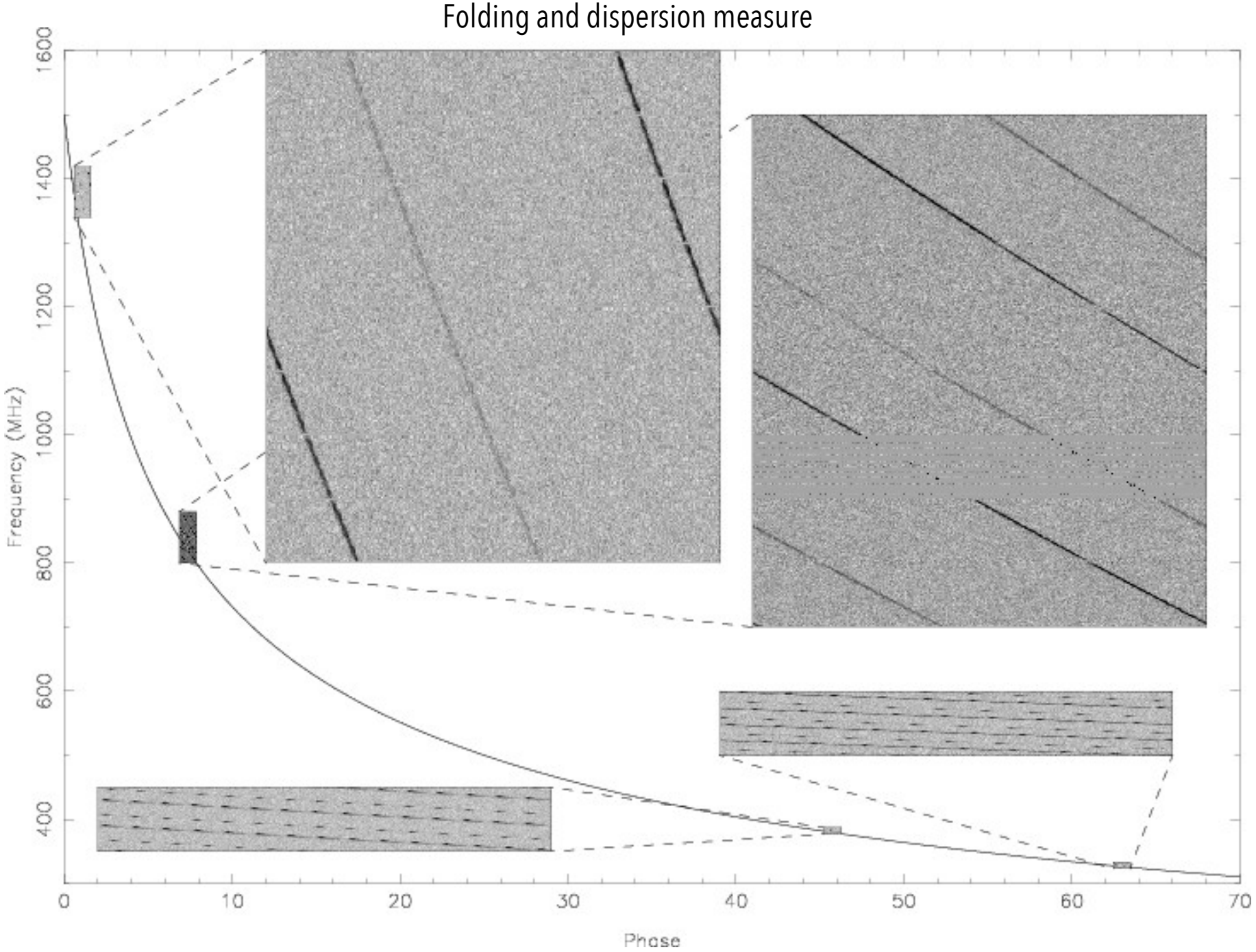
Folding and dispersion measure
Frequency (MHz)
1600
1400
1200
1000
800
600
400
0
10
20
30
40
50
60
70
Phase

Origin:

- Intrinsic (coherent emission, dependent on λ, and zone)
- Extrinsic (diffraction)

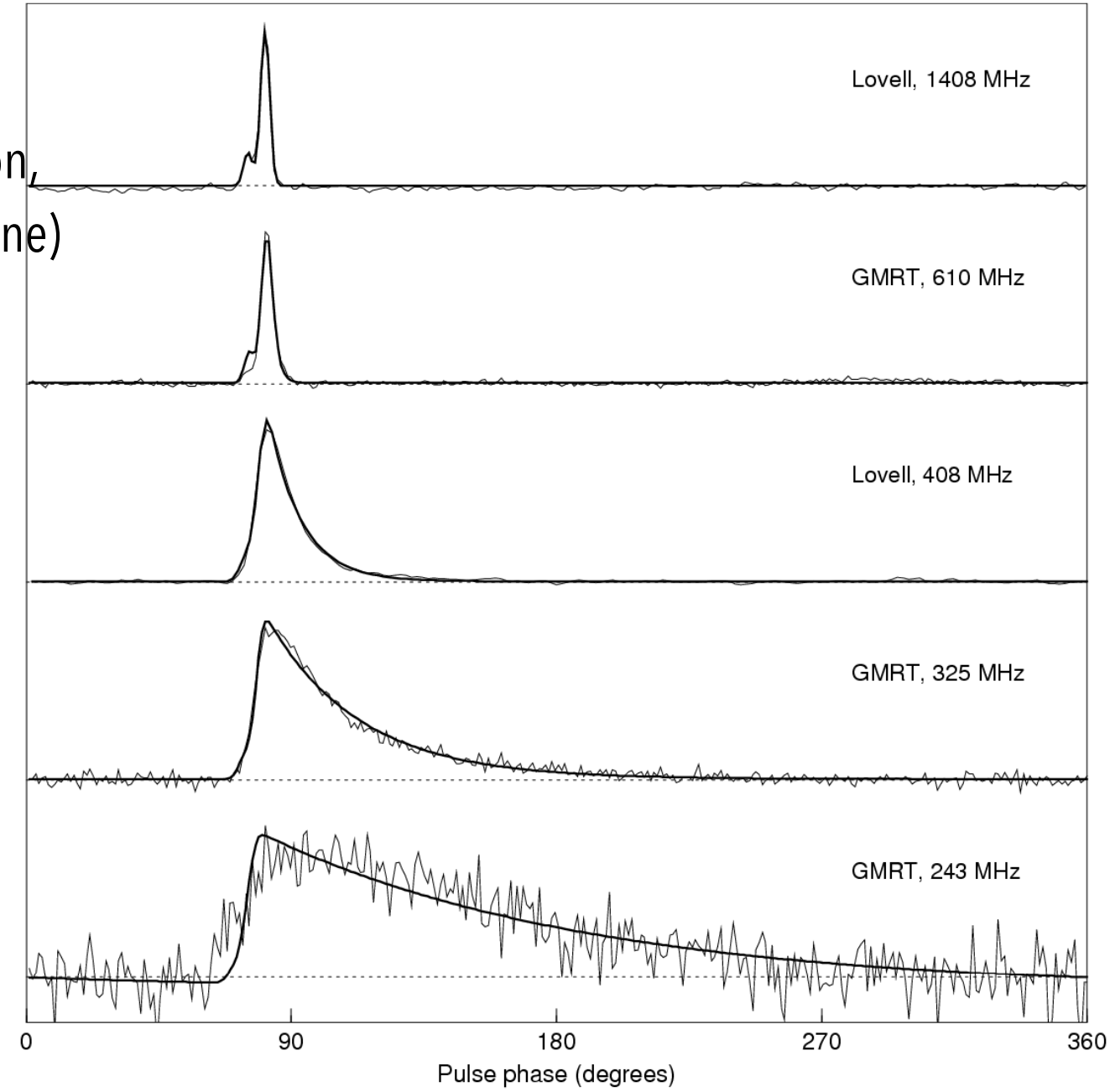

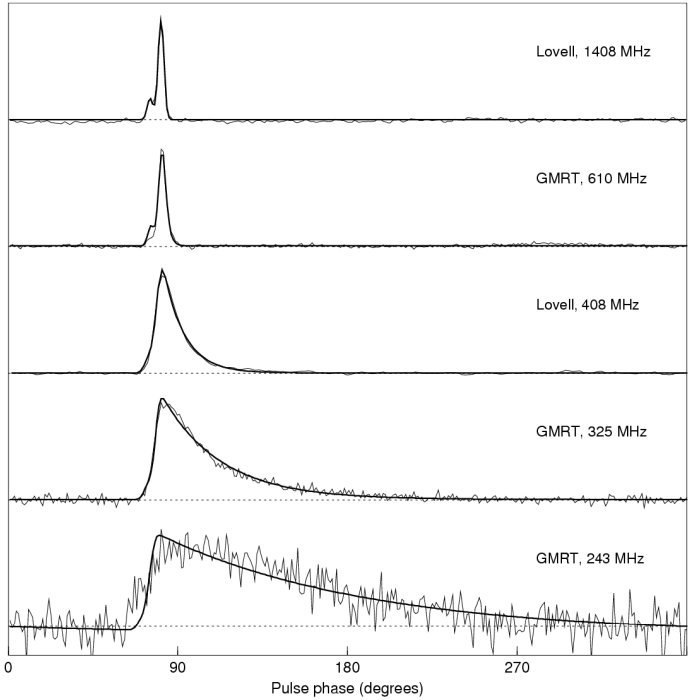

Thin Screen Diffraction/Scattering model. Inhomogeneities in the ISM cause small-angle deviations in the paths of the radio waves. These deviations result in time (and therefore phase) delays that can interfere to create a diffraction pattern, broaden the pulses in time, and make a larger image of the pulsar on the sky. (From the Handbook of Pulsar Astronomy, by Lorimer & Kramer)

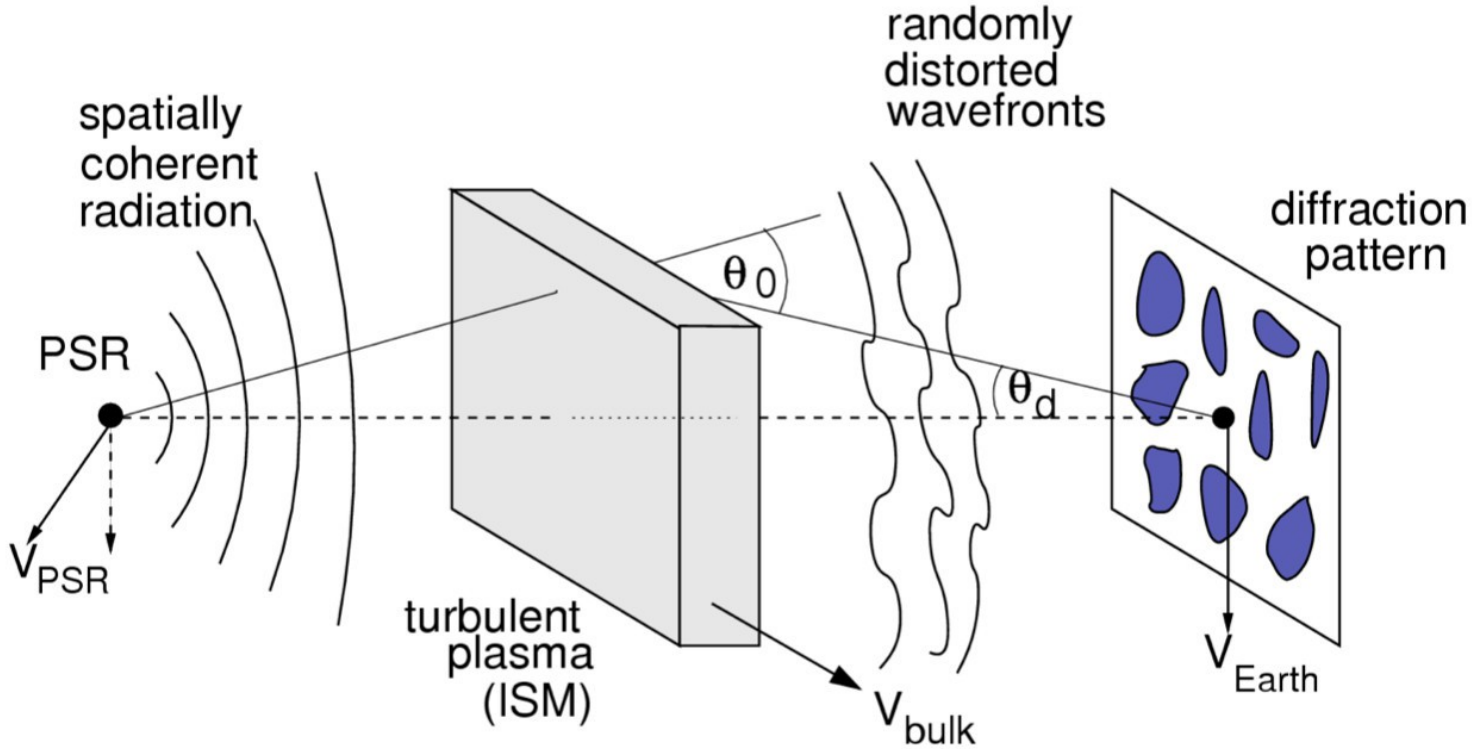

Pulsars: detection of a weak signal: FT & folding

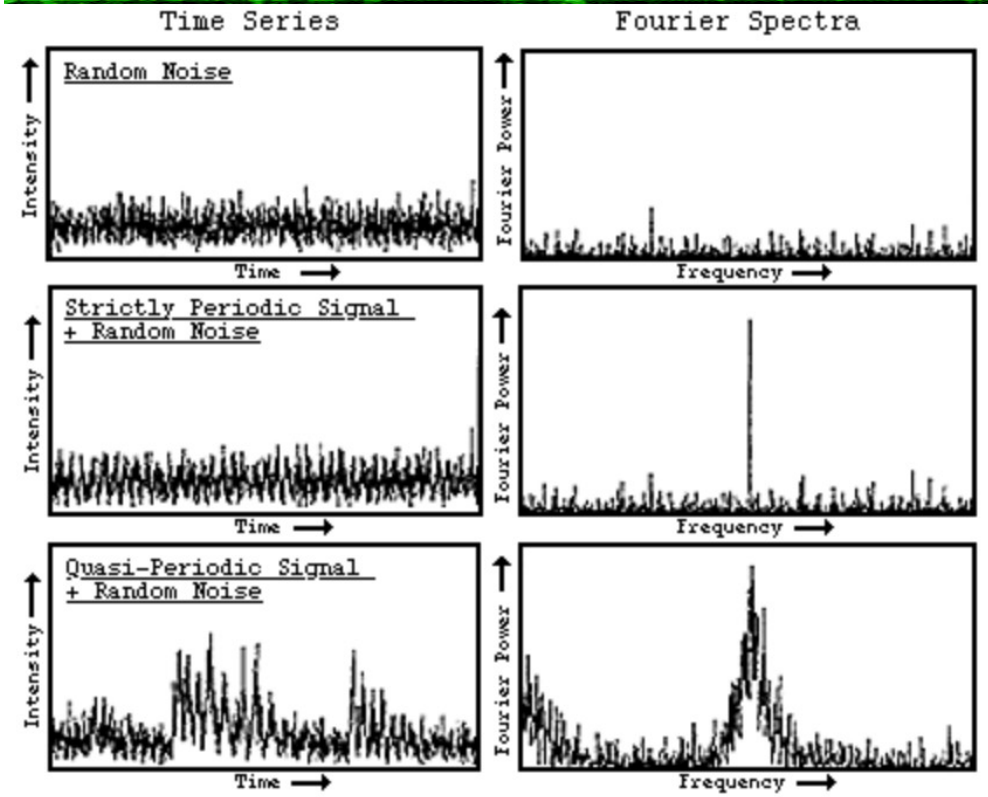

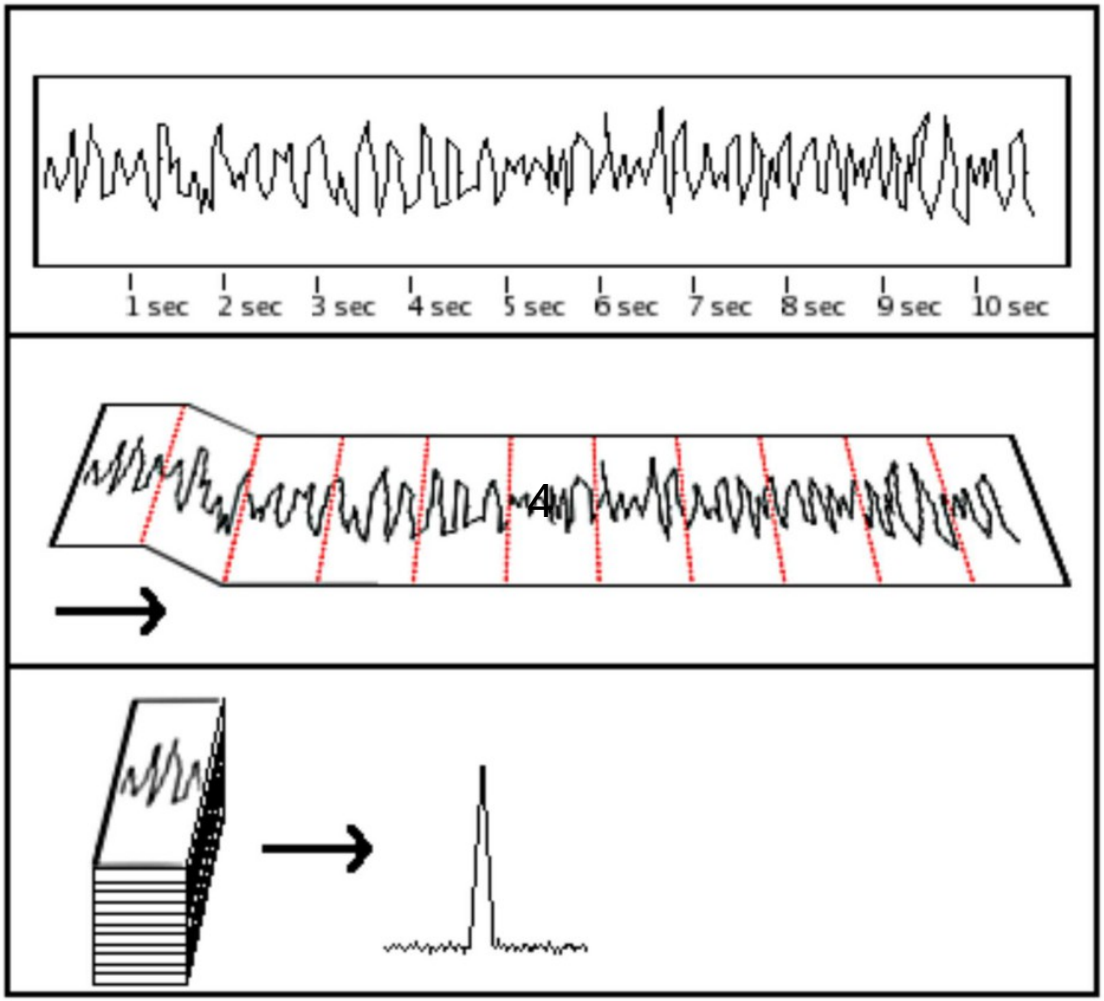

Pulsars: how folding produces the pulsed signal

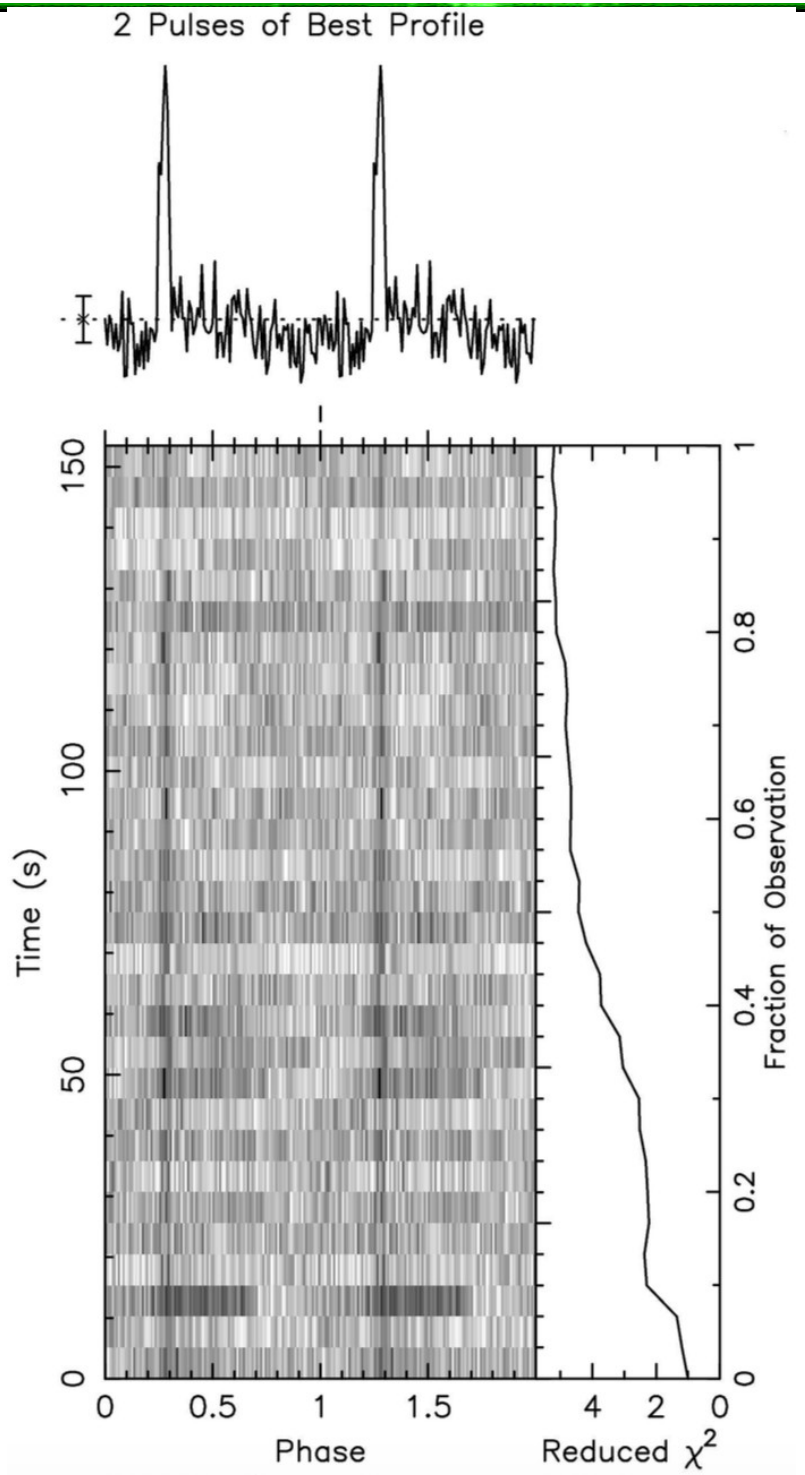

Pulsars: period & derivative

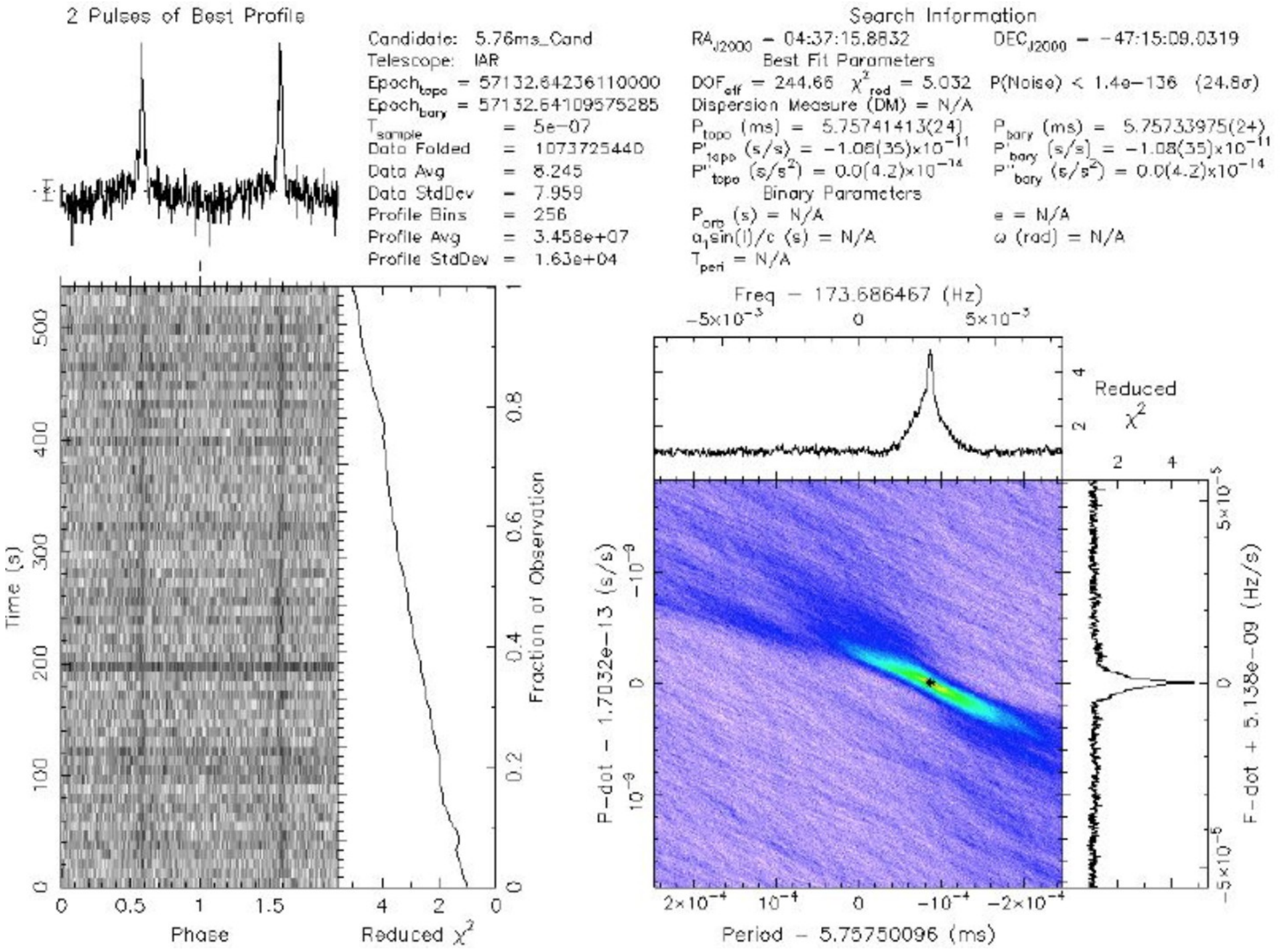

See also https://arxiv.org/pdf/1704.00027.pdf

The radio spectra:

Very steep:

- (flattening: low frequencies)
- (steepening: high frequencies)

Very compact objects!!!!

High brightness temperature

$$T_B = \frac{\lambda^2}{2k} \frac{S_\nu}{\theta_1 \cdot \theta_2}$$

Exceeding any Compton catastrophe!!!!

(>> 10^{25} ° K)

Not true for T_B in other bands, depends on the "coherent emission length (i.e. λ)"

Self-Abs: No relationship with DM

Intrinsic to the emission mechanism

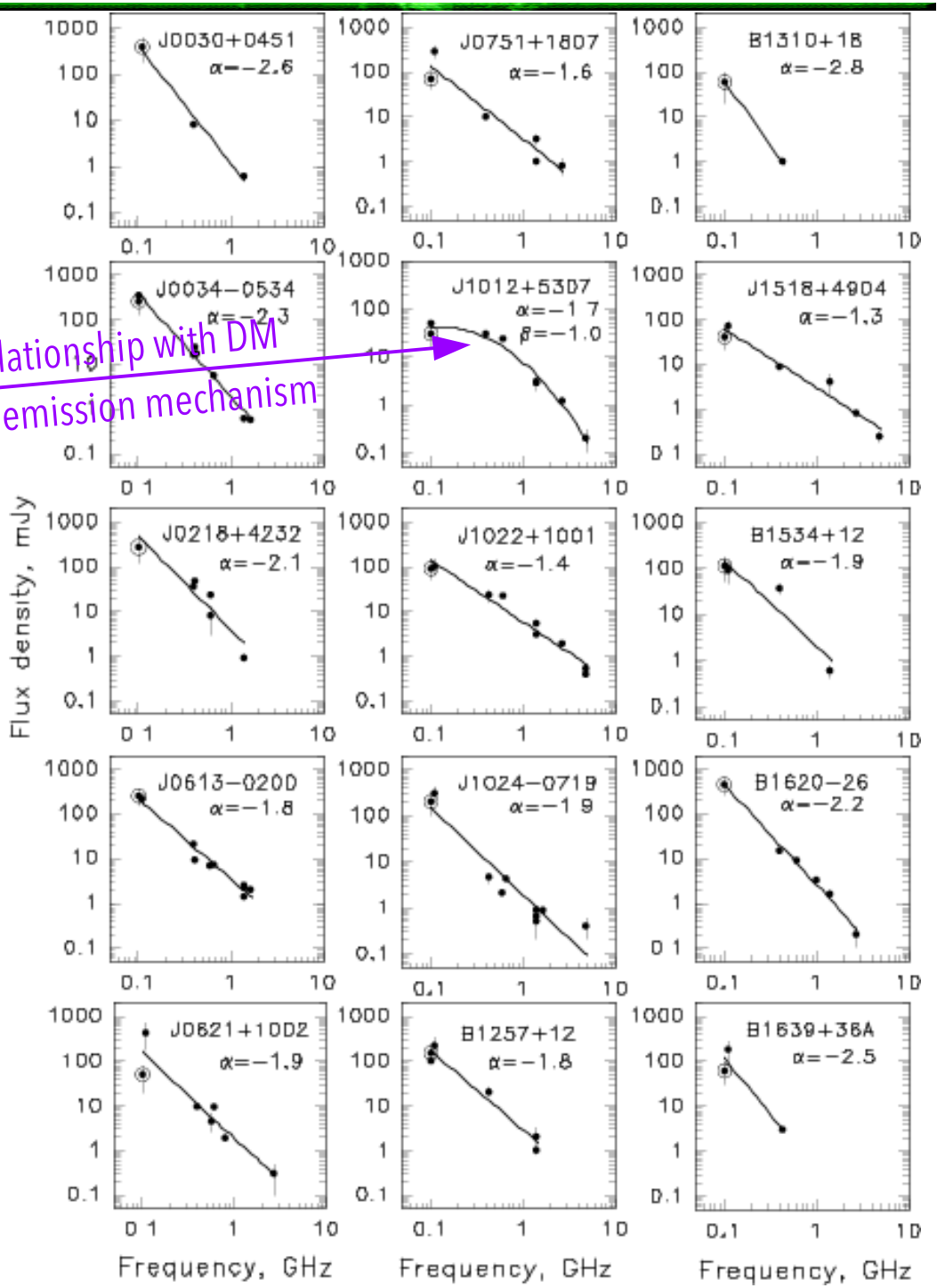

Pulsars: the SED of the Crab pulsar

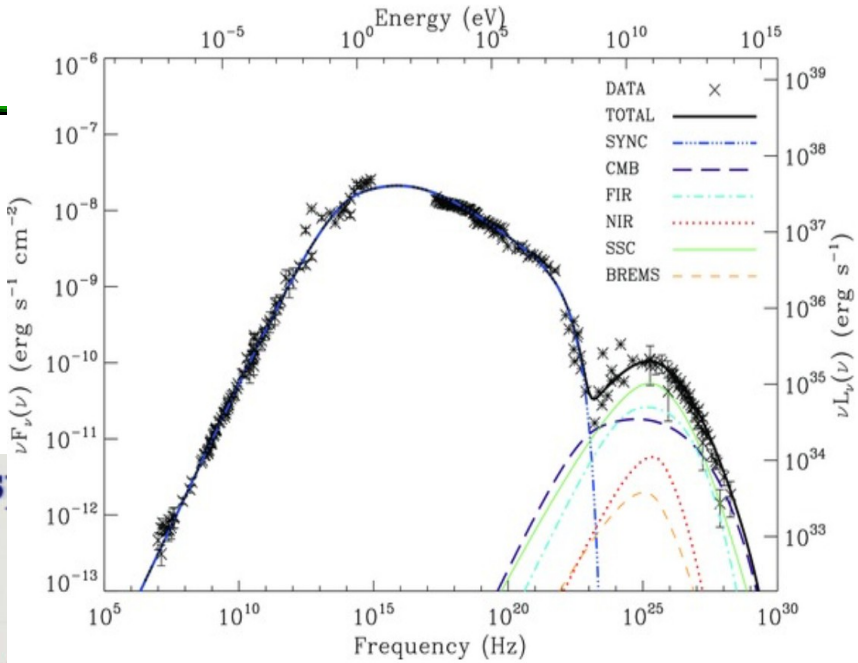

Pulsars shine throughout the electromagnetic s

The Crab pulsar

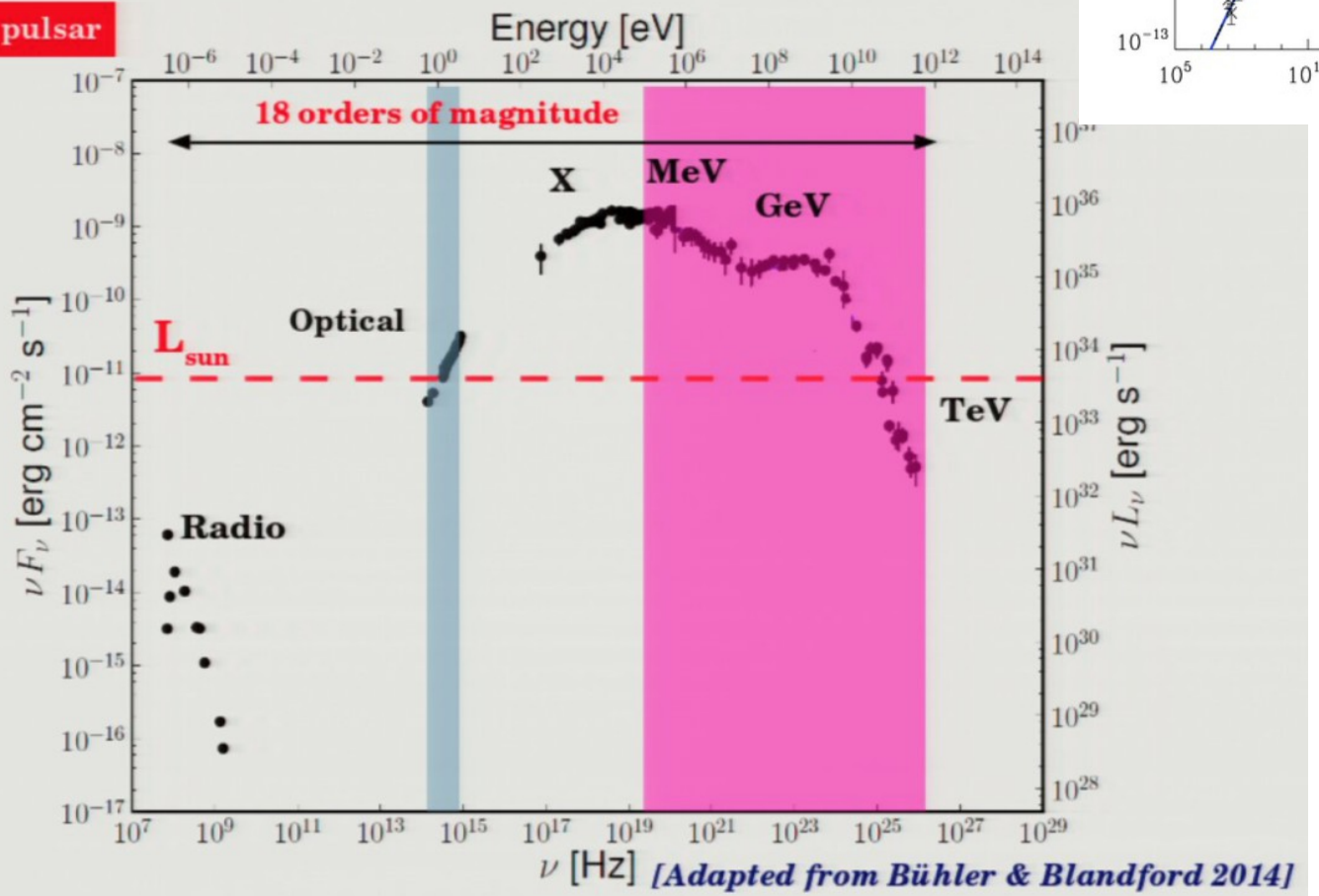

[Adapted from Bühler & Blandford 2014]

A large fraction of the pulsar spindown is released in light, in particular in the gamma-ray band => Efficient particle acceleration !

The extremely high T_B of pulsars are explained by coherent radiation.

Electrons do not radiate as independent charges

- *instead bunches of N electrons in volumes whose dimensions are less than a wavelength emit in phase as charges N e.*
- *Larmor's formula indicates that the power radiated by a charge q is proportional to q^2, so the radiation intensity can be N^2* times brighter than incoherent radiation from the same total number N of electrons. Coherent radiation is N times stronger than incoherent radiation

Because the coherent volume is smaller at shorter wavelengths, most pulsars have extremely steep radio spectra.

- *Polarized emission, mainly linear, a bit of circular, variable within the period.*

- *Also spectral index is variable within the period.*

Linear and circular polarization

Dai et al. 2015, MNRAS, 449, 3223

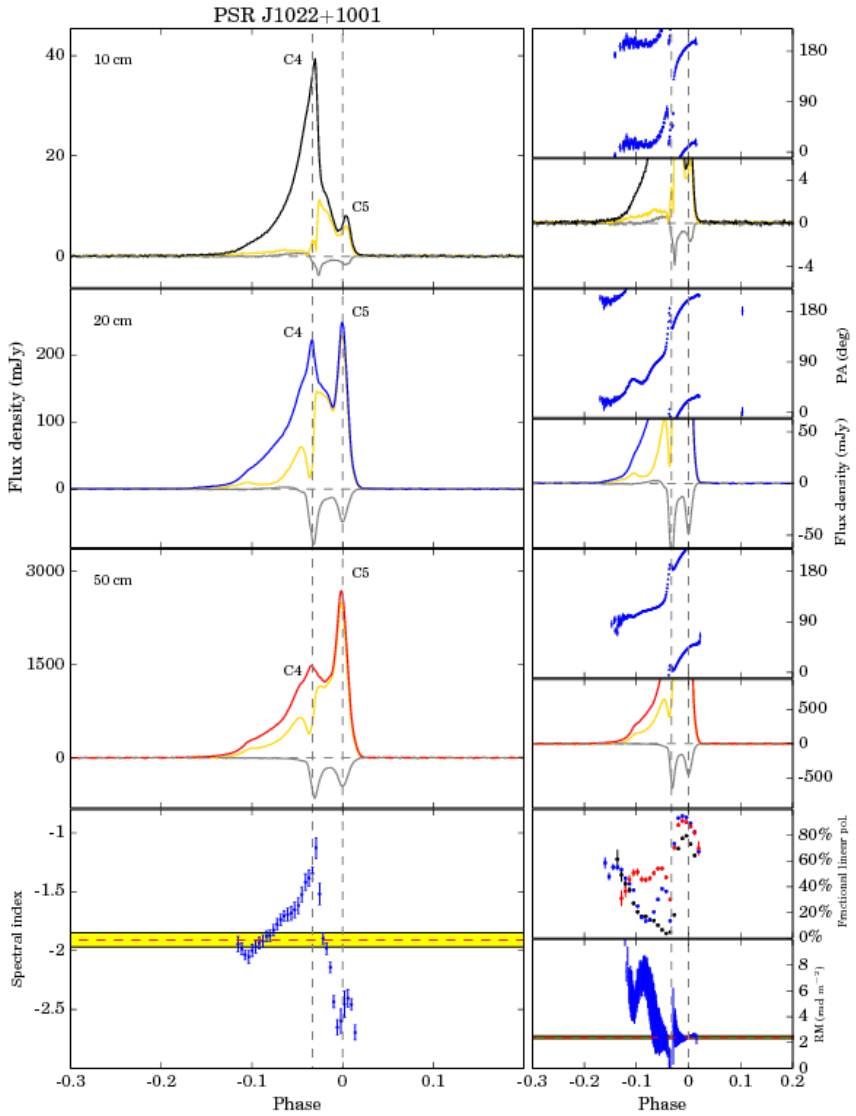

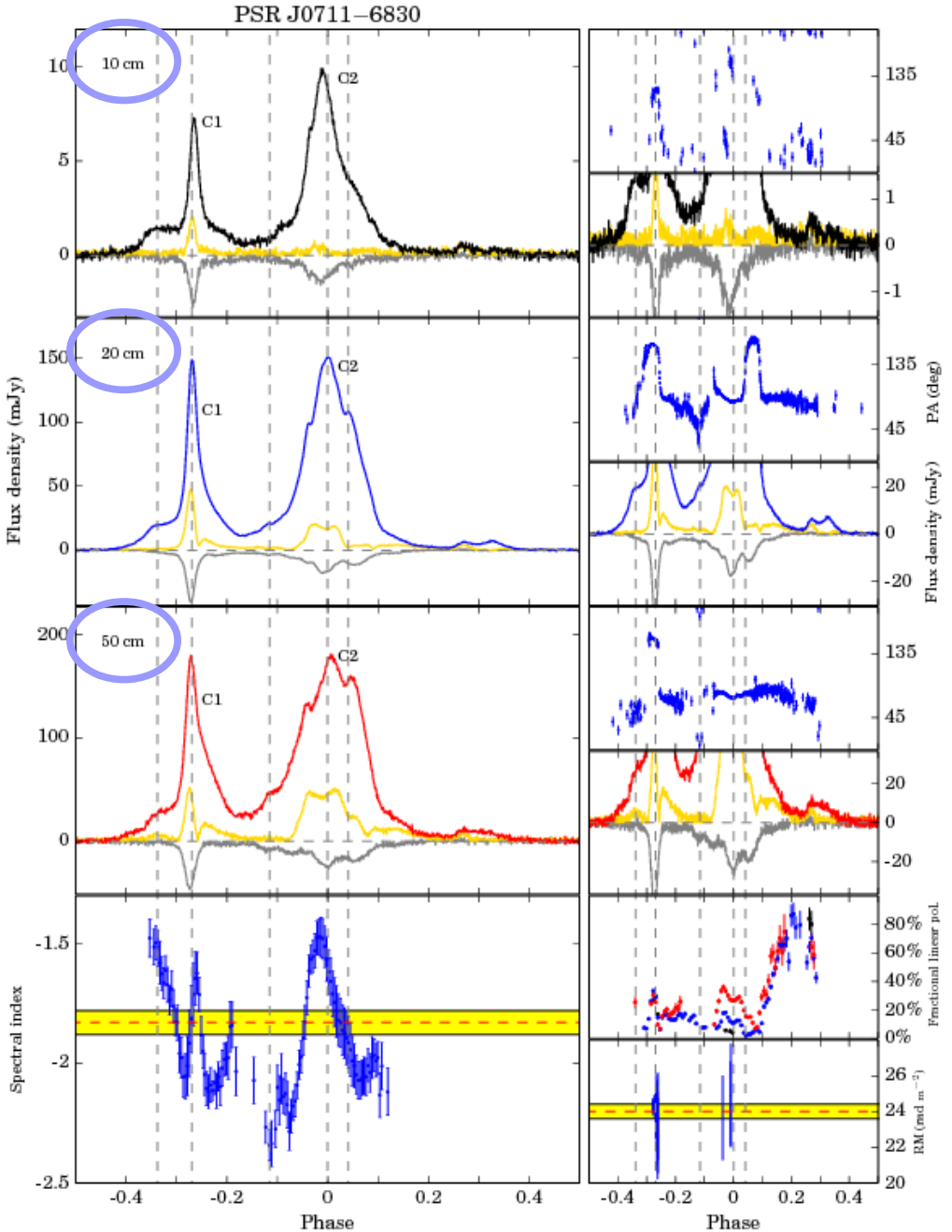

The black, blue and red lines indicate the total intensity profile in the three obsvering bands. The yellow and grey lines show linear and circular polarization respectively.

Pulsars: distribution of pulsars in the MW

Yellow points: known pulsars (as of 2012?)

Grey points: predicted distribution of pulsars, expected to be discovered by SKAs

Pulsars have been detected in the LMC and in globular clusters

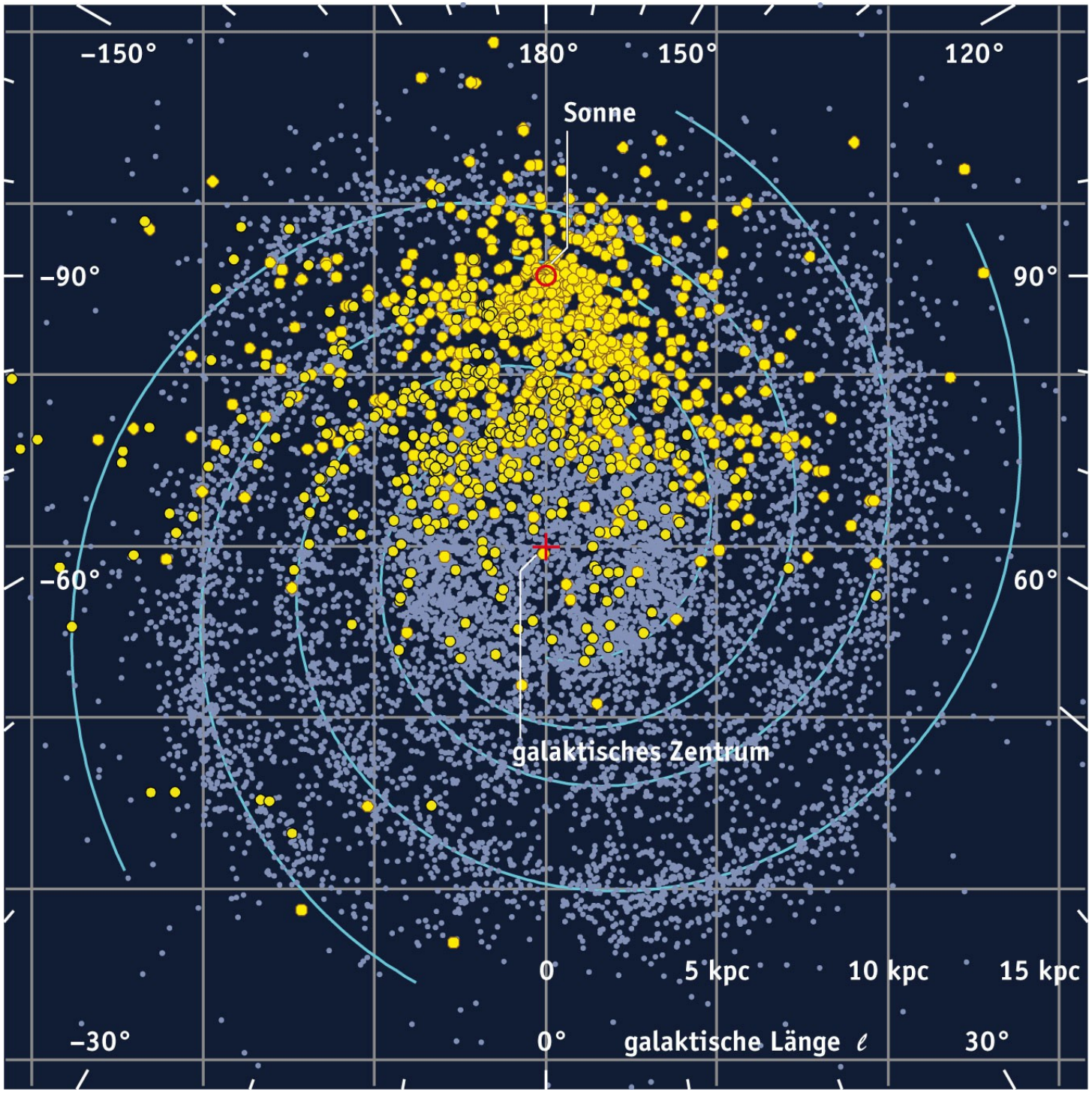

Pulsars: Gamma-ray detection

Last Updated: 2016 February 22 (# everything below this line is machine-generated

Summary Statistics Total number of pulsars: 205

Young, radio selected : 53

Young, gamma selected : 54

Young, X-ray selected : 5

Total number young PSRs : 112

MSP, radio selected : 92

MSP, gamma selected : 1

Total number of MSPs : 93

Total number of binaries : 73

Found in radio searches of LAT sources : 54

EGRET/COMPTEL pulsars: 7

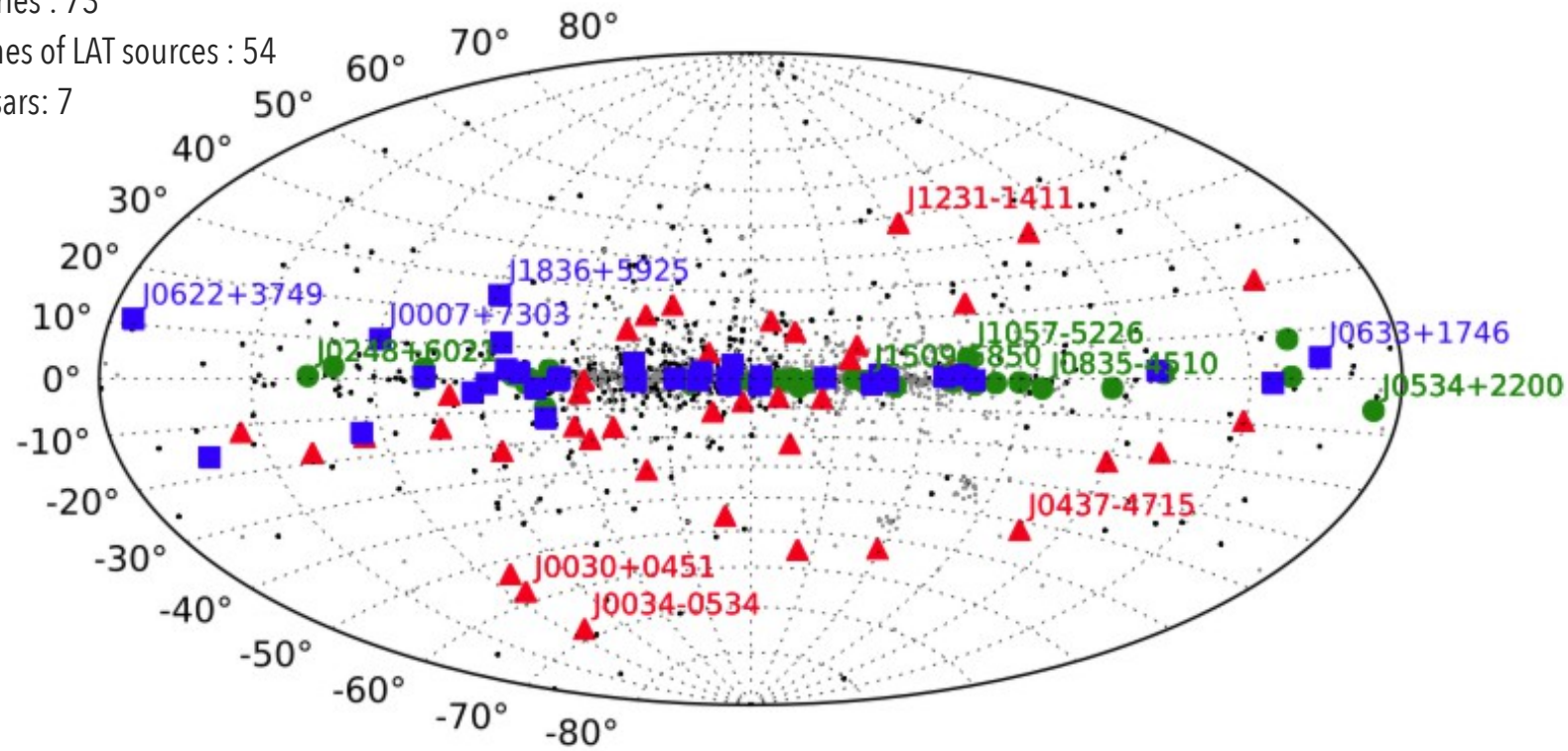

Skymap in Galactic coordinates showing the gamma-ray pulsars of different types detected by Fermi: Blue squares: radio quiet pulsars. Red triangles: millisecond gamma-ray pulsars. Green circles: radio loud gamma-ray pulsars. Black dots: Gamma-rays were phase-folded using a rotation ephemeris. Gray dots: Pulsars for which no rotation ephemeris was available. (Harding 2013, from Abdo, + 2013)

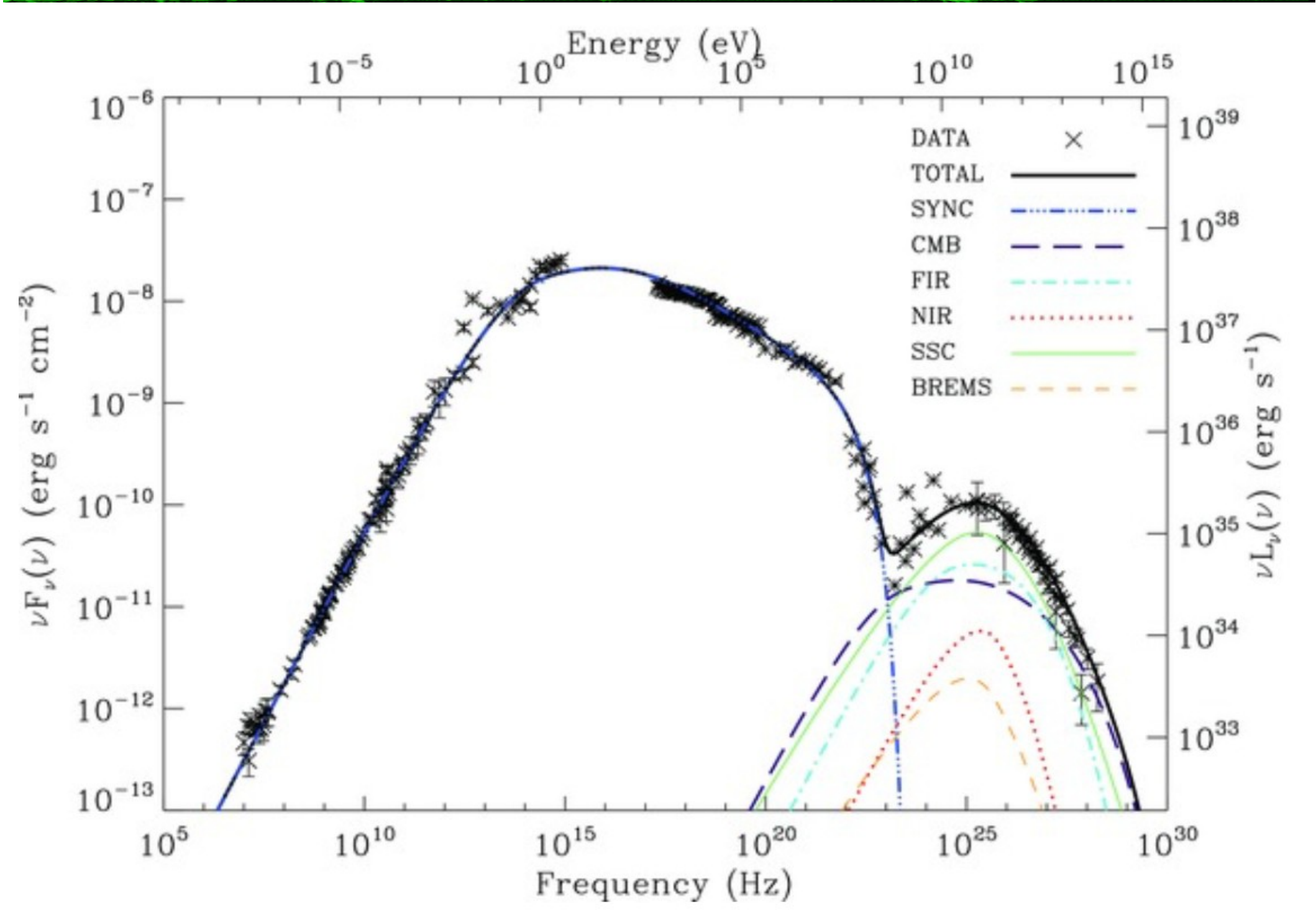
Energy (eV)
10^{-5}
10^{0}
10^{5}
10^{10}
10^{15}
DATA
TOTAL
SYNC
CMB
FIR
NIR
SSC
BREMS
$\nu F_\nu(\nu)$ (erg s^{-1} cm^{-2})
$\nu L_\nu(\nu)$ (erg s^{-1})
10^{-6}
10^{-7}
10^{-8}
10^{-9}
10^{-10}
10^{-11}
10^{-12}
10^{-13}
10^{39}
10^{38}
10^{37}
10^{36}
10^{35}
10^{34}
10^{33}
10^{5}
10^{10}
10^{15}
10^{20}
10^{25}
10^{30}
Frequency (Hz)

"The" pulsar diagram: Every pulsar is *slowly slowing down*

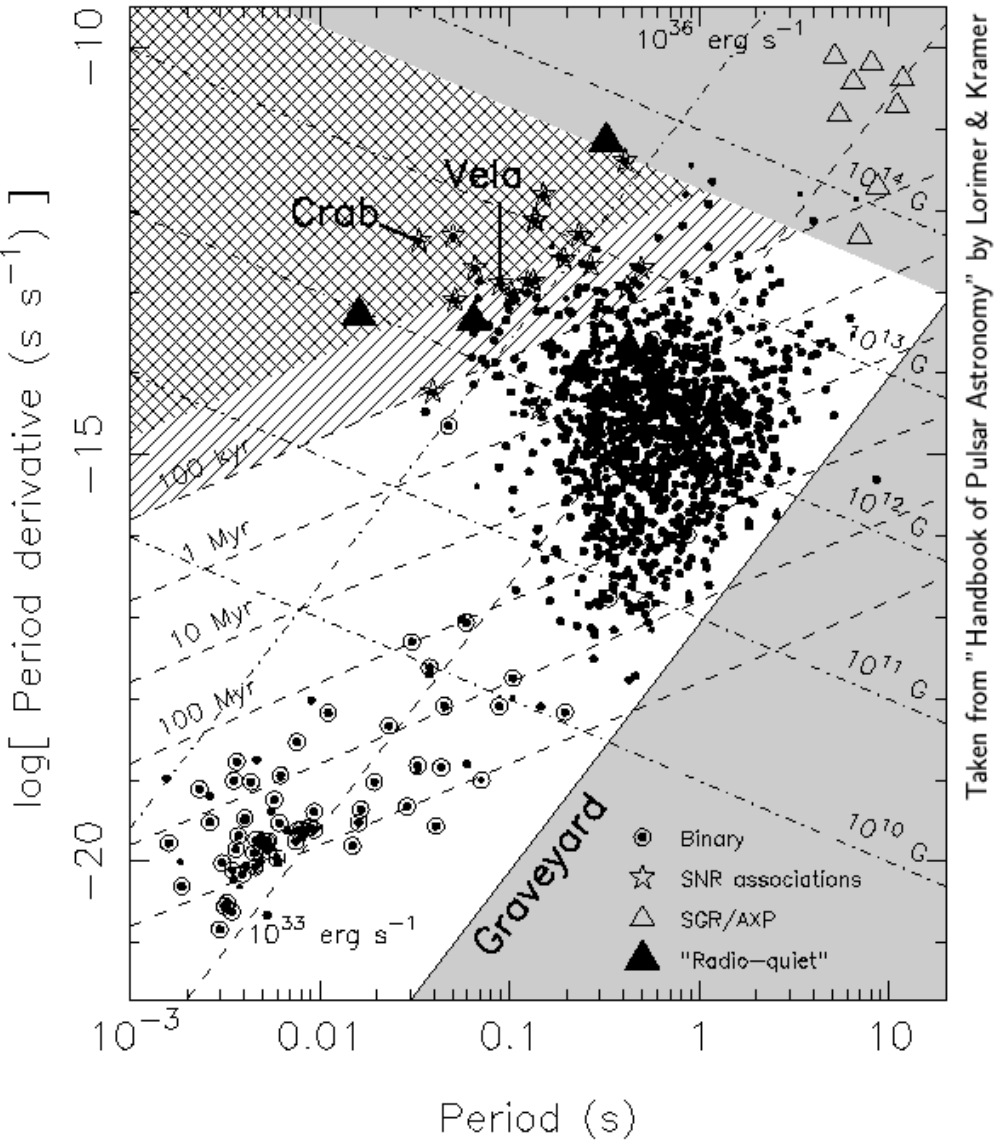

Magnetars

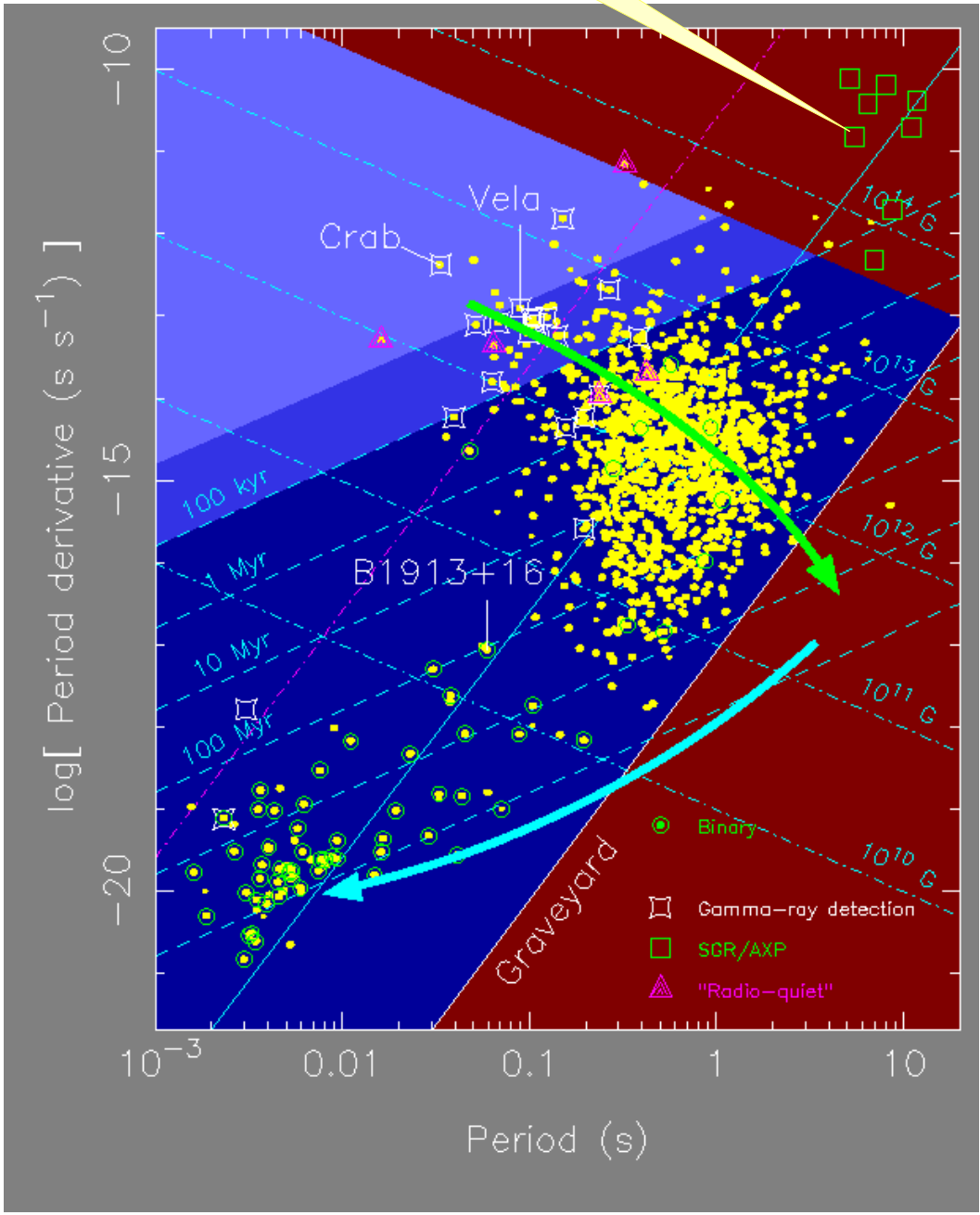

Magnetars:

- *NS with large magnetic fields (10^{14-15} G) in relatively slow rotation (P ~ 2 – 10 s)*

Such strong fields heavily distorts atomic structure

- *Strong bursts in the X-rays and soft γ-rays, interleaved with quiescent periods (SGR & AXP)*

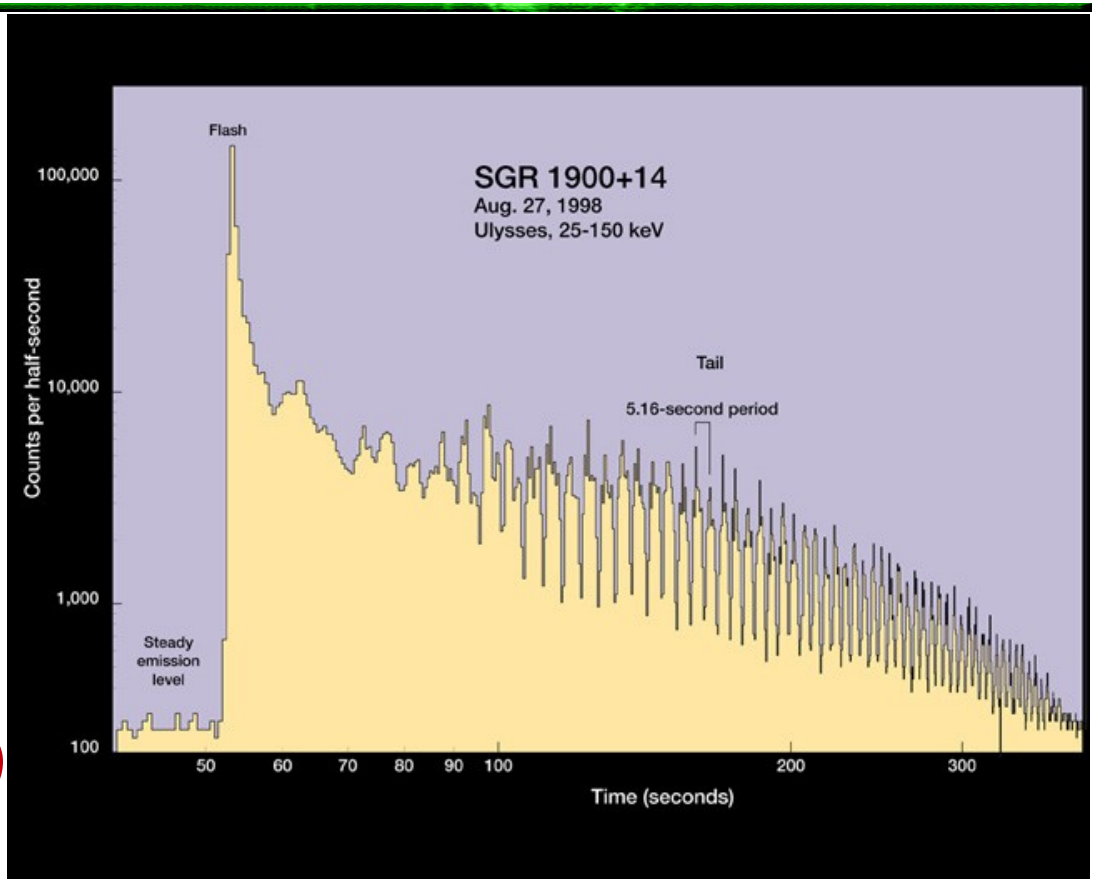

- *Energy from Magnetic field which decays rapidly, in about 10^4 yr ($dE/dt > [dE_{rot}/dt]$)*

- SGR bursts commonly last for only a small fraction of a second, although some last for several seconds.

Normal SGR bursts can radiate away as much energy in a single second as the Sun does in a year. ("normal" exclude the giant flares of March 5, 1979 and August 27, 1998 which were more than 1,000 times brighter.)

Pulsars: the lighthouse model (artist's view)

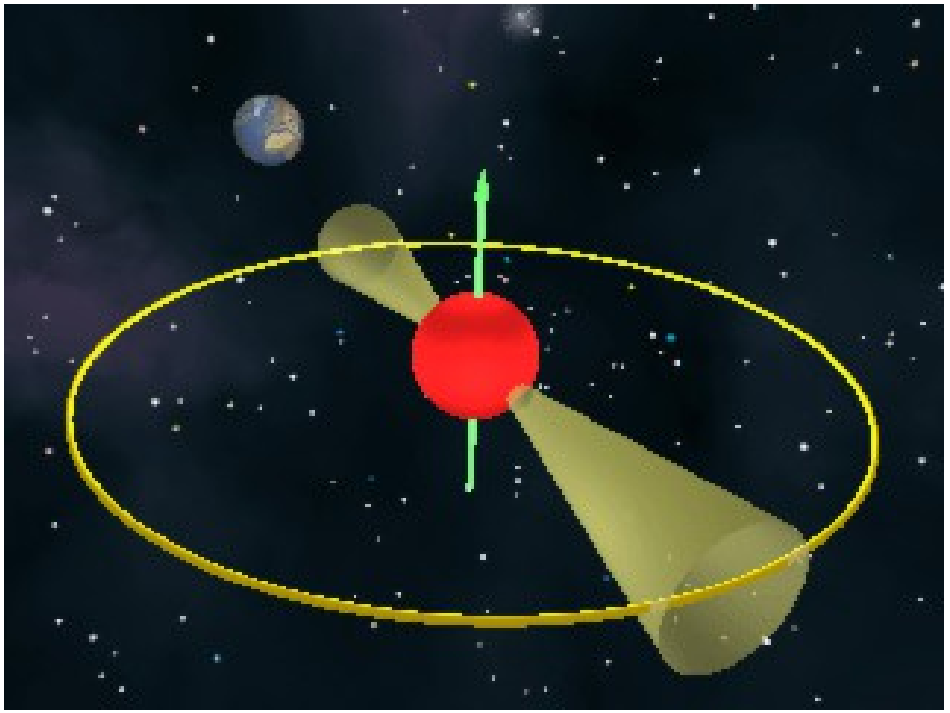

Name	P (sec)	(# turns in 1 sec)
PSR B0329+54	P=0.714519	1.4
PSR B0833-45=The Vela Pulsar	P=0.089	11
PSR B0531+21=The Crab Pulsar	P=0.033	30
PSR J0437-4715	P=0.0057	174
PSR B1937+21	P=0.00155780644887275	642
PSR J1748-2446	P=0.0013966	716

⟹ Listen to

http://www.jb.man.ac.uk/pulsar/Education/Sounds/

Pulsars: light cylinder, magnetosphere, et al.

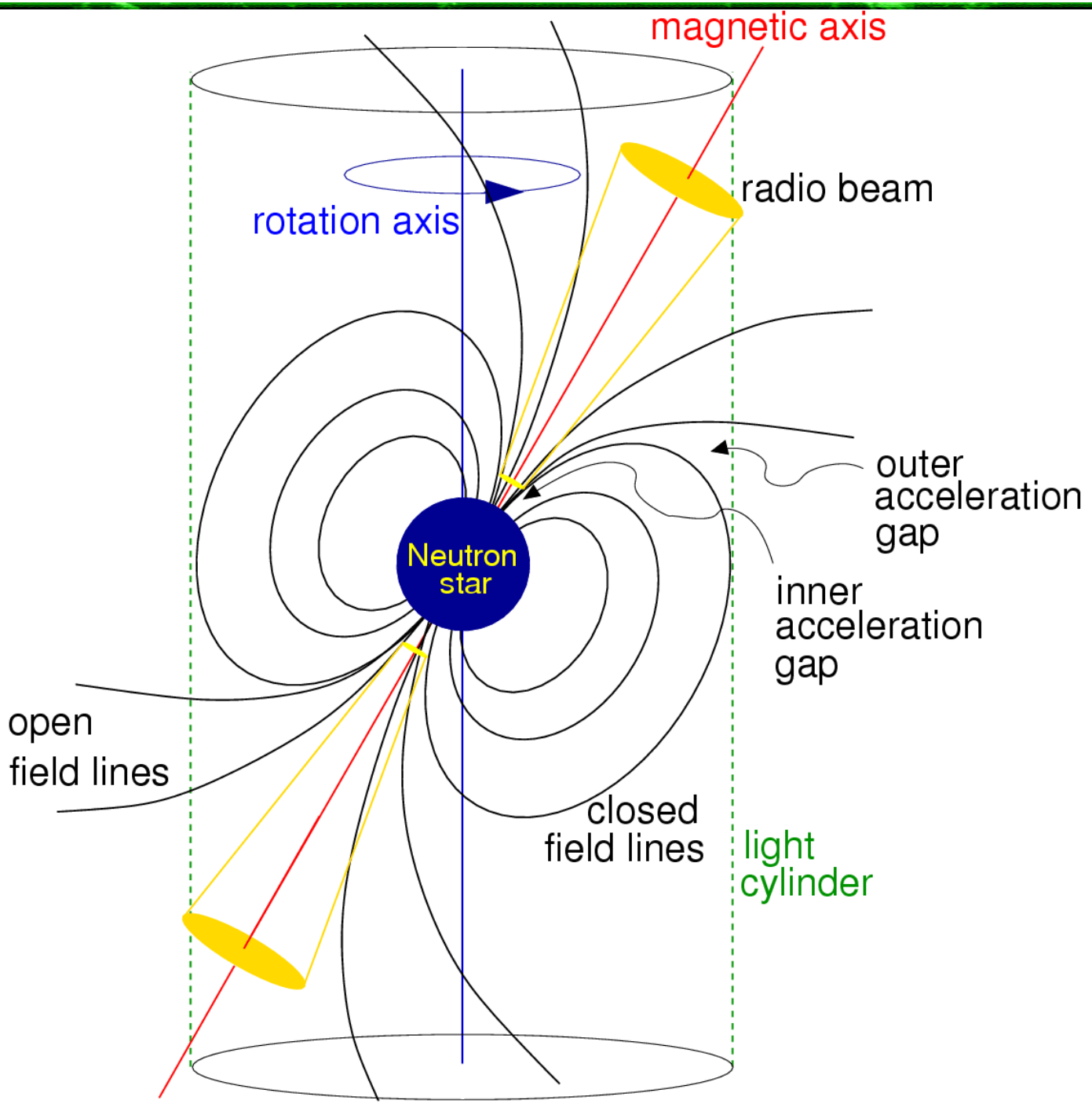

2 phenomenological models: (for inhomogeneous pulses)

- Core & (nested) cones
- Patchy beam

Best is a combination of the two like in the cartoon ⟹

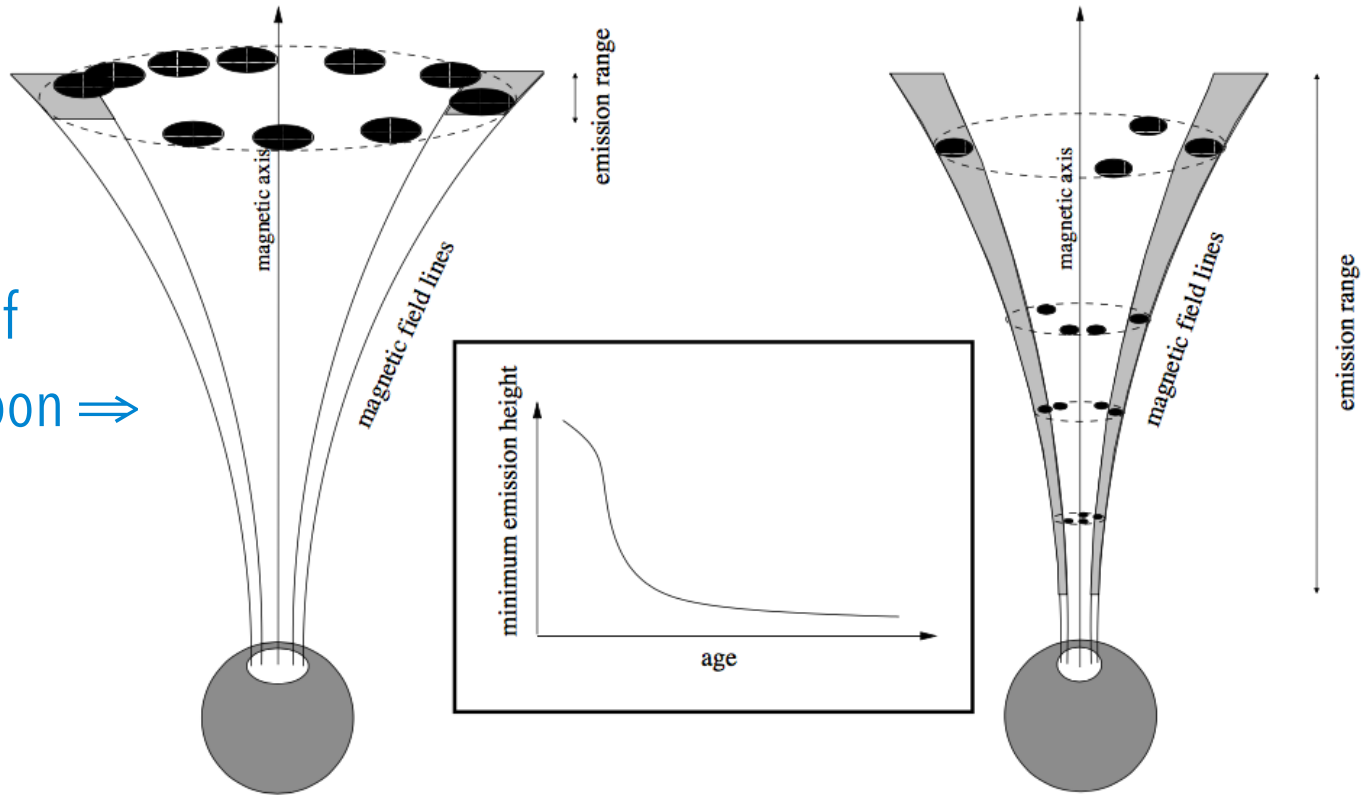

Figure 5: A recent phenomenological model for pulse shape morphology. The neutron star is depicted by the grey sphere and only a single magnetic pole is shown for clarity. Left: a young pulsar with emission from a patchy conal ring at high altitudes from the surface of the neutron star. Right: an older pulsar in which emission emanates from a series of patchy rings over a range of altitudes. Centre: schematic representation of the change in emission height with pulsar age. Figure designed by Aris Karastergiou and Simon Johnston [179].

Facts:

- Associated to neutron stars (near/within SNR in relatively young objects)
- Stable period (~1 ms to a few s) and its derivative (and second derivative)
- P and $\dot{P}$ are grossly correlated
- Individual pulses are different, average profile is characteristic of each pulsar
- Variable (circular and linear) polarization and spectral index during pulse
- Very steep radio spectra
- Brightness temperatures far too high for incoherent radiation ($> 10^{25}\,^{o}K$)

Models:

- Pacini (1967): a NS with a strong magnetic field whose axis is not aligned with the rotation axis emits a lot of energy in the form of electromagnetic waves extracting kinetic energy from the rotation of the NS: $\nu = \nu_{rot}$
- Goldreich & Julian (1969): Unipolar Machine
- Ruderman & Sutherland (1975)

Franco Pacini (1939-2012)

Peter Goldreich (1939)

- Pacini (1967): a NS with a strong magnetic field whose axis is not aligned with the rotation axis emits a lot of energy in the form of electromagnetic waves extracting kinetic energy from the rotation of the NS. $\nu = \nu_{rot}$

Radiated power by a magnetic dipole $\vec{m}$ whose rotation axis is displaced by an angle α wrt the magnetic axis

$$-\left(\frac{dE}{dt}\right) = \frac{2}{3}\frac{1}{c^3}\left(\frac{d^2\vec{m}}{dt^2}\right) = \frac{2}{3c^3}\,\omega_{NS}^4\,(\vec{m}\sin\alpha)^2$$

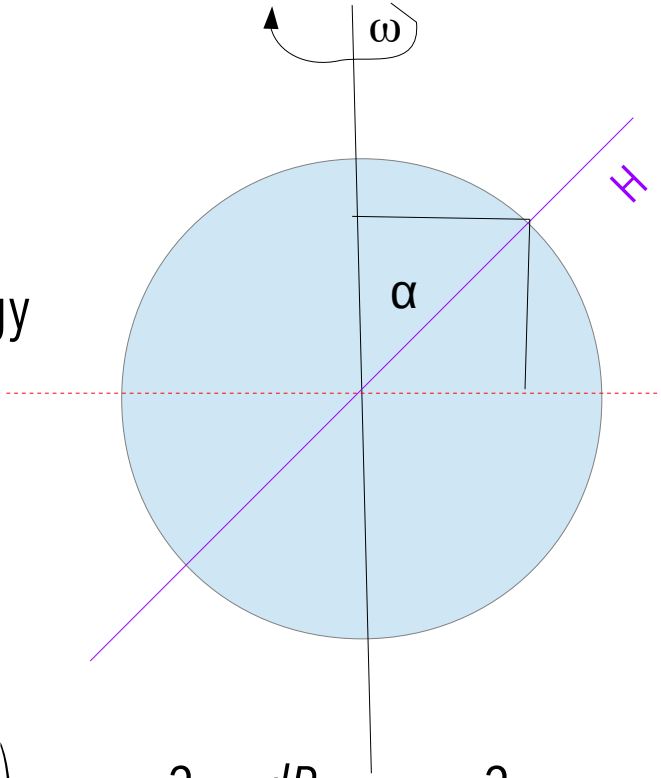

the emitted power is at expenses of the rotational kinetic energy

$$-\left(\frac{dK_{NS}}{dt}\right) = -I_{NS}\,\omega_{NS}\,\dot{\omega}_{NS}$$

$$\dot{\omega}_{NS} = -\frac{2}{3c^3}\,\omega_{NS}^3\,\frac{(\vec{m}\sin\alpha)^2}{I_{NS}}$$

$$\omega_{NS} = 2\pi\nu_{NS} = \frac{2\pi}{P} \rightarrow \dot{\omega}_{NS} = \frac{d\,\omega_{NS}}{dt} = \frac{d}{dt}\left(\frac{2\pi}{P}\right) = -\frac{2\pi}{P^2}\frac{dP}{dt} = -\frac{2\pi}{P^2}\dot{P}$$

If H_{NS} is the field on the NS surface

$$\vec{m} \sim H_{NS} R_{NS}^3 \quad \text{and assuming } \alpha = 90^o \quad \text{we have}$$

$$\dot{\omega}_{NS} = -\frac{2}{3c^3}\,\omega_{NS}^3\,\frac{(H_{NS}^2 R_{NS}^6)}{I_{NS}} \quad \rightarrow \quad \textit{namely} \quad \rightarrow \quad P\dot{P} = \frac{8\pi^2}{3c^3}\,\frac{(H_{NS}^2 R_{NS}^6)}{I_{NS}}$$

P and $\dot{P}$ are measured with high precision, once I_{NS} is assumed, then

$$H_{NS} = \left(\frac{3c^3}{8\pi^2}\,\frac{I_{NS}}{R_{NS}^6}\,P\dot{P}\right)^{1/2} \simeq (10^{39} P\dot{P})^{1/2} = 3.2\cdot 10^{19}(P\dot{P})^{1/2} = 10^{12}\left(\frac{P}{s}\right)^{1/2}\left(\frac{\dot{P}}{10^{-15}}\right)^{1/2}[G]$$

$$\text{where } I_{NS} = \frac{2}{5} M_{NS} R_{NS}^2$$

In case of a non-homogeneous sphere $I_{NS} = k\,M_{NS} R_{NS}^2$ with $k \in [0.2, 0.45]$

In case $M_{NS} = 1.4\,M\odot$, $R_{NS} = 10\,km$ and $k = 0.4$, then $I_{NS} \approx 10^{45}\,erg\,cm^2$

$$-\left(\frac{dK_{NS}}{dt}\right) = -I_{NS}\,\omega_{NS}\,\dot{\omega}_{NS} \approx 10^{30}-10^{33}\,erg\,s^{-1} \qquad \text{(in most cases)}$$

In general it is 2 -- 4 orders of magnitude larger than the total (radio) luminosity

Crab has a $-\left(\frac{dK_{NS}}{dt}\right) = 5\cdot10^{38}\,erg\,s^{-1}$

while the total luminosity from radio to γ rays is $L \approx 10^{38}\,erg\,s^{-1}$

Most of the energy is carried away in an invisible form except for plerions

η_ν is the efficiency of conversion from kinetic energy to radiation as a function of frequency:

$$\eta_\nu = \frac{L_\nu}{(dK_{NS}/dt)}$$

In the X and γ rays, η_ν is larger than in the radio band

$$\dot{\omega}_{NS} = -\frac{2}{3c^3}\,\omega_{NS}^3\,\frac{(\vec{m}\sin\alpha)^2}{I_{NS}} \quad \rightarrow \textit{namely} \rightarrow \quad P\dot{P} = \frac{8\pi^2}{3c^3}\,\frac{(\vec{m}\sin\alpha)^2}{I_{NS}}$$

→ which can be used to determine the characteristic age of the pulsar

The relationship $\dot{\omega} \sim \omega^n$ provides information on the mechanism which slows down the rotation of the NS.

n is known as braking index.

In case of dipole radiation n=3, while n=5 for quadrupole (both magnetic and gravitational)

Table 1: Pulsars with observed braking index.

Ho & Andersson, 2012, Nature Physics, 8, 787

Pulsar name	Supernova remnant	Period (s)	Period derivative (s s^{-1})	Characteristic age τ_c (yr)	Braking index n	Age (yr)
B0531+21	Crab	0.0331	4.23×10^{-13}	1,240	2.51(1) (ref. 4)	958
J0537−6910	N157B	0.0161	5.18×10^{-14}	4,930	−1.5(1) (ref. 20)	$2{,}000_{-1{,}000}^{+3{,}000}$ (ref. 21)
B0540−69	0540−69.3	0.0505	4.79×10^{-13}	1,670	2.140(9) (ref. 22)	$1{,}000_{-240}^{+660}$ (ref. 23)
B0833−45	Vela	0.0893	1.25×10^{-13}	11,300	1.4(2) (ref. 24)	$11{,}000_{-5{,}600}^{+5{,}000}$ (ref. 25)
J1119−6127	G292.2−0.5	0.408	4.02×10^{-12}	1,610	2.684(2) (ref. 26)	$7{,}100_{-2{,}900}^{+500}$ (ref. 27)
B1509−58	G320.4−1.2	0.151	1.54×10^{-12}	1,550	2.839(3) (ref. 22)	<21,000 (ref. 28)
J1846−0258	Kesteven 75	0.325	7.08×10^{-12}	729	2.65(1) (ref. 22)	$1{,}000_{-100}^{+3{,}300}$ (ref. 29)
J1734−3333	G354.8−0.8	1.17	2.28×10^{-12}	8,120	0.9(2) (ref. 3)	>1,300

The periods and period derivatives are taken from ref. 19. The numbers in parentheses show the braking index uncertainty in the last digit. For J1734−3333, we give a lower limit of the age, which we estimate by considering the supernova remnant size (21 parsecs; ref. 30) and remnant expansion velocity v_{SNR}, to obtain an age ~2,000 yr ($10^4 km s^{-1}/v_{SNR}$); and considering the pulsar's distance away from the centre of the supernova remnant (46 parsecs; ref. 30) and pulsar space velocity v_{pulsar}, to obtain an age ~23,000 yr ($2{,}000 km s^{-1}/v_{pulsar}$).

Let's derive $\dot{\omega} \sim \omega^n \rightarrow \ddot{\omega} = n\,\omega^{n-1}\dot{\omega}$ from which we have

$$n = \frac{\ddot{\omega}}{\omega^{n-1}\dot{\omega}} \quad \text{but} \quad \omega^{n-1} = \frac{\omega^n}{\omega} = \frac{\dot{\omega}}{\omega} \quad \text{and then} \quad n = \frac{\omega\,\ddot{\omega}}{\dot{\omega}^2} = 2 - \frac{P\,\ddot{P}}{\dot{P}^2}$$

In case $n \neq 3$, beyond e-m wave emission, other processes may influence $\dot{P}$ and $\ddot{P}$

a (relativistic) stellar wind (PWN)

an accretion disk made of debris of the explosion

instabilities of the internal structure (glitches)

A braking index different from 3 can be easily explained, but due to the degeneracy of the parameters, little information can be obtained

From the period and its derivative, it is possible to determine a characteristic age: τ_c

$$\dot{P} = \frac{dP}{dt} = a P^{-1}$$

$$\int_{P_o}^{P} P\, dP = a \int_{o}^{\tau_c} dt$$

$$\frac{P^2}{2} - \frac{P_o^2}{2} = a\,\tau_c$$

To be taken with care...

$$\tau_c \simeq \frac{P^2}{2a} \simeq \frac{P}{2\dot{P}}$$

Max rotation rate, aka minimum rotation period

$$\omega_{NS}^2 R_{NS} = \frac{4\pi^2}{P^2} R_{NS} \leq \frac{GM_{NS}}{R_{NS}^2}$$

$$P \geq \sqrt{\frac{4\pi^2 R_{NS}^3}{GM_{NS}}} \simeq \frac{3}{\sqrt{G\rho_{NS}}}$$

Pulsar models: oblique rotator

The e-m wave originated by rotation can accelerate particles out of the light cylinder at very high energies

e- and nuclei: which origin?

from SN explosion?

emitted from the NS itself?

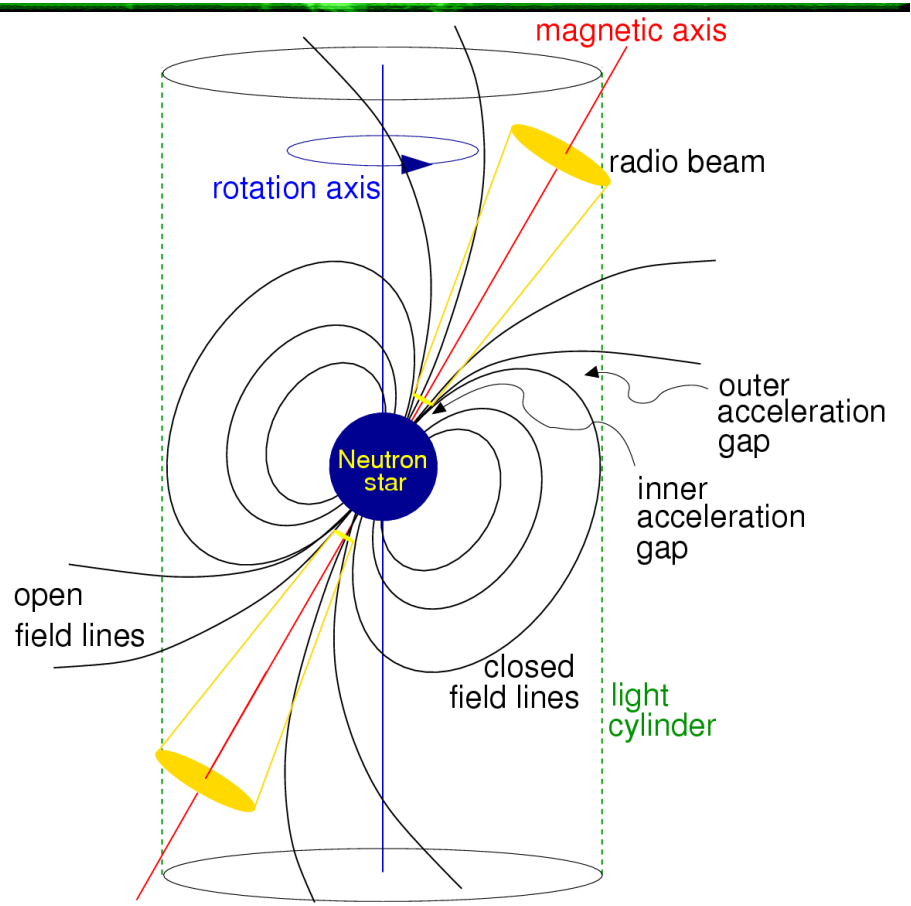

Let's consider a pulsar with P = 1 s (rotates at $\nu = 1$ Hz) and emits radiation with $\lambda = c/\nu \sim 3 \cdot 10^{10} cm$

At a given distance (e.g. λ) the energy flux of the emitted e-m wave is = (rotational) kinetic energy loss, and we can infer the value of the $\vec{E}$ field (the whole loss is converted into e-m wave energy flux)

$$4\pi\lambda^2 \cdot \frac{|\vec{E}'|^2}{8\pi} \cdot c \approx -\left(\frac{dK_{NS}}{dt}\right)$$

Summary of **Goldreich & Julian 1969:**

$\vec{\omega}_{NS}$ and $\vec{H}$ are aligned: (very unlikely, but maths much simpler)

E-m effects extract charges from NS surface and then they are trapped into the magnetosphere.

NS interior:

rotation and Lorentz force generate a $\vec{E}$ field which separate charges:

Positive (negative) charges are at the poles and negative (positive) at the equator depending on $\vec{\omega}_{NS} \cdot \vec{H}$ being < 0 (>0).

NS exterior:

Quadrupole potential, except to the equator, a E component parallel to H exists (max at the poles)

This field largely exceeds gravity and can extract charges from the NS surface

=> the space around the NS is not empty but filled by the magnetopshere co-rotating with the NS

up to a cylindric surface (light cylinder) $R_{LC}\,\omega_{NS} = c \quad \rightarrow \quad R_{LC} = 5 \cdot 10^9 \dfrac{P}{sec} \; [cm]$

θ_p $\rightarrow$ open field lines, cross the light cylinder but cannot co-rotate

$\rightarrow$ $\vec{H}$: spiral structure is seen in the polar view

Goldreich & Julian 1969

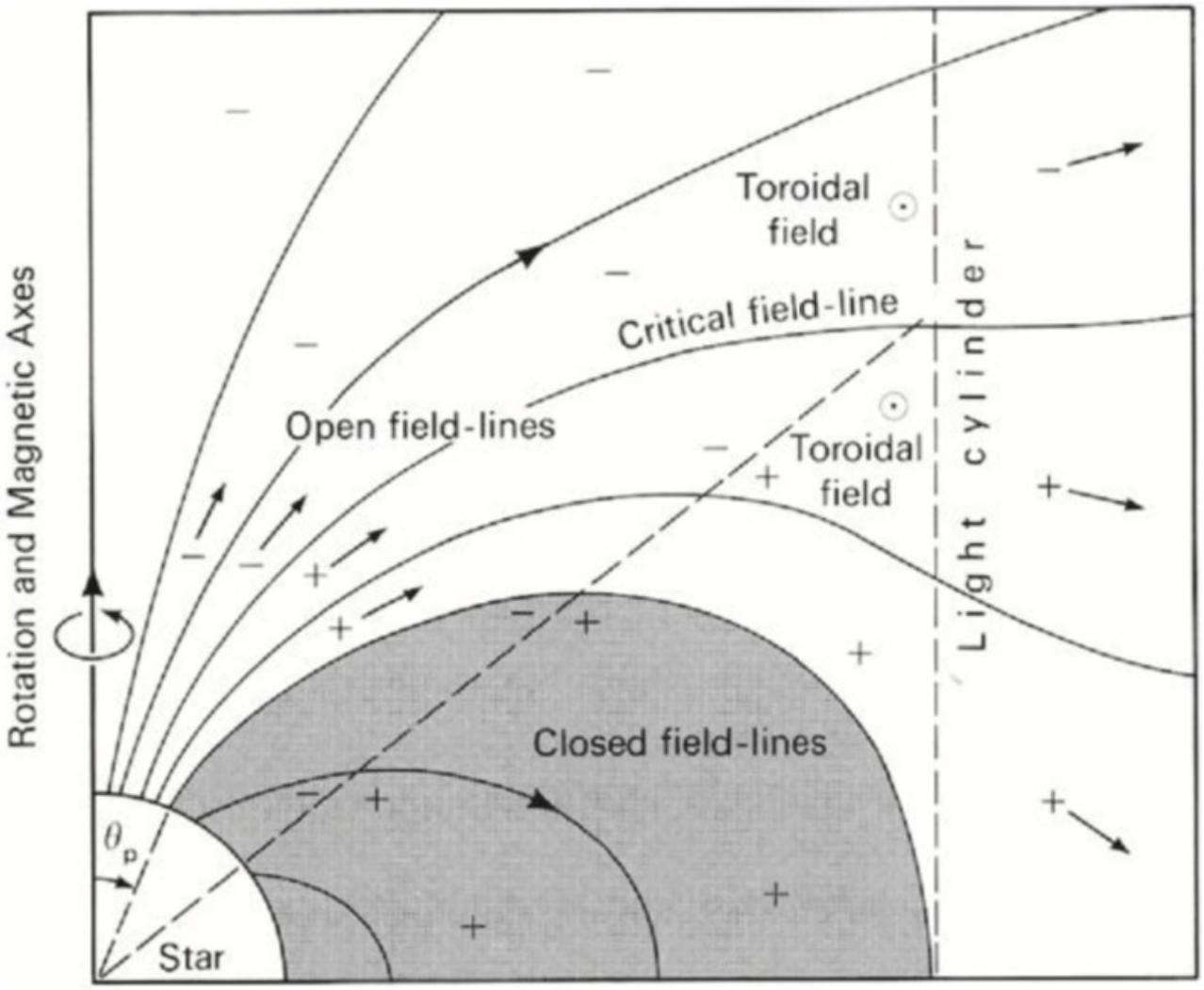

θ_p

The magnetic and electric field lines in the magnetosphere have a complex distribution: The induced local electric field from the rotating (i.e. variable) B field is "neutralized" by the flow of charges in the plasma and locally may be 0

Pulsars: polar view of the field lines

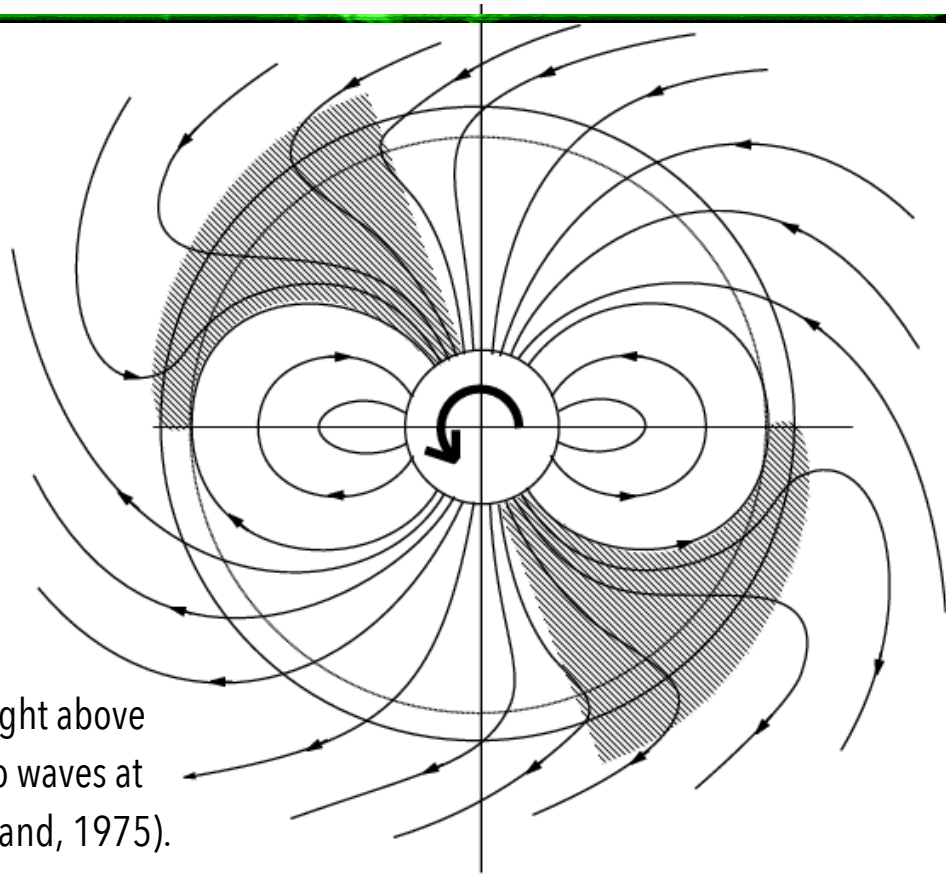

The frequency of the radiation which is produced in a zone depends on the height above The neutron star's surface: Ä and X rays are produced close to the surface, radio waves at greater heights, where the density is lower (adapted after Ruderman & Sutherland, 1975).

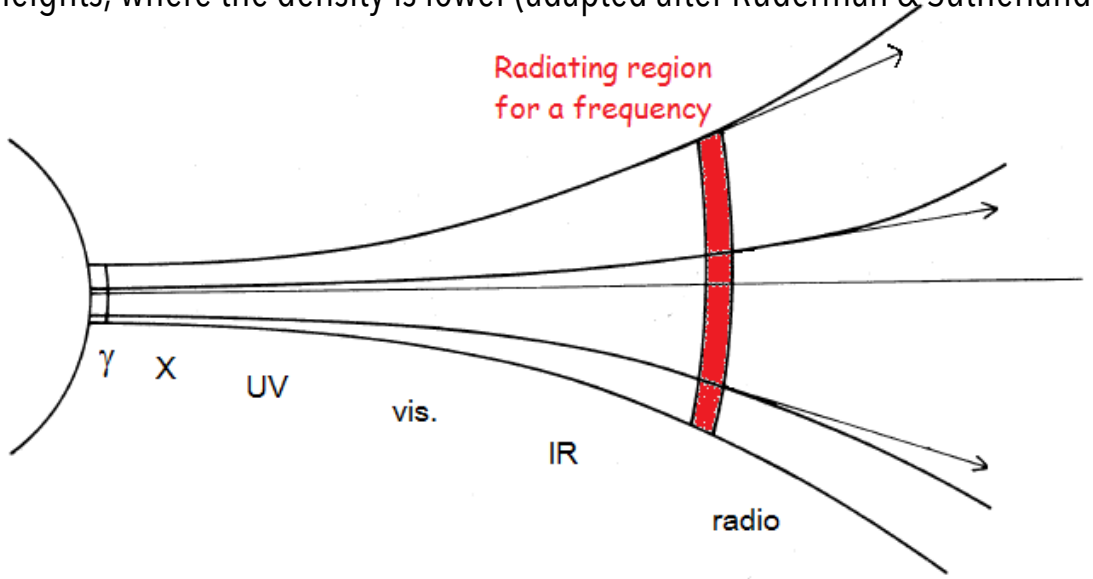

The opening angle of the beam
Is frequency dependent

Model with ω || H

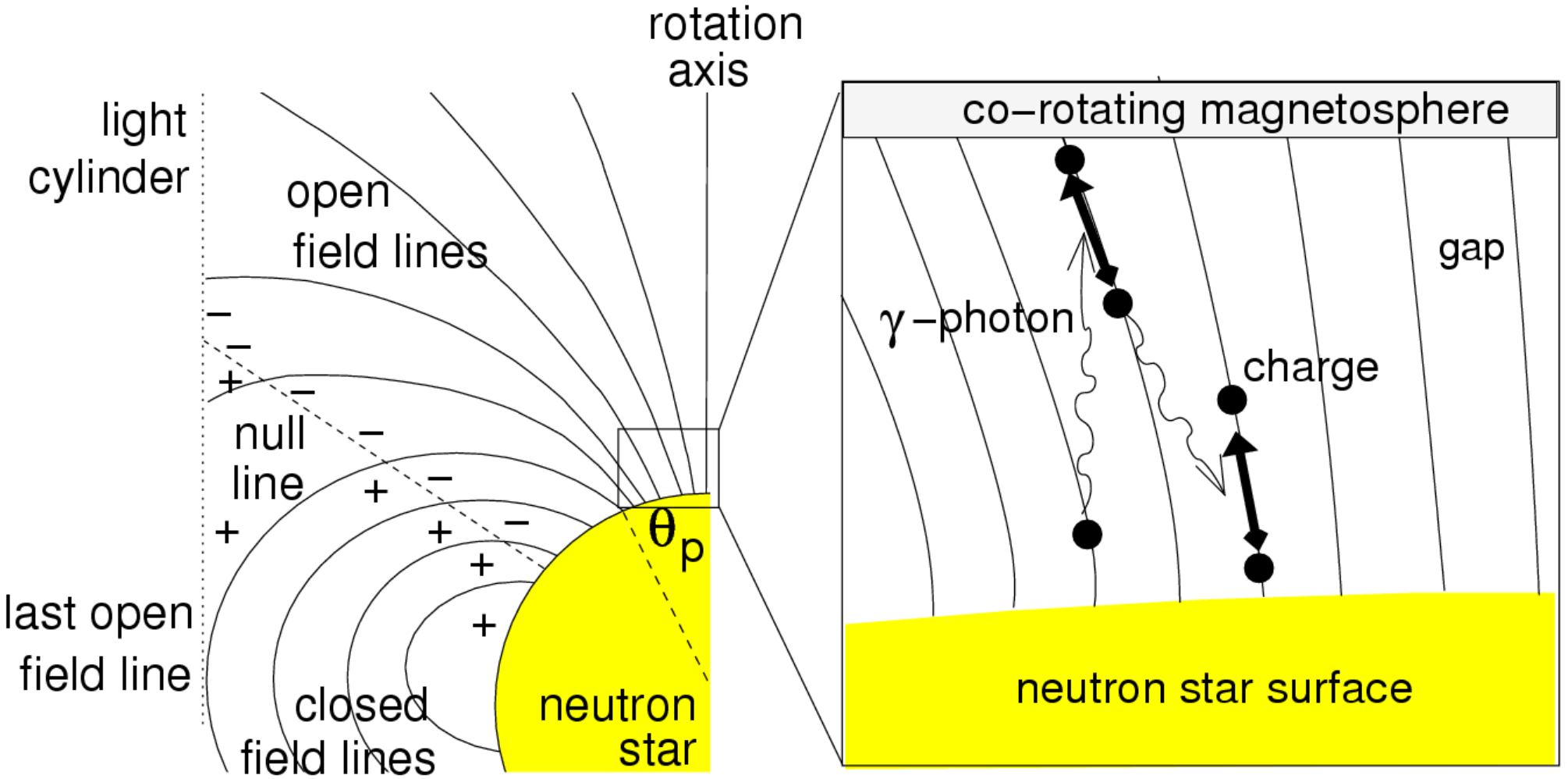

How to get θ_p:

$$\frac{\sin^2\theta_p}{R_{NS}} = \frac{\sin^2(90^o)}{R_{LC}}$$

$$\sin^2\theta_p = \frac{R_{NS}}{R_{LC}} = \frac{R_{NS}\,\omega_{NS}}{c} = \frac{2\pi}{c}\frac{R_{NS}}{P} = 2\cdot 10^{-4}\left(\frac{P}{sec}\right)^{-1}$$

Pulsars: Input to models and a sample output of a numerical simulation (taken from Cerutti's presentation)

The light cylinder

The light cylinder radius defines the location where the co-rotation velocity equals the speed of light: $R_{LC}\Omega=c$ (~5000km for a 100ms pulsar)

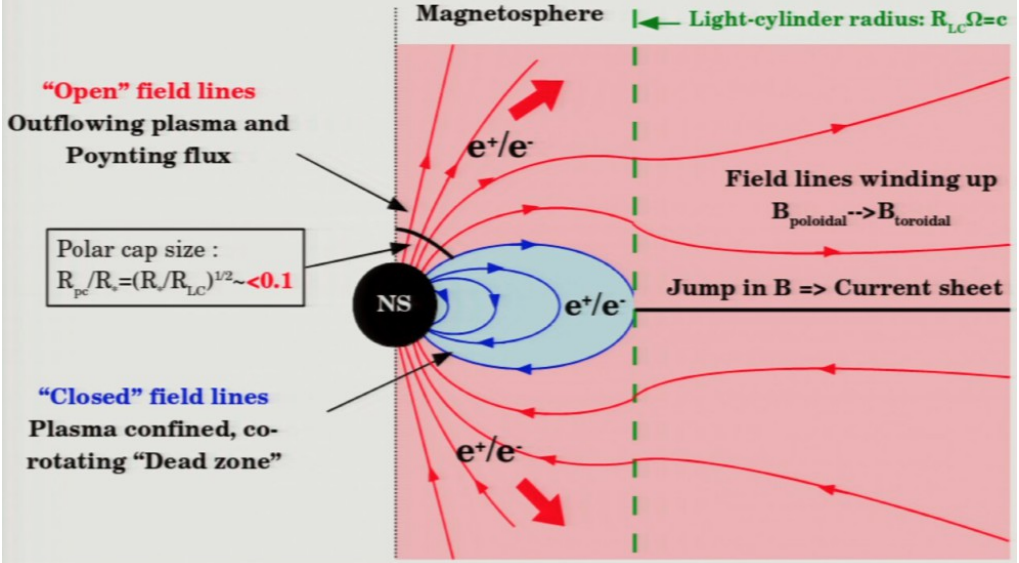

...but vacuum is not a good approximation

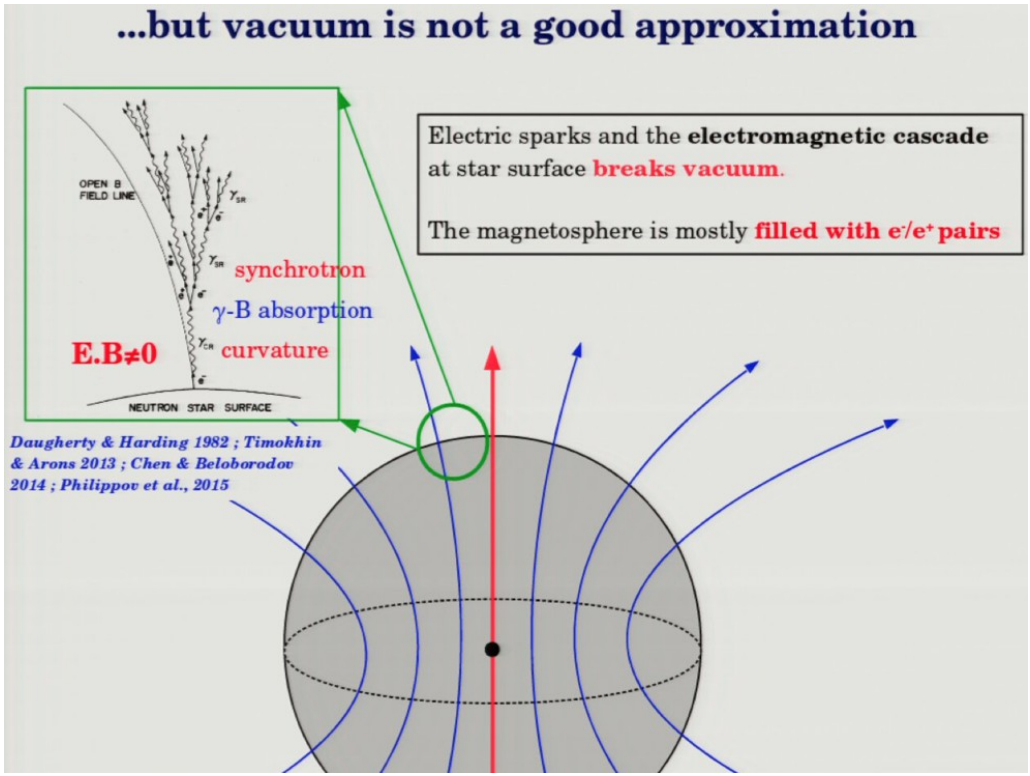

Particle / radiation mean energy (χ=30°)

Cerutti et al. 2016

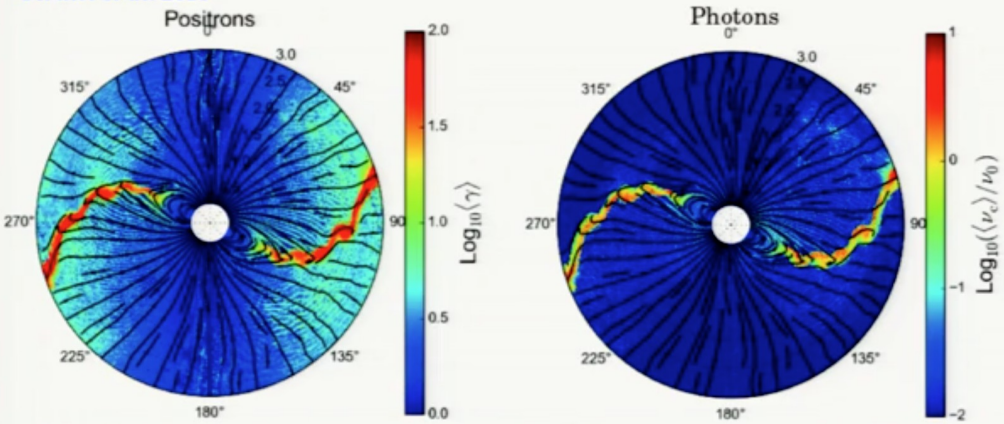

Relativistic reconnection

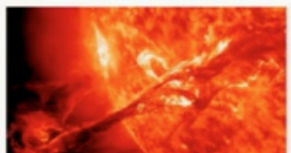

Mostly synchrotron radiation

Ruderman & Sutherland (1975)

Proton extraction from NS is not effective, while electrons would be allowed to leave NS would be progressively charged while it must be neutral

Critical line of the magnetosphere detached from the surface (gap), a small region charge free

Electrons (positrons) necessary to do the "work", are not extracted from the NS

- External γ – rays inteacting with the H field turn into pairs (e+/e-).
- Out of the polar gap they produce high energy curvature radiation, i.e. new γ – rays …
- Infalling charges null (reduce) the E field quenching (reducing) the process/polar gap
- > inhomogeneous pulses

- conditions:

(e+/e-) must reach high energies to produce γ – rays: formula ?

Free mean path of γ – rays smaller that the H scale length: formula ?

Pulsars: Polar & Outer Gaps (to explain pulsars visibile in the Ä – rays only)

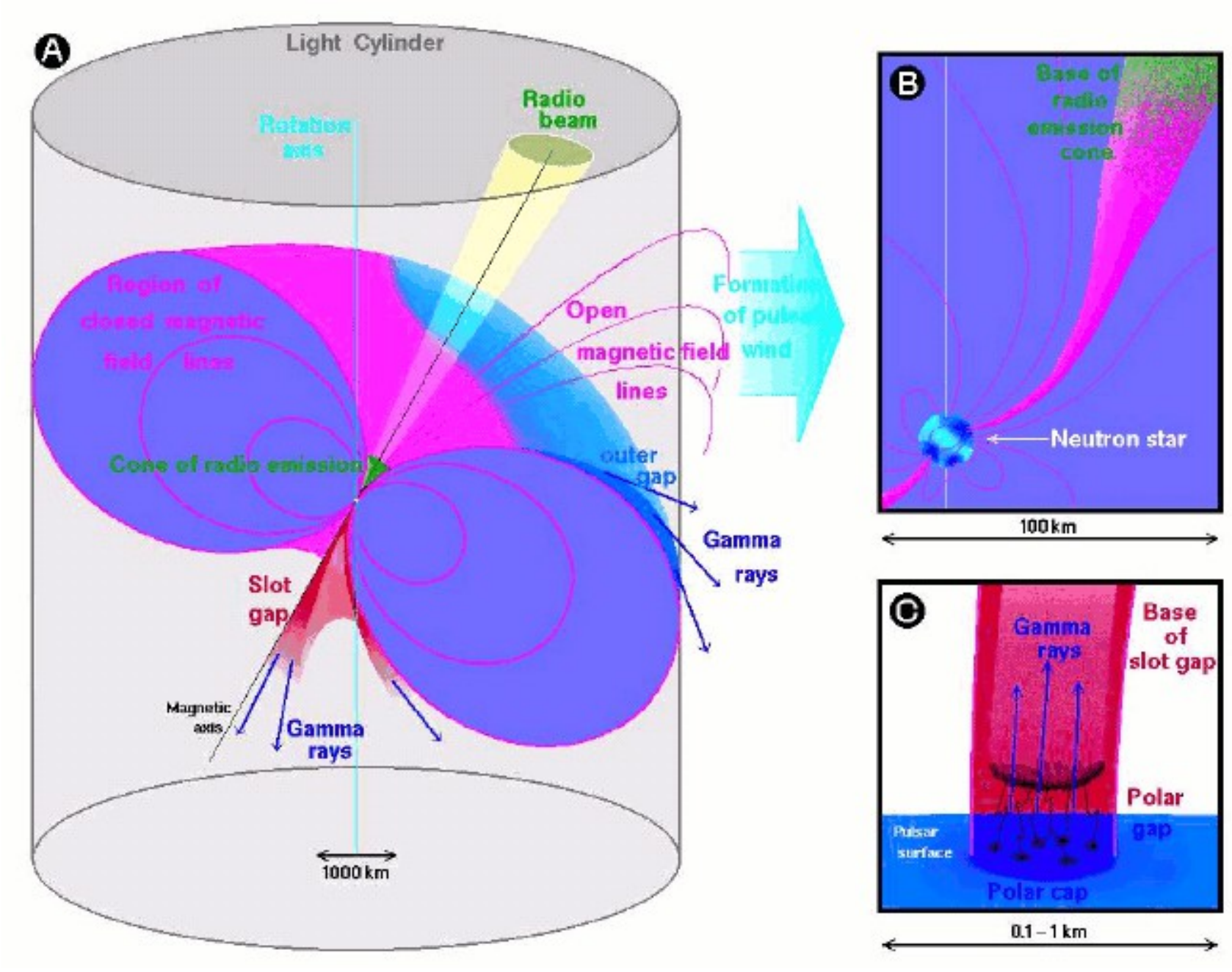

Pulsar Wind Nebulae *(Plerions but it is not the whole story)*

Pulsar wind nebulae main properties:

- Increasing brightness towards the center, without a shell-like structure as seen in most other supernova remnants.
- Highly polarized flux, flat spix in the radio band, á =0–0.3.
- Spix steepens at X-ray energies due to synchrotron radiation losses and on the average has an X-ray photon index of 1.3–2.3
- (spectral index of 2.3–3.3).

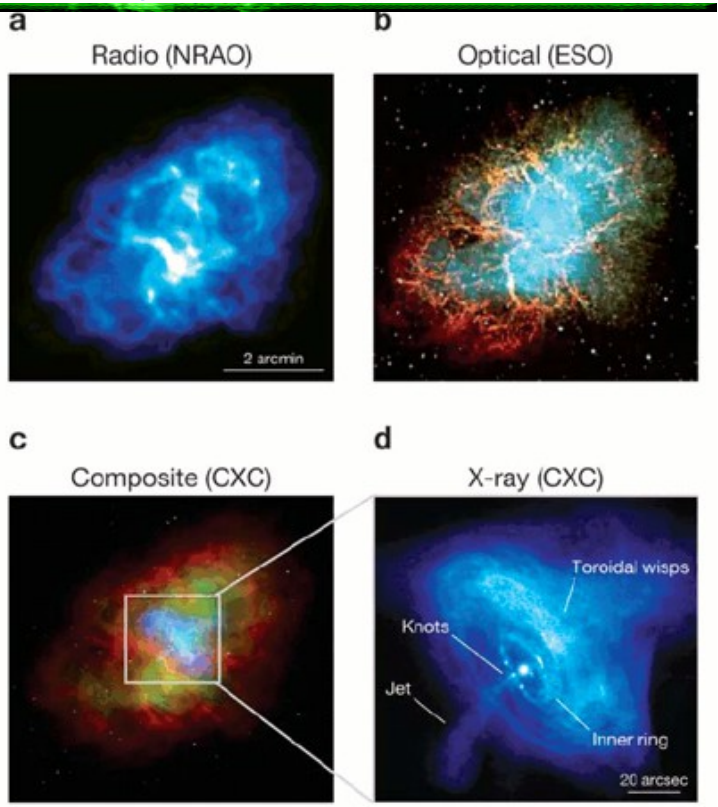

- An X-ray size that is generally smaller than their radio and optical size (shorter synchrotron lifetimes of the higher-energy electrons)
- A photon index at TeV gamma-ray energies of ~2.3.

PWN probes of a pulsar/neutron star's interaction with its surroundings.

They can be used to infer the geometry, energetics, and composition of the pulsar wind, the space velocity of the pulsar itself, and the properties of the ambient medium.

Pulsars in binary systems

Orbiting pulsars in binary systems have P (and $\dot{P}$) affected by "acceleration" arising from the Doppler shift induced by the orbital motion. In case of a constant a (which is not!) during an integration time T,

the pulsation is shifted by $\frac{aT}{Pc}$

Acceleration is largest for massive and close system (short orbital period, < 1 day).

Knowing the orbital period, the variable shift can be compensated and corrected

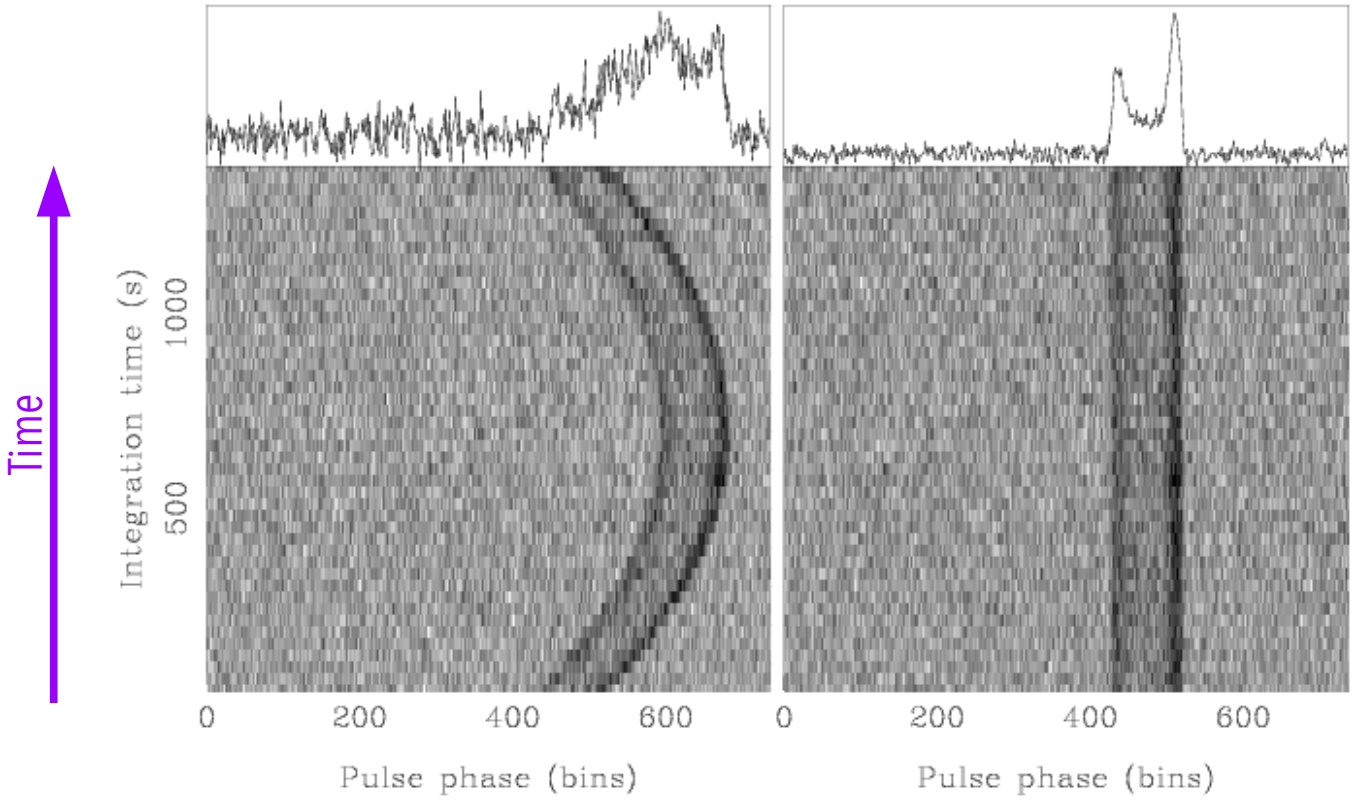

Left: 22.5 observation of the binary pulsar B1913+16 with Arecibo. A constant period has been assumed. Right: acceleration search applied, recovering the pulse shape and improving the S/N

Pulsars in binary systems

Formation:

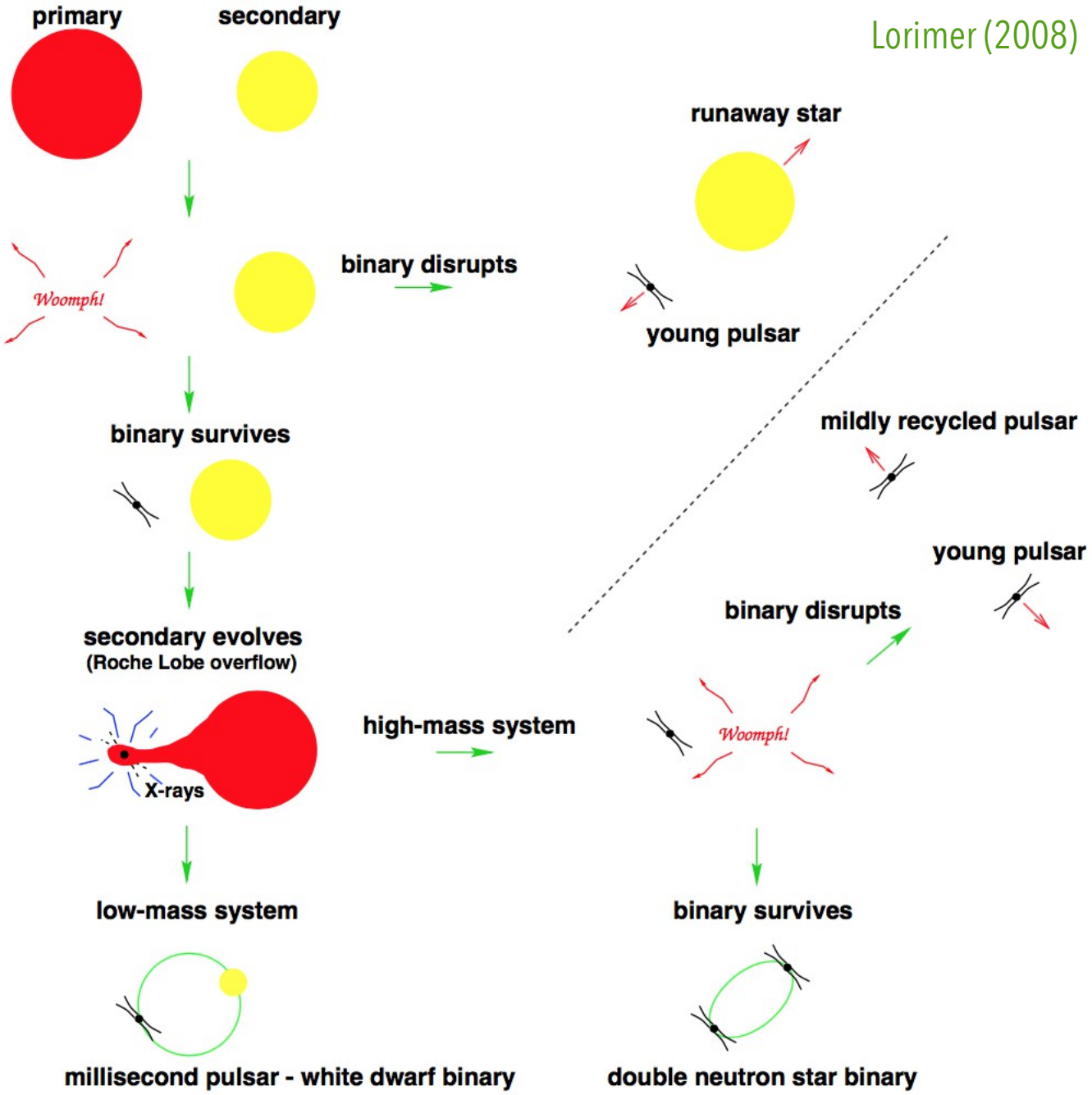

Lorimer (2008)

Pulsars in binary systems

1974: Joseph Taylor and Russell Hulse (Princeton U) discovered the first binary pulsar, PSR 1913+16, which consists of two neutron stars (one seen as a pulsar) orbiting around their center of mass.

Einstein's general theory of relativity predicts that massive objects in short binary orbits should emit gravitational waves, and thus that their orbit should decay with time.

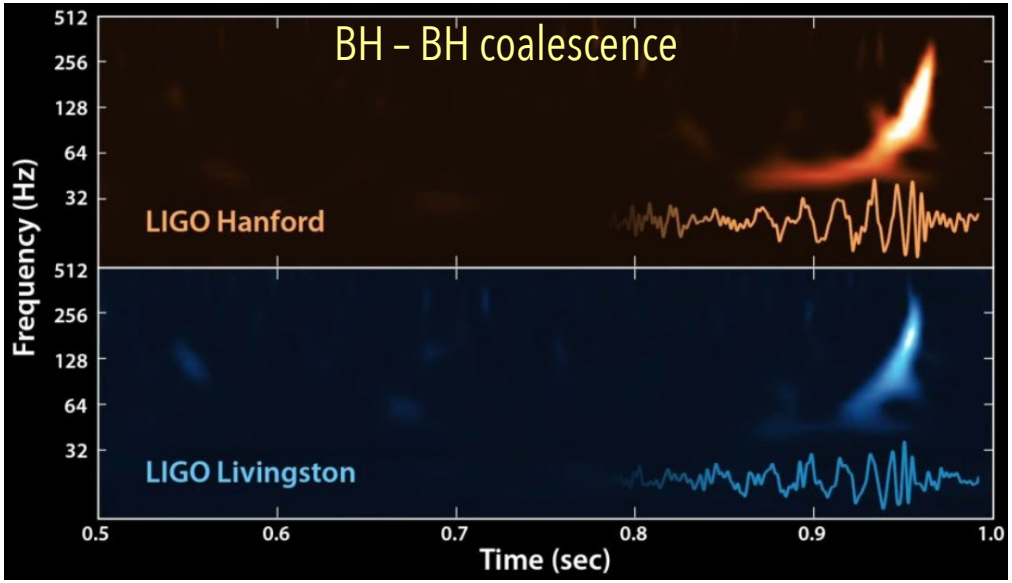

This was indeed observed, precisely as general relativity predicts, and in 1993, Taylor and Hulse were awarded the Nobel prize in Physics for this discovery.

(next page shows the Hulse & Taylor prediction [solid line] and the observation of the decay of the orbit [filled circles])

Orbital decay: periastron shift (GR accurate within 0.2%, after ~ 30 yr of observation)

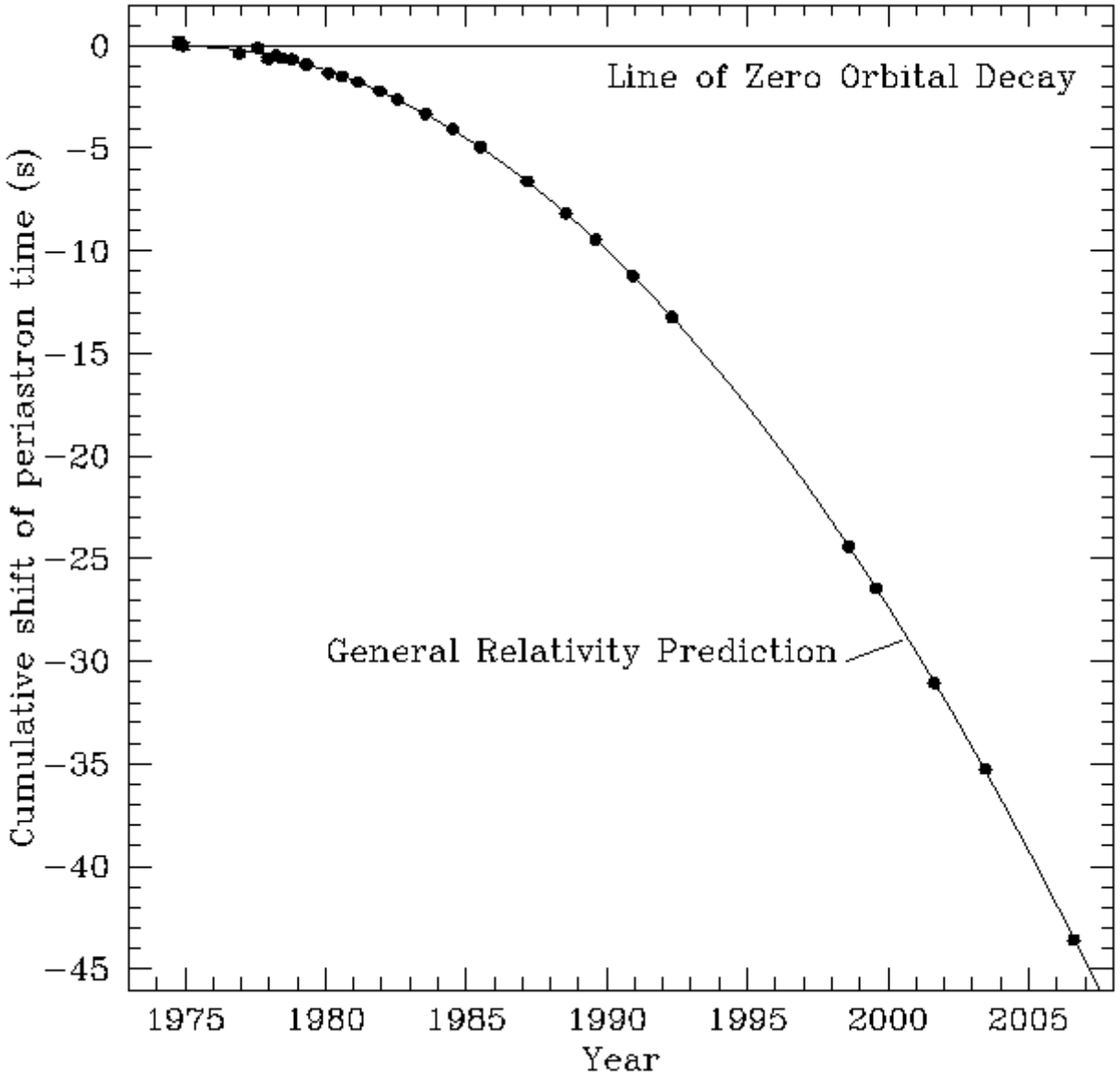

Pulsars in binary systems

Binary systems: Examples of Doppler variations observed in binary systems containing pulsars. Left: The Doppler variations of the globular cluster MSP J1748 – 2446N in Terzan 5. This pulsar is in a nearly circular orbit ($e = 4.6 \times 10^{-5}$) with a companion of minimum mass 0.47 Mo. The difference between the semi-major and semi-minor axes for this orbit is only 51±4 cm! The red lines show the periods as measured during GBT observations. Right: Similar Doppler variations from the highly eccentric binary MSP J0514−4002A in the globular cluster NGC 1851. This pulsar has one of the most eccentric orbits known (e=0.888) and a massive white-dwarf or neutron-star companion.

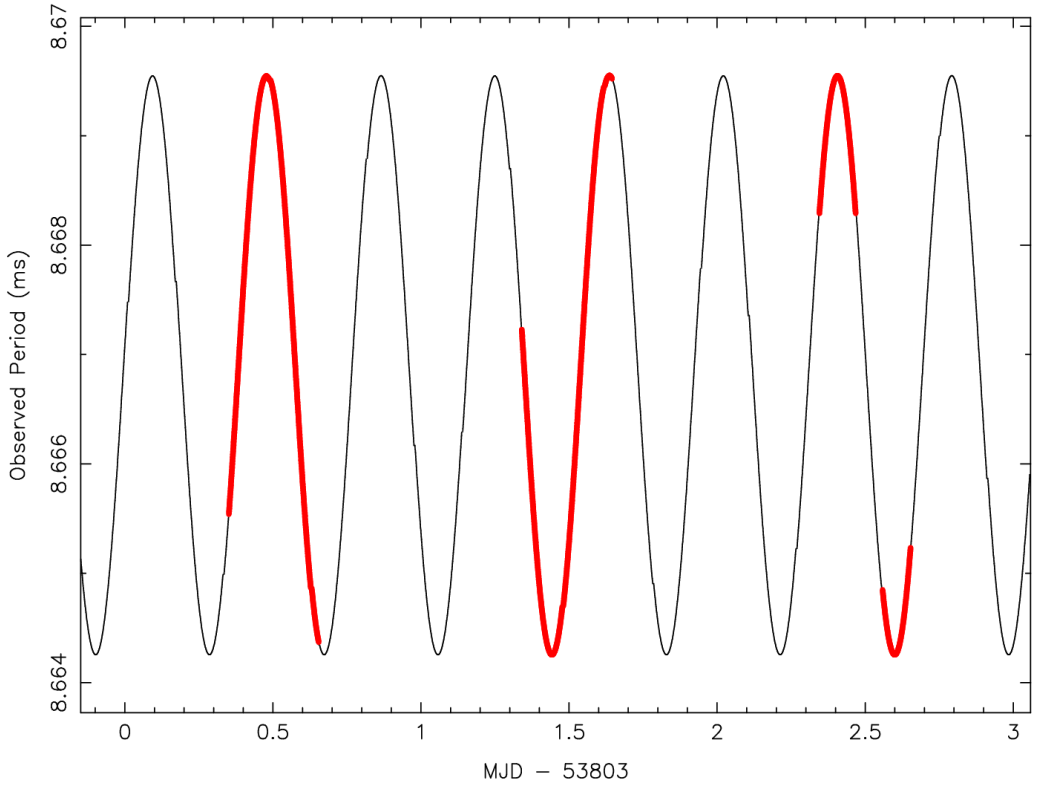

MSP J1748 – 2446N

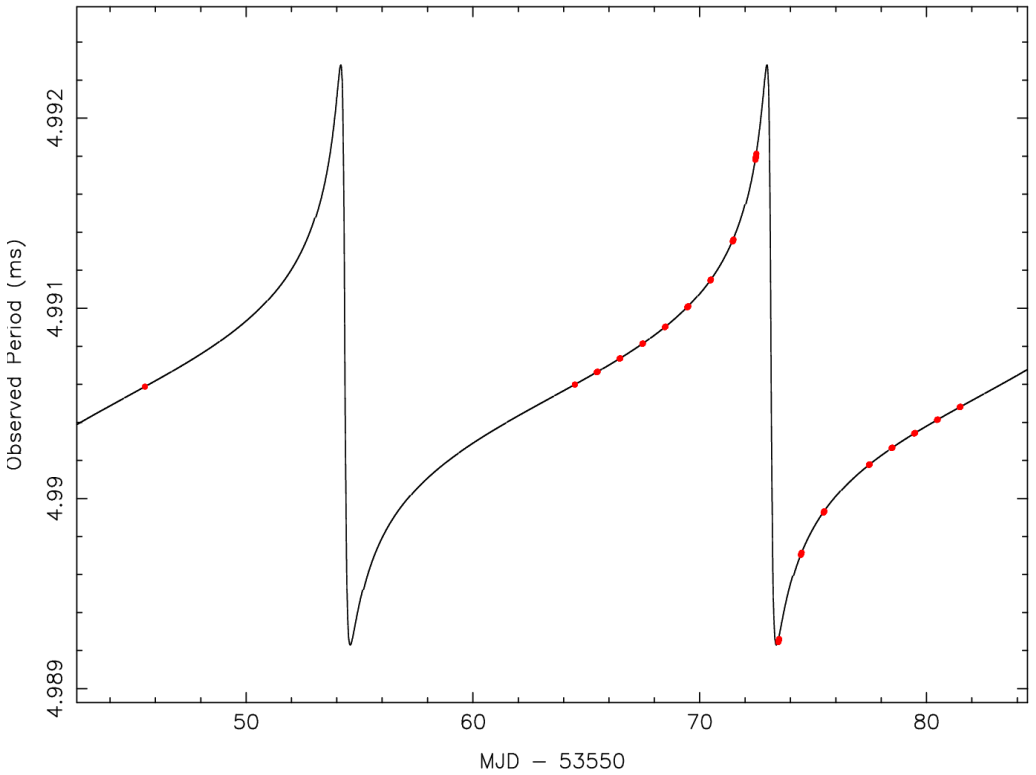

MSP J0514−4002A

The double pulsar system J0737-3039A (22.7 ms) & B (2.8 s) & Mass determination [Burgay + 2003]:

After 12 months of observations
timing measurements for A
already provide five PK parameters.
Shaded regions are those excluded
by the K mass functions of the two pulsars.
Further constrains (pair of lines)
are predicted by GR.

$$m_A + m_B = 2.59 M_e$$

$$i = 88 \pm 1^0$$

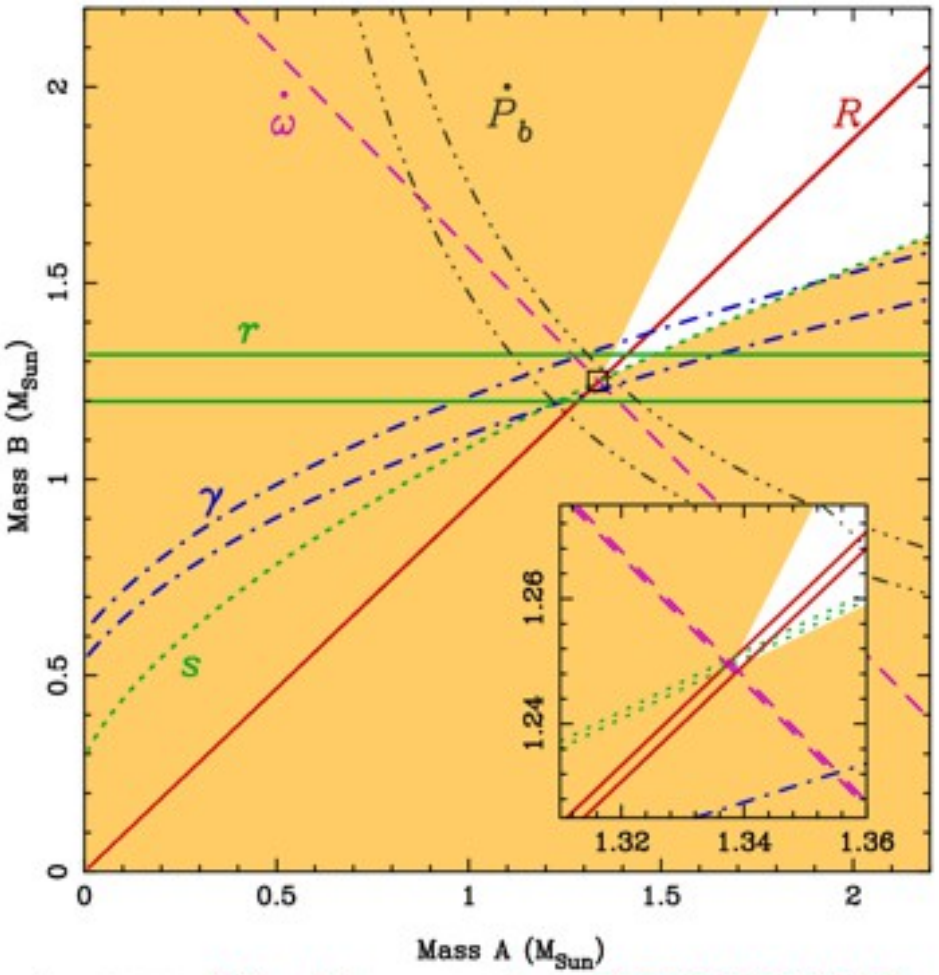

masses of the binary system J0737-3039A&B

The double pulsar system J0737-3039A (22.7 ms) & B (2.8 s) & Mass determination [Burgay + 2003]:

Advance of Periastron $$\dot{\omega} = 3\left(\frac{P_b}{2\pi}\right)^{-5/3}(T_o M)^{2/3}(1-e^2)^{-1}$$

Gravitational redshift (time dilation) $$\gamma = e\left(\frac{P_b}{2\pi}\right)^{1/3} T_o^{2/3} M^{-4/3} m_c (m_p + 2m_c)$$

Rate of orbital decay (GW emission)

$$\dot{P}_b = -\frac{192\pi}{5}\left(\frac{P_b}{2\pi}\right)^{-5/3}\left(1+\frac{73}{24}e^2+\frac{37}{96}e^4\right)(1-e^2)^{-7/2} T_o^{5/3} m_p m_c M^{-1/3}$$

Range of Shapiro Delay $$r = T_o m_c$$

Shape of Shapiro Delay $$s = x\left(\frac{P_b}{2\pi}\right)^{-2/3} T_o^{-1/3} M^{2/3} m_c^{-1}$$

where $M = m_p + m_c$ $x = a_p \sin i / c$ $s = \sin i$ $T_o = GM_{sun}/c^3 = 4.925490947\,\mu s$

The number density of pulsars is related to many assumptions

- Beaming correction:

f = fraction of total pulsars visible or probability of having the pulsar beam intercepting the LoS

Dependent on

- Beam shape (circular)
- (randomly distributed) Inclination angle between rotation axis and H axis

(n.b. Shorter periods may have broader beams ?

f ~ 20% for normal pulsars

f ~ 50 – 100% for ms pulsars)

- luminosity distribution ⇒

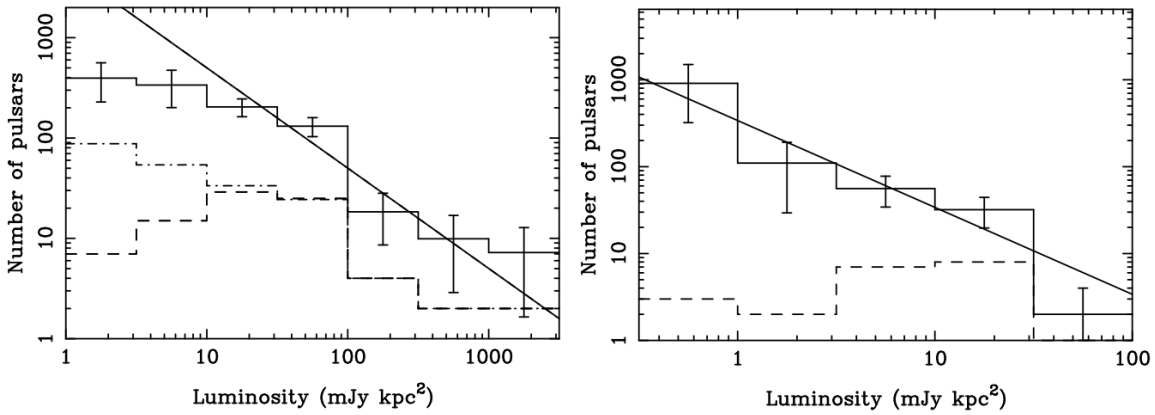

Figure 17: Left panel: The corrected luminosity distribution (solid histogram with error bars) for normal pulsars. The corrected distribution *before* the beaming model has been applied is shown by the dot-dashed line. Right panel: The corresponding distribution for millisecond pulsars. In both cases, the observed distribution is shown by the dashed line and the thick solid line is a power law with a slope of −1. The difference between the observed and corrected distributions highlights the severe under-sampling of low-luminosity pulsars.

Based on a sample of pulsars within 1.5 kpc

With luminosities > 1.5 mJy kpc^2 @ 430 MHz

Surface density:

Normal pulsars 156 ± 31 pulsars kpc^{-2} f=20%

Millisecond pulsars 38 ± 16 pulsars kpc^{-2} f=75%

Pulsar populations

Within the Milky way

Assuming distribution similar to other stellar population,

- 160.000 active normal pulsars
- 40.000 msp

If pulsar lifetime ~ 10^7 yr then birth rate ~1 every 100 yr

Inactive NS within the MW are supposed to be ~ 10^8 – 10^9 (Sartore + 2010, A&A, 510, A23)

Millisecond pulsars more difficult to observe but have longer lifetime!

`mean birth rate ~ 1 every 350.000 yr

– consistent with the LMXRB birth rate

Relativistic binaries:

Pulsar in a narrow binary sistem with a compact object:

Short orbital periods, high velocity, significant timing effects but not only!

- WD – NS
- NS – NS (~10)
- BH – NS (0)

N.B. Very eccentric binary systems may remain undetected, due to high acceleration

Coalescence time (analytic approximation to a few %)

$$\tau_g = 9.83 \cdot 10^6 \,\mathrm{yr} \left(\frac{P_b}{\mathrm{hr}}\right)^{8/3} \left(\frac{m_1 + m_2}{M_\odot}\right)^{-2/3} \left(\frac{\mu}{M_\odot}\right)^{-1} (1 - e^2)^{7/2}$$

$$\text{where } \mu = \frac{m_1 m_2}{(m_1 + m_2)}$$

Galactic merger rates based on binary pulsar data only $118^{+174}_{-79}\,\mathrm{Myr}^{-1}$

Taking into account all MW NS binaries as well as those detectable in nearby galaxies, the expected event rate for advanced LIGO becomes $265^{+390}_{-178}\,\mathrm{yr}^{-1}$

Summary of pulsar radio astronomy

- Easier to be detected in the radio because of transparency of the ISM, but DM!
- Enormous T_B $\Rightarrow$ coherent radiation mechanism, Ne instead of a single e

  coherence length $\sim\lambda$, volume $\sim \lambda^3$ $\Rightarrow$ very steep radio spectral index
- Polarized emission
- Unknown (initial) accelerations mechanism(s), although they are the most effective producers of relativistic particles
- Energy extracted from rotation (and magnetic field)
- Analytic models viable in aligned rotators in vacuum, but....
- Millisecond pulsars are recycled objects in multiple systems
- Pulsars in multiple systems are probes for GR

Pulsar with P = 1 s rotates at ν = 1 Hz and emits radiation with ƛ = c /ν ~3 10^{10} cm

Let' determine $\vec{v}_X = \frac{c}{H^2}\left(\vec{E} \times \vec{H}\right)$ *then* $\left|\vec{v}_X\right| = c\frac{\left|\vec{E}\right|}{H} \approx c$

for a plane wave (fields have the same intensity)
Such a speed is reached in a very short time and the acceleration comes from the electric field

$$\tau_X \approx \frac{v_X}{a} = v_X\frac{m_e}{eE} \approx \frac{cm_e}{eH} = \tau_L \ll \frac{2\pi}{\omega_{NS}}$$

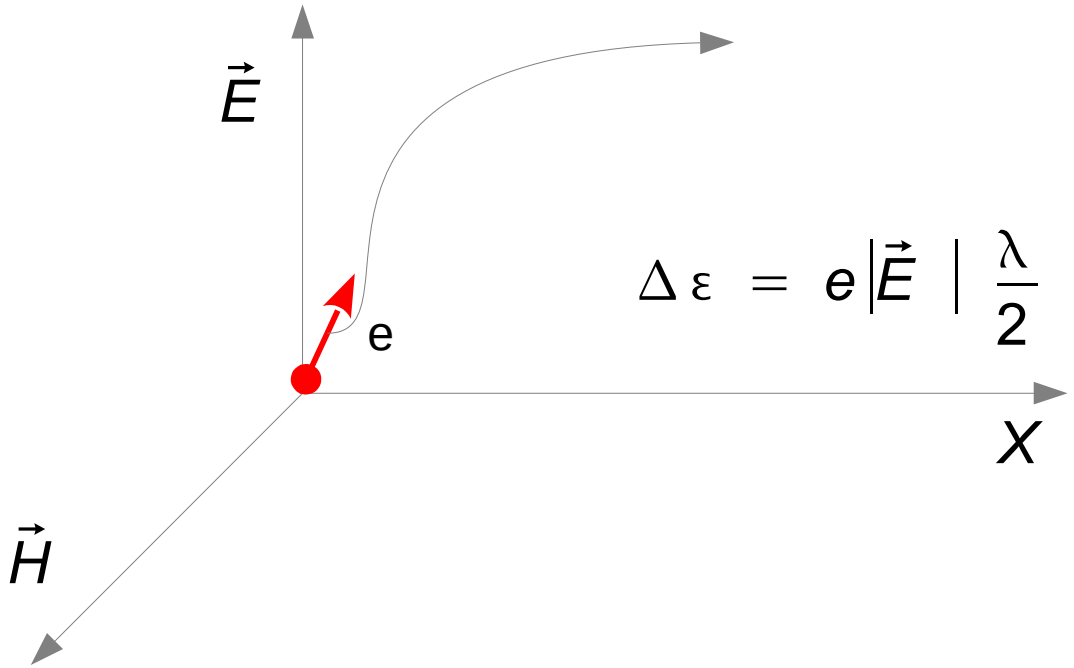

$$\Delta\varepsilon = e\left|\vec{E}\right|\frac{\lambda}{2} \sim 10^{14}\,eV \qquad \left[\left|\vec{E}\right| = 10^6\,Volt\,sec^{-1}\right]$$

See Fanti & Fanti Section 17.5.3

Pulsar with P = 1 s rotates at ν = 1 Hz and emits radiation with $\lambda = c/\nu \sim 3\ 10^{10}$ *cm*

At a given distance (e.g. λ) the energy flux of the emitted e-m wave is = (rotational) kinetic energy loss, and we can infer the value of the electric field

$$\frac{|\vec{E}^2|}{8\pi} \times c = -\frac{1}{4\pi\lambda^2}\frac{dT_{NS}}{dt}$$

*a charge in , **in its own reference frame**:* $m_e \dot{\vec{v}} = e\left(\vec{E} + \frac{\vec{v}}{c} \times \vec{H}\right)$

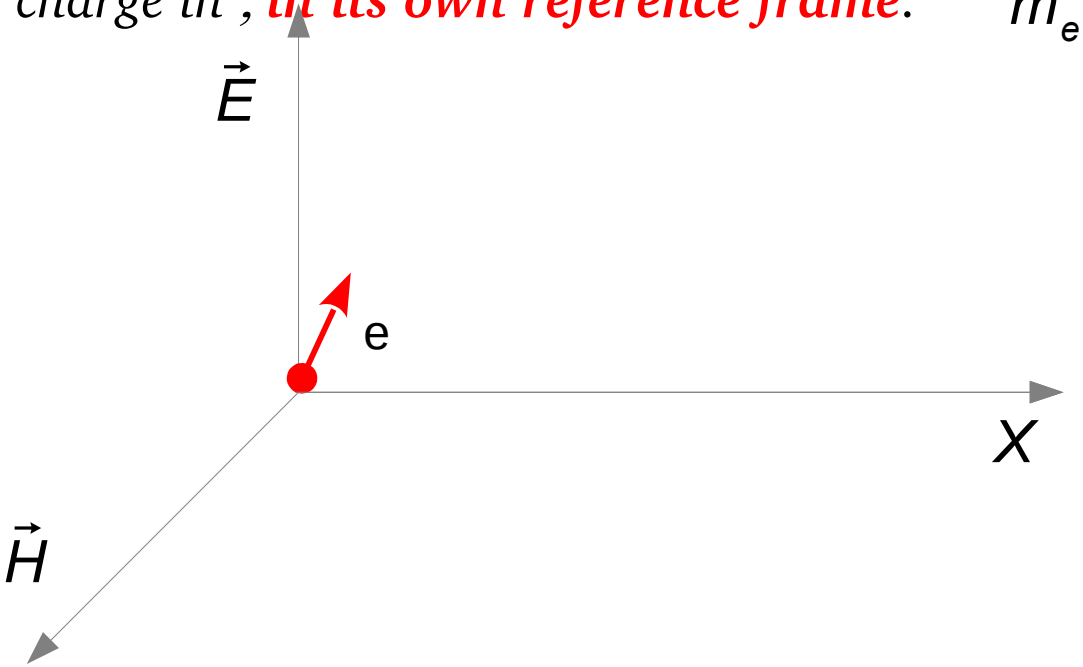

Let's write $\vec{v}_X = \frac{c}{H^2}\left(\vec{E} \times \vec{H}\right)$ (constant, E and H stationary)

$\vec{v}' = \vec{v} - \vec{v}_X$ i.e. $\vec{v} = \vec{v}_X + \vec{v}' = \frac{c}{H^2}\left(\vec{E} \times \vec{H}\right) + \vec{v}'$

given that $\frac{\vec{v}_X}{c} \times \vec{H} = \frac{c}{H^2}\left(\vec{E} \times \vec{H}\right) \times \vec{H} = -\vec{E}\,\frac{H^2}{H^2} = -\vec{E}$

$m_e \dot{\vec{v}} = e\left(\vec{E} + \frac{\vec{v}}{c} \times \vec{H}\right) = e\left(\vec{E} - \vec{E} + \frac{\vec{v}'}{c} \times \vec{H}\right) =$

$= m_e \dot{\vec{v}}'$

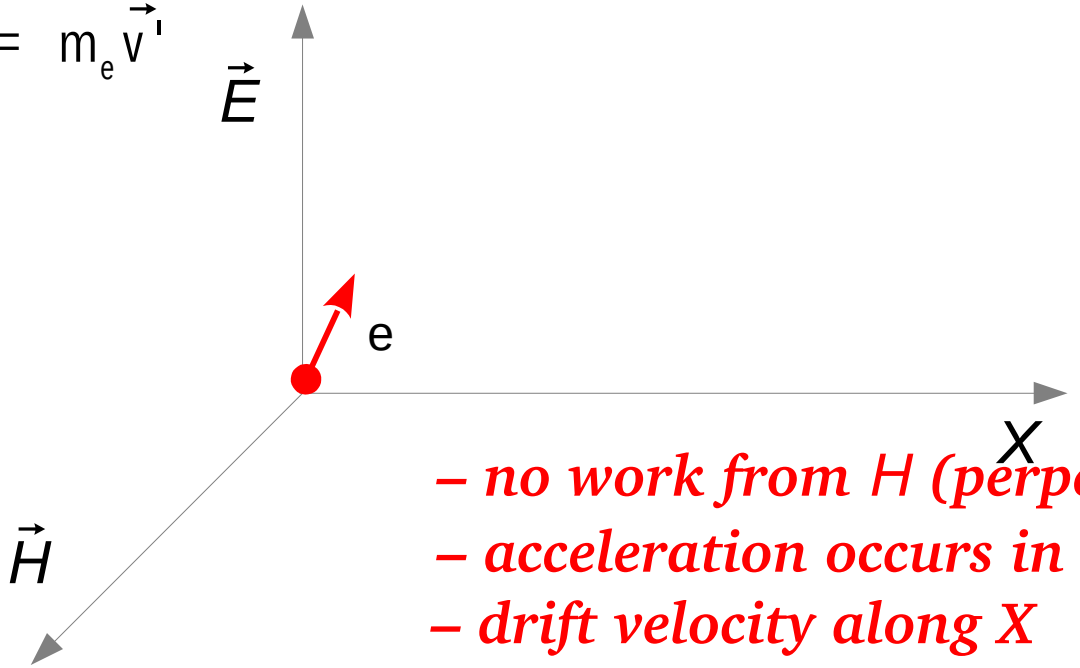

– *no work from H (perpendicular to v) (ΔK from E field)*
– *acceleration occurs in the E,X plane*
– *drift velocity along X*

Let's consider two static fields $\vec{H} \perp \vec{E}$. An electron moving at $\vec{v}$ feels:

$$m_e \dot{\vec{v}} = e\left(\vec{E} + \frac{\vec{v}}{c} \times \vec{H}\right)$$

Let $\vec{v} = \vec{v}_X + \vec{v}'$ and write $\vec{v}_x = c \cdot \frac{\vec{E} \times \vec{H}}{H^2}$ then the Lorentz force becomes

$$\frac{\vec{v}}{c} \times \vec{H} = \frac{\vec{v}_X}{c} \times \vec{H} + \frac{\vec{v}'}{c} \times \vec{H} = -\vec{E} + \frac{\vec{v}'}{c} \times \vec{H}$$

$$\vec{v} = \vec{v}_X + \vec{v}' = \frac{c}{H^2} \vec{E} \times \vec{H} + \vec{v}' \quad \text{then} \quad \dot{\vec{v}} = \dot{\vec{v}}'$$

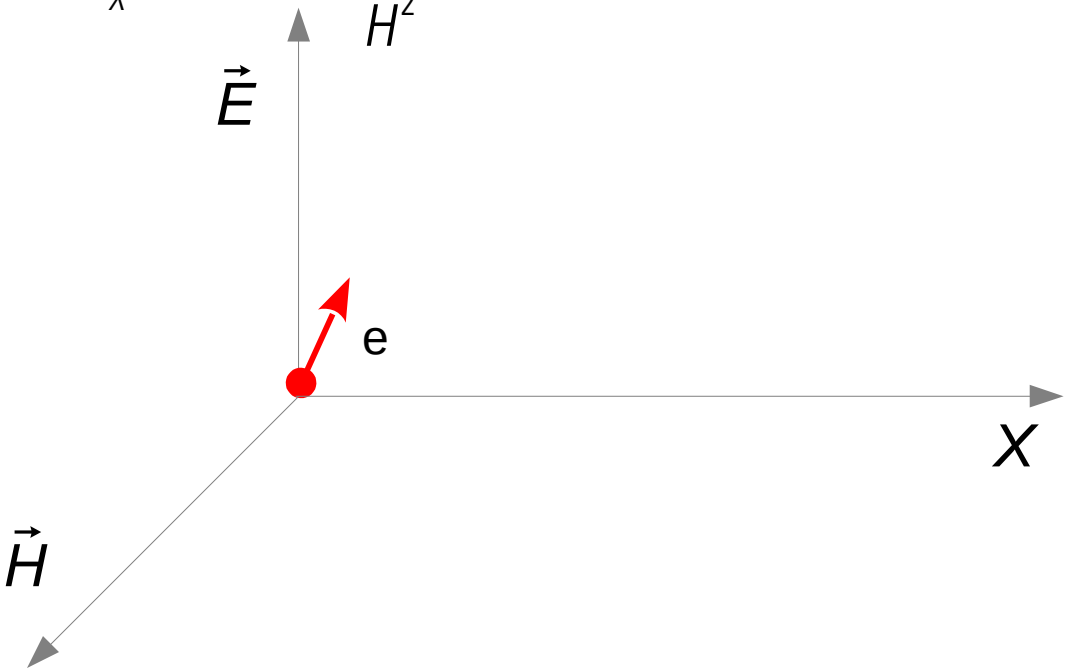

Pulsar with P = 1 s rotates at ν = 1 Hz and emits radiation with ! = c /ν ~3 10^{10} cm

Let' determine $\vec{v}_X = \frac{c}{H^2}\left(\vec{E} \times \vec{H}\right)$ *then* $|\vec{v}_X| = c\frac{|\vec{E}|}{H} \approx c$

for a plane wave (fields have the same intensity)
Such a speed is reached in a very short time and the acceleration comes from the electric field

$$\tau_X \approx \frac{v_X}{a} = v_X\frac{m_e}{eE} \approx \frac{cm_e}{eH} = \tau_L \ll \frac{2\pi}{\omega_{NS}}$$

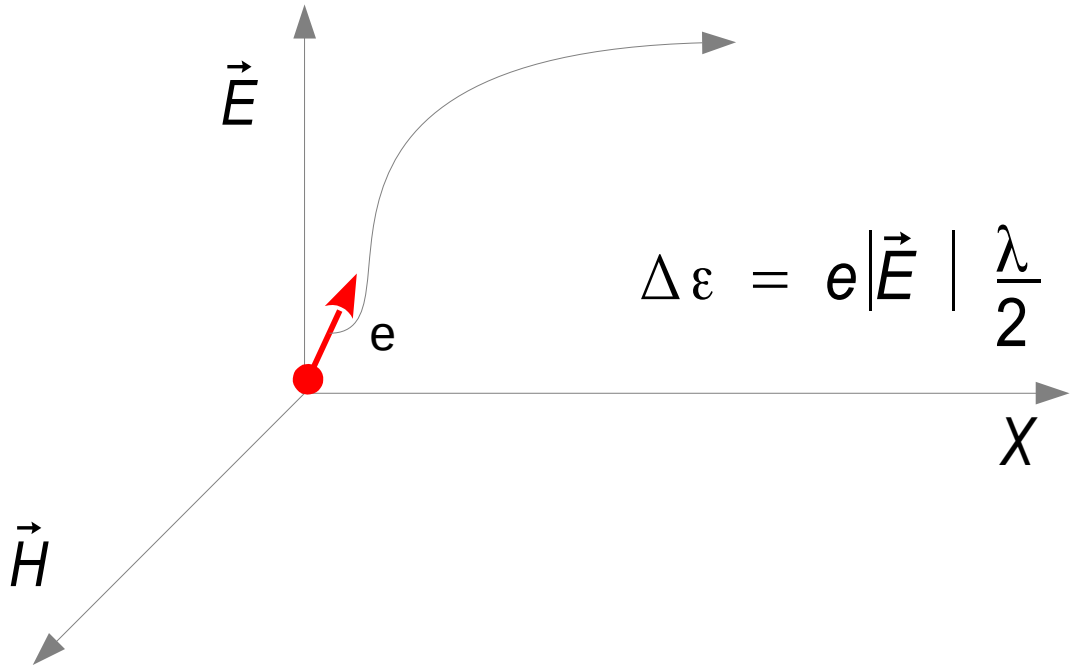

$$\Delta\varepsilon = e|\vec{E}|\frac{\lambda}{2} \sim 10^{14}\,eV \qquad [|\vec{E}| = 10^6\,Volt\,sec^{-1}]$$

The Lorentz force is then $m_e \dot{\vec{v}} = \frac{e}{c} \vec{v}' \times \vec{H} = m_e \dot{\vec{v}}'$

Only $\vec{v}'$ contributes to the acceleration $\perp \vec{H}$ in the $\vec{E} - X$ plane; v_X is a constant drift velocity

$\vec{H}$ in the Lorentz force is $\perp \vec{v}$ $\rightarrow$ no work!

the increase of the kinetic energy of the electrons comes from $\vec{E}$

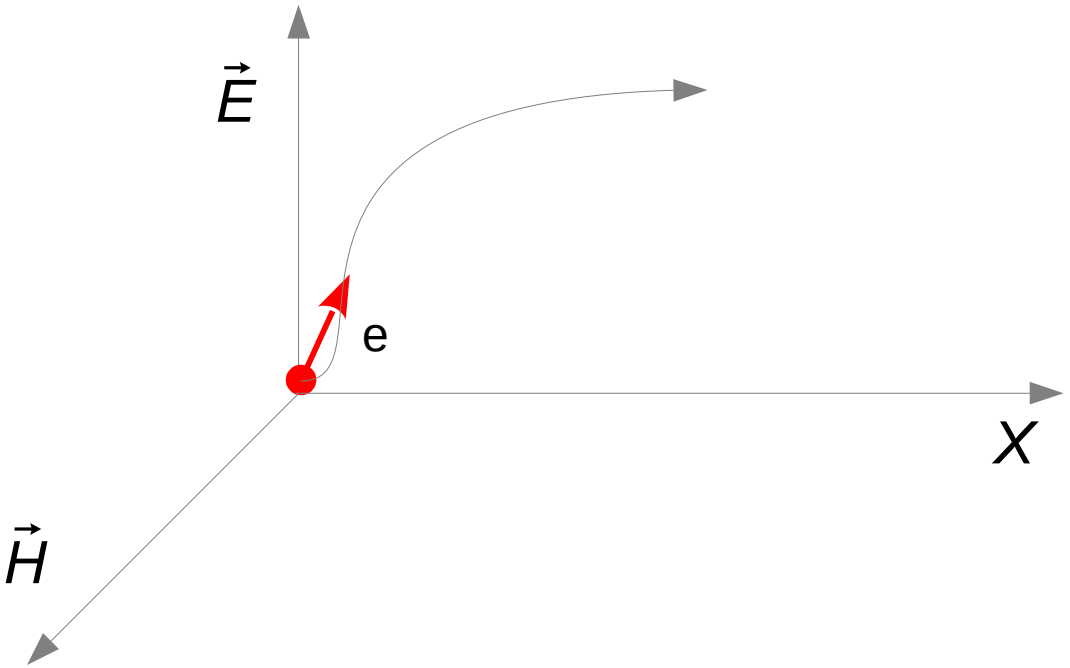

H. L
J. RI
z[1,5],
PE[7]

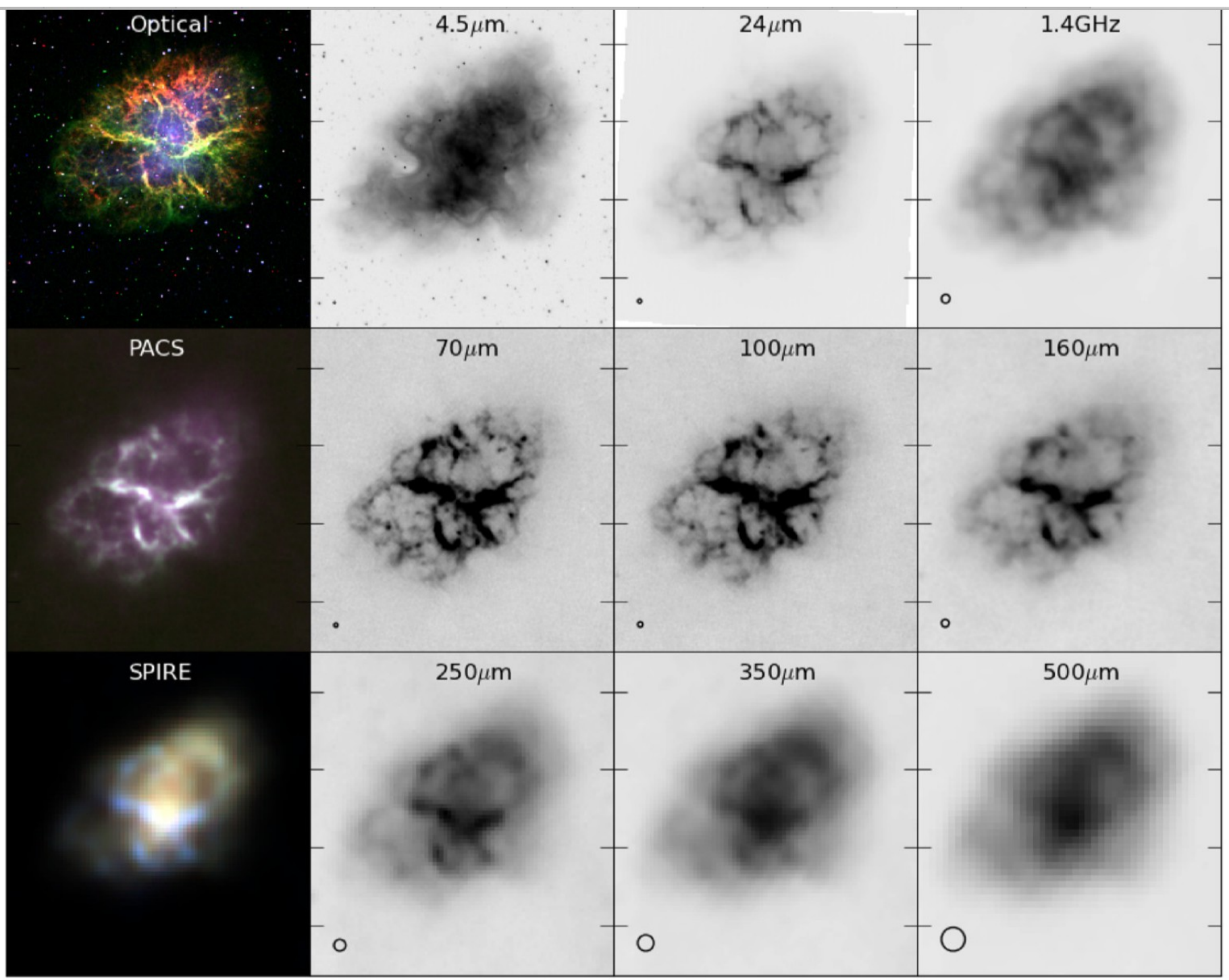

Figure 2. Multiwavelength montage of the Crab SNR centered on the pulsar (R.A. = 262.°671, decl. = 22.°0145, J2000.0) with diameter 4.′2 × 4.′2. Top (from left to right): three-color image in Hα (red), [O III] (green), and Bessel *B* (blue) using images obtained from the Faulkes Telescope North (Appendix A). *Spitzer* IRAC 4.5 μm, MIPS 24 μm, and VLA archive data at 1.4 GHz (taken in 1996). Middle: *Herschel* PACS three-color image and individually the 70, 100, and 160 μm images. Bottom: *Herschel* SPIRE three color image and individually, 250, 350, and 500 μm images. Beam sizes are indicated with the black circle in the lower left corner.

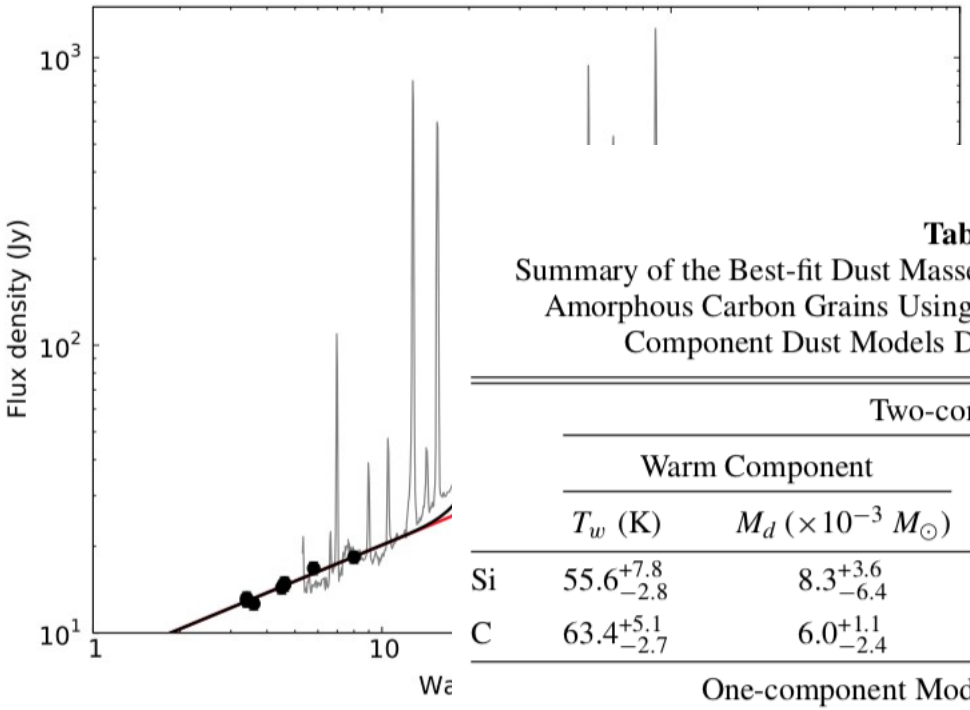

Figure 4. IR SED of the Crab Ne
Herschel, the new *Spitzer* calibrati
errors include the photometric error
the error in the synchrotron extrap
contribution (Table 2) added in qua
100 μm flux is overplotted in gray.
et al. 2005) *Spitzer* spectroscopy (fr
is overplotted for comparison. The synchrotron power law is shown in red. Two temperature components of amorphous carbon dust at 63 and 34 K required to fit the SED are plotted (blue dashed) with the sum of these plotted in solid blue. A single-temperature amorphous carbon fit (40 K) to the FIR is also shown (green dot-dashed). The sum of the two-component dust and synchrotron contributions is shown by the solid black curve.

Table 3
Summary of the Best-fit Dust Masses and Temperatures for Silicate and Amorphous Carbon Grains Using the Two (Top) and One (Bottom) Component Dust Models Displayed in Figures 4 and 5

	Two-component Model				
	Warm Component		Cool Component		
	T_w (K)	M_d ($\times 10^{-3}$ $M_\odot$)	T_c (K)	M_d ($M_\odot$)	χ^2
Si	$55.6^{+7.8}_{-2.8}$	$8.3^{+3.6}_{-6.4}$	$28.1^{+3.2}_{-5.5}$	$0.24^{+0.3}_{-0.1}$	0.05
C	$63.4^{+5.1}_{-2.7}$	$6.0^{+1.1}_{-2.4}$	$33.8^{+2.3}_{-1.8}$	0.11 ± 0.01	0.23
	One-component Model				
	T_d (K)	M_d ($M_\odot$)	χ^2		
Si	34	0.14	3×10^{-5}		
C	40	0.08	7×10^{-3}		

Note. The reduced χ^2 statistic is also included.

GOMEZ ET AL.

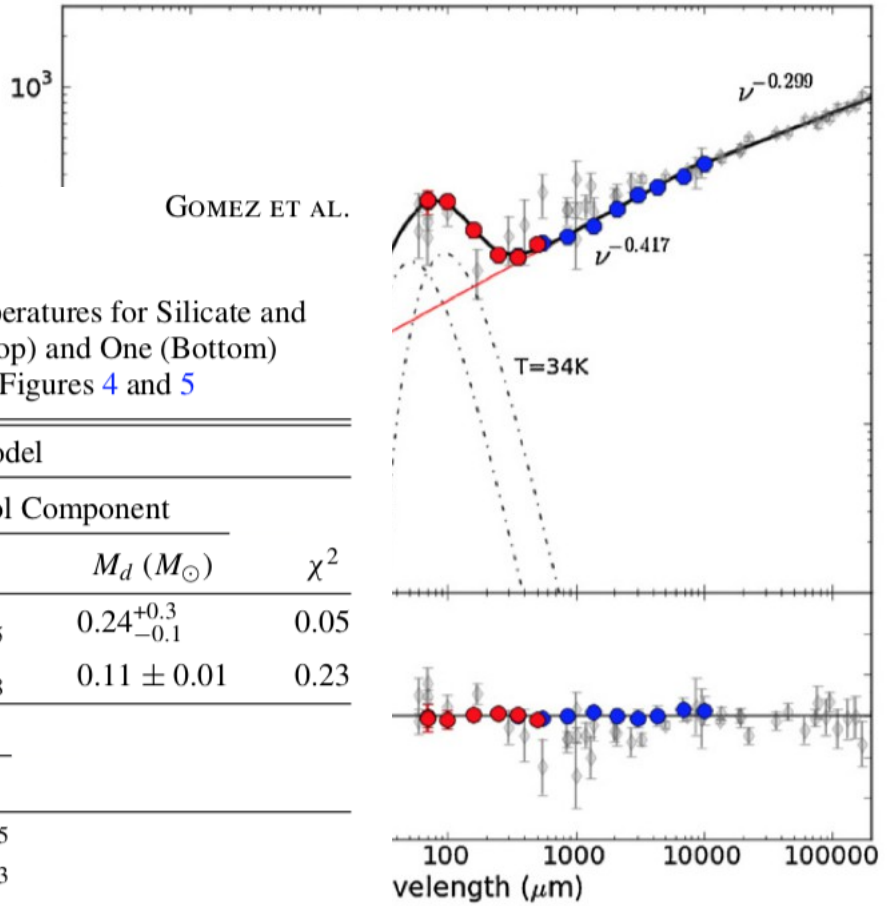

a from the IR-radio including *Hersch*
E (purple) photometry, and *Planck* flux
(Planck Collaboration 2011, blue points). Previous fluxes from the literature (s
Table 4 and references therein) are shown with gray diamonds. The synchrotr
law fitted to the 3.6–10^4 μm data points is the dashed black line. Dot-dashed lin
are the fitted components from thermal emission by amorphous carbon grai
(see Figure 4). The solid black line is the total flux obtained from summi
the synchrotron and the two dust components (with the residual shown below
Note the total integrated fluxes plotted here also include a contribution from li
emission at 24, 70, and 100 μm (Section 3.1), which has not been added to t
total black SED curve plotted here.

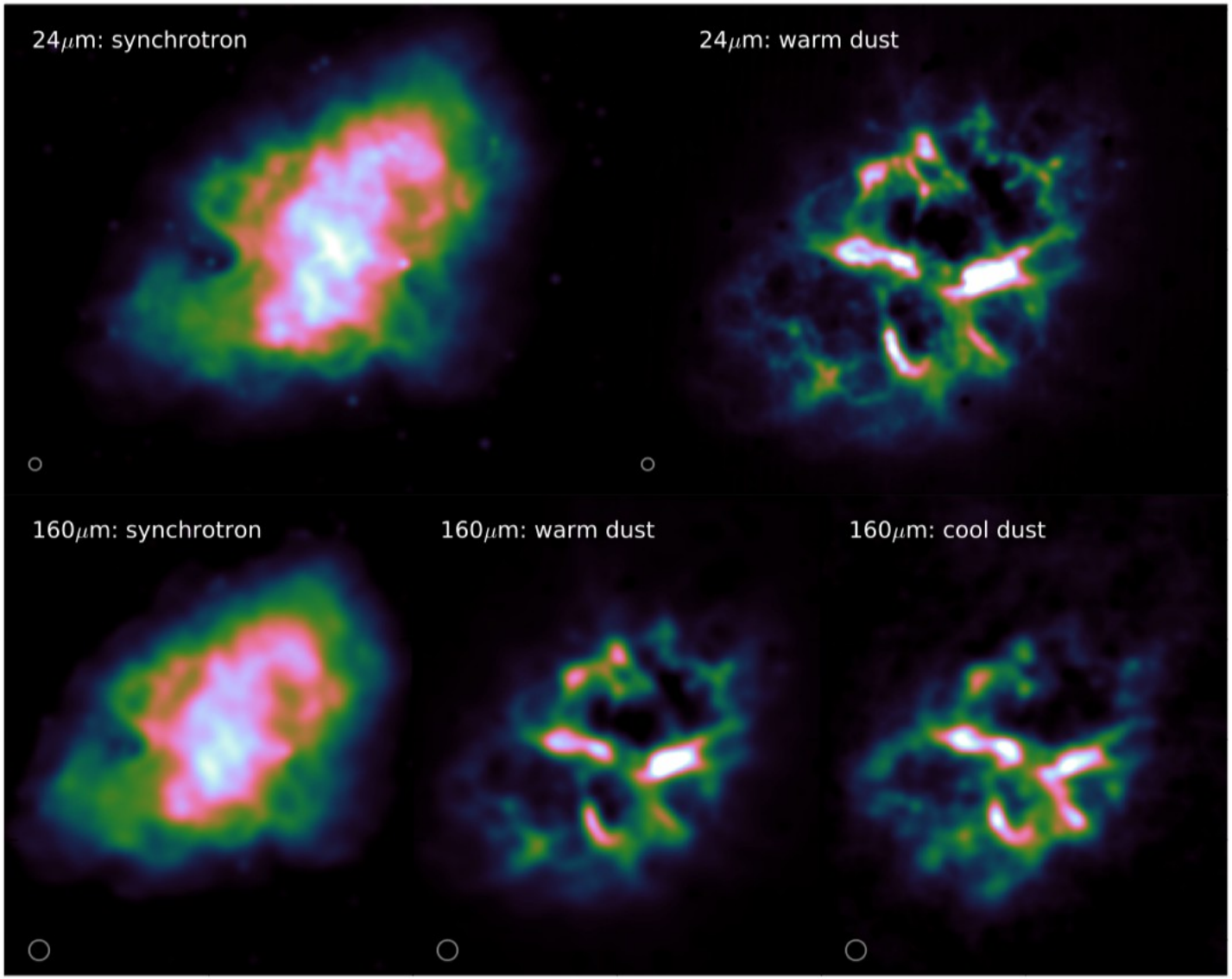

Figure 6. Top: the distribution of synchrotron and thermal emission from the warm dust component at 24 μm. Bottom: the *Herschel* SPIRE 160 μm emission separated into the synchrotron component (left), the warm dust component (as traced by the emission at 24 μm) (middle), and the newly identified cool dust component (right). The color palette used in the online version of this figure is the cubehelix scheme in which color monotonically increases in terms of perceived brightness (Green 2011).